Title
Fluorogenic and Covalently Targeted Voltage Sensitive Dyes

Author
Grenier, Vincent

Publication Date
2018

Peer reviewed|Thesis/dissertation

Fluorogenic and Covalently Targeted Voltage Sensitive Dyes

By

Vincent Grenier

A dissertation submitted in partial satisfaction of the
requirements for the degree of
Doctor of Philosophy
in
Chemistry
in the
Graduate Division
of the
University of California, Berkeley

Committee in charge:

Professor Evan W. Miller, Chair
Professor Christopher J. Chang
Professor Marla B. Feller

Fall 2018

Fluorogenic and Covalently Targeted Voltage Sensitive Dyes

By Vincent Grenier

Abstract

Fluorogenic and Covalently Targeted Voltage Sensitive Dyes

by

Vincent Grenier

Doctor of Philosophy in Chemistry

University of California, Berkeley

Professor Evan W. Miller, Chair

Fluorescent reporters of membrane potential are important tools in neuroscience, offering a non-invasive, real-time optical readout of neuronal activity. Voltage sensitive dyes of the VoltageFluor family report neuronal activity with high sensitivity and sub-millisecond response times, but lack the cell-type specific targetability of genetically encoded tools, placing certain constraints on their applicability in complex environments (i.e. tissue slice, *in vivo*, sub-cellular localization).

The work presented in this thesis addresses these problems through two distinct strategies. In Chapters 1 and 2 I describe the development of weakly-fluorescent, photoactivatable "caged" VoltageFluors. Spatial control of illumination allows for release of VoltageFluor at the single cell and subcellular levels in cultured mammalian neurons, and subsequent recording of evoked action potentials. This caging strategy has proven to be generalizable, and Chapter 3 and Appendix 1 detail the synthesis of enzymatically-activatable probes. In Chapter 4 I present a strategy for the selective labeling of cells with a VoltageFluor derivative, which harnesses the known covalent interaction between a short peptide, SpyTag, and its cognate binding protein, SpyCatcher. I synthesized a series of VoltageFluor-SpyTag conjugates, or VoltageSpy dyes, which specifically label the outer membranes of cells expressing SpyCatcher at the cell surface, with minimal off-target labeling, and without requiring a wash step. I demonstrate the application of this system to imaging spontaneous activity in cultured mammalian neurons, as well as imaging evoked activity in axons and dendrites. Appendix 2 describes efforts to apply VoltageSpy dyes in mouse brain slice. Finally, Chapter 5 presents a general strategy for minimizing phototoxic effects sometimes encountered when imaging with VoltageFluor dyes, using either bath applied triplet state quenchers or an intramolecularly-stabilized VoltageFluor derivative. Cyclooctatetraene was found to be an effective protective agent – a result which may prove broadly useful in imaging VoltageFluor dyes, improving the applicability of the fluorogenic and covalently-targeted tools presented in Chapters 1-4.

For My Parents

Table of Contents

Acknowledgements

I am tremendously grateful to my advisor, Evan Miller, for five years of outstanding mentorship and support. Evan's unfailing positivity and enthusiasm often kept me motivated when I felt that a particular experiment was too challenging or doomed to fail (it always worked in the end). I was first exposed to his work on voltage sensitive dyes in 2011, when, as a curious and impressionable undergraduate I saw his postdoctoral advisor Roger Tsien present at the Canadian Chemistry Conference. This was my first exposure to the world of fluorescent probes and I distinctly remember thinking "I want to do *that*". Naturally when I arrived at Berkeley I had little choice but to join his lab – which, all in all, seems to have worked out rather well. I hope that as I progress through my own career I will be able to exemplify the same qualities that have made Evan such a great person to work for.

If my time at Berkeley has been so rewarding it is due in large part to my wonderful friends and colleagues in the Miller lab. Belonging to the first generation of grad students in a lab was an important aspect of my grad school experience, but it wouldn't have been the same without my classmates Parker Deal, Rishi Kulkarni and Alisha Contractor. I have no doubt they'll go far. Special thanks to Parker for introducing me to soccer. We were soon joined by an incredibly talented postdoc, Alison Walker, from whom I learned most of what I know about microscopy, electrophysiology and tissue culture. Alison was a great mentor and collaborator, and I'm a far better scientist for having had the opportunity to work with her. In the younger cohorts of Miller Lab students, I'd particularly like to thank Pei Liu for being a great collaborator across multiple projects, and Steven Boggess, Julia Lazzari-Dean, Gloria Ortiz and Molly Kirk for their friendship.

I've been lucky to mentor a number of younger students, which has been of the most rewarding elements of grad school. I'd like to acknowledge Brittany Daws, Johnathan Maza and Anneliese Gest for their hard work as rotation students. Anneliese and Brittany have since joined the lab, and it's been a pleasure seeing them continue to develop as scientists. I'd also like to thank Wootack Hong, who worked with me as an undergraduate, for his hard work and friendship.

I would never have succeeded at Berkeley without having had several excellent mentors as an undergraduate, throughout both my internships and academic research. I would like to thank Jean-Philippe Levesque-Sergerie and Sophie Dahan at PerkinElmer Biosignal, Alexandre Champagne, Christopher Wilds and Anne Noronha at Concordia University, Geneviève Huppé and Martine Lamarche at the Laboratoire de sciences judiciaires et de médecine légale du Québec, and Matthias Schönberger at LMU Munich for those formative experiences.

Here at Berkeley I'm grateful to Ming Hammond and Ehud Isacoff for allowing me to rotate in their labs – both rotations were a great experience. I'd also like to thank David Savage, Marla Feller and Christopher Chang for serving on my qualifying exam committee.

Finally, I would like to thank my family. I'm sure it can't always have been easy on my parents to have their eldest child three thousand miles away from home for five years, but they have always supported me unconditionally in all my endeavors and grad school was no different. My siblings, Anne-Sophie and Philippe, are two of the coolest, kindest and funniest people I know, and it was always a joy to host them when they came to visit.

Chapter 1

A Small Molecule Photoactivatable Sensor of Transmembrane Potential

Portions of this work have been published in the Journal of the American Chemical Society:

Grenier, V.; Walker, A.S.; Miller, E.W. *J. Am. Chem. Soc.*, **2015**, *137* (34), 10894-10897.

Portions of this work were completed in collaboration with others:

Neuronal cell culture was performed by Dr. Alison S. Walker. Optical recording of evoked action potentials was performed in collaboration with Dr. Alison S. Walker.

Introduction

Changes in neuronal membrane potential encode the vast range of thoughts, feelings, and behaviors that comprise the human experience. Despite the central importance of the brain to human health and disease, the molecular and cellular mechanisms underlying brain and neuronal function remain incompletely characterized, prompting efforts at the national and international level to develop more comprehensive maps of neuronal activity.[1–3] Much of modern neurobiology stands upon the electrophysiological recordings of the activity of single neurons embedded within a network context. While this approach has proven incredibly powerful, real limitations exist. Specifically, the invasive requirement of impaling cells with electrodes in biological samples severely disrupts overlying tissue and restricts recordings to the cellular soma, making multi-site recording challenging or impossible.

Fluorescence imaging uniquely addresses this problem because the technique is non-invasive, can provide spatial information on membrane potential changes in multiple cells or in sub-cellular regions distant from the soma, and can be high-throughput. Voltage imaging with autofluorescent proteins,[4–7] small molecules,[8–13] or a combination of both,[14–16] remains an attractive solution because it can enable the direct measurement of membrane potential while providing the spatial resolution, throughput, and parallel recording capabilities of Ca^{2+} imaging approaches. Recently, voltage-sensitive small molecules based on molecular wires emerged as an intriguing class of fluorophores for voltage sensing.[17,18]

VoltageFluors, or VF dyes, sense changes in transmembrane potential by a photoinduced electron transfer (PeT) mechanism. PeT from an electron-rich aniline through a molecular wire to a fluorescent reporter is controlled by the electric field across the plasma membrane of an excitable cell, such as a neuron. At rest, where typical mammalian neuronal membrane potentials are approximately -60 mV inside the cell, PeT is enhanced, resulting in diminished fluorescence. As the membrane depolarizes, during an action potential or upon integration of excitatory inputs from connected neurons, PeT decreases, resulting in enhanced fluorescence.[19] Consequently, VF dyes display large voltage-sensitive change in fluorescence while maintaining the fast response time needed for resolving single action potential spikes. Because PeT within the VF dye scaffold is fast compared to the biological event of interest, VF dyes add no capacitive load, making them ideal candidates for non-disruptive sensors of neuronal activity.

Despite these important characteristics, the amphipathic nature of VF dyes results in non-specific uptake into all plasma membranes within a biological sample, obscuring the boundary between adjacent stained cells and making it difficult to detect voltage-induced fluorescence changes against a high background of non-excitable cells stained with the dye. The ability to sparsely label neurons with VF dyes would address this problem. Restricted labeling of a subset of neurons within a neuronal network would improve signal-to-noise by lowering background fluorescence and pave the way for optical interrogation of local neuronal circuits both in culture and in more complex preparations. To achieve selective labeling of only a fraction of defined neurons, we envisioned quenching VF fluorescence with a photolabile protecting group (Scheme 1-1).

Design of a Photoactivatable Voltage Indicator

Photolabile protecting groups have found broad utility in both organic synthesis and chemical biology.[20,21] Originally developed as a protecting group for amino acids that could be

removed under mild conditions,[22] the o-nitrobenzyl protection group and its derivatives have since found broad utility in masking the physiological activity of biologically active molecules, including nucleotides,[23–25] metal ion ligands,[26–29] ionophores,[30] neuro-transmitters,[31] reactive oxygen species,[32] receptor agonists,[33] and amino acid residues.[34] Nitrobenzyl motifs have also been applied to fluorophores for super-resolution microscopy.[35,36] We propose to use photoactivatable VF dyes based on DMNB photocages to spatially control the apparent staining of cells in biological samples. The caged VoltageFluor would localize to cell membranes and remain weakly fluorescent until uncaging or photoactivation via illumination liberated the parent VF fluorophores (Scheme 1-1). Restricting uncaging illumination by scanning a region of interest (ROI) or through spatial light modulation (SLM) technology would provide targeted fluorescent labeling of defined sub-populations of neurons. Toward this end, we now present the design, synthesis, and application of a small-molecule photoactivatable optical sensor of transmembrane potential, or SPOT (compound 1-1), as a first class of voltage sensing fluorophores that enable targeted photoactivation of VF dyes in cells of interest via selective photo-uncaging.

Results and Discussion

SPOT2.1.Cl is readily available in one step from previously reported VF compounds.[17,18] Alkylation of VF2.1.Cl with 2-nitro-4,5-dimethoxybenzylbromide in DMF provides SPOT2.1.Cl in 94% yield (Scheme 1-1). We examined the photophysical behavior and characteristics of SPOT2.1.Cl under simulated physiological conditions (PBS, pH 7.4). As synthesized, SPOT2.1.Cl displays an absorbance profile significantly altered from the parent VF dye (Figure 1-1, grey and black traces), with a λ_{max} centered at 400 nm (ε=44,000 $M^{-1}cm^{-1}$) attributed to the molecular wire absorbance and a minor absorbance centered at 500 nm (ε=21,000 M-1cm-1) corresponding to the alkylated fluorescein scaffold. At 522 nm, the λ_{max} for VF2.1.Cl, SPOT2.1.Cl shows only weak absorbance (ε=6,200 $M^{-1}cm^{-1}$). In contrast, the free VF dye demonstrates strong absorbance at 522 nm, with a shoulder at 488 nm. Emission from SPOT2.1.Cl is minimal (Figure 1-2a, black trace), as reflected by its low fluorescence quantum yield (Φ=0.002), which is 28-fold lower than VF dye (Φ=0.057). UV illumination of SPOT2.1.Cl promptly delivers VF, as measured by complete recovery of absorbance profiles characteristic of VF2.1.Cl (Figure 1-1a, green and black traces) and a 25-fold increase in fluorescence emission (Figure 1-2a, green trace). HPLC comparison against VF2.1.Cl confirmed the photochemical conversion of SPOT2.1.Cl into VF2.1.Cl (Figure 1-3). Identical UV irradiation had no effect on VF2.1.Cl absorbance or emission (Figure 1-1b and c). The photochemical quantum yield was determined by actinometry to be 0.007. SPOT has an ε_{365} of 33,000 $M^{-1}cm^{-1}$ giving an overall efficiency (Φ x $\varepsilon_{365\ nm}$) of 230, comparable to reported values for o-nitro photocages.[20]

We next turned our attention to photoactivation of SPOT2.1.Cl in living cells. Bath application of SPOT2.1.Cl to human embryonic kidney cells (HEK 293) resulted in very little cellular fluorescence staining, due to the low intrinsic brightness of SPOT2.1.Cl (Figure 1-2c). Illumination with 390 nm (30 x 1 s) light results in an immediate increase in cell membrane-associated fluorescence characteristic of VF staining (Figure 1-2d) over the entire field, indicating that SPOT2.1.Cl had localized to cell membranes and remained optically silent until photoactivation. Quantification of the mean cellular fluorescence intensity pre- and post-UV indicates that SPOT2.1.Cl provides a 12 ± 1.2-fold (*n*=3 separate experiments) increase in fluorescence intensity following irradiation. Membrane-associated fluorescence depends on prior UV illumination, as examination of fields of view not exposed to light show little fluorescence (Figure 1-4a, c, e). However, subsequent photoactivation of these regions (390 nm, 30 s) results in

a similar fluorescence increase (Figure 1-4b, d, f), demonstrating that patterns of spatially restricted light can selectively photoactivate distinct cell populations.

Having established the ability of SPOT2.1.Cl photoactivation to control apparent staining at a region-specific level, we next examined the ability of SPOT2.1.Cl to label individual cells, using confocal microscopy. By defining a photoactivation ROI around several cells, SPOT2.1.Cl could be selectively activated in the cells of interest (Figure 1-5a, b), giving an approximately11-fold increase (±0.8, *n*=5 cells, Figure 1-5d) in fluorescence intensity in cells illuminated with 405 nm light (25 x 1 s illumination, Figure 1-5a-c). Upon release by light, SPOT2.1.Cl remained localized in single cells; the dye did not migrate away from the originally uncaged cells (Figure 1-5b). Uncaged SPOT2.1.Cl, however, freely diffuses within cell membranes. Confocal imaging of HEK cells loaded with SPOT2.1.Cl show minimal fluorescence prior to photoactivation, as before (Figure 1-6a). Photoactivation of one half of a HEK cell (yellow area, Figure 1-6a) delivered a prompt increase in VF2.1.Cl fluorescence in the illuminated half of the cell (Figure 1-6b). After 10 minutes, the rest of the cell "fills" with dye, as photoactivated SPOT2.1.Cl diffuses laterally through the plasma membrane (Figure 1-6c). The neighboring cell (Figure 1-6d) remains darker (Figure1-6b and c), and shows minimal fluorescence increase. Directly uncaged regions increase fluorescence by 520% (±60%) while neighboring regions increase fluorescence by only 40% (±17%, SEM for n = 4 experiments, Figure 1-7). Diffusion of SPOT away from the uncaging site in confluent monolayers is minimal (Figure 1-8), and VF2.1.Cl behaves nearly identically to the canonical lipophilic tracer dye, DiO, in FRAP experiments in confluent monolayers of HEK cells (Figure 1-9). Taken together, these experiments establish that uncaged SPOT diffuses rapidly within cells, but much more slowly across plasma membranes, in a manner similar to DiO.

Following illumination, cells stained with SPOT2.1.Cl become bright and voltage-sensitive. Whole-cell patch clamp electrophysiological measurements in HEK cells reveal that post-illumination, activated SPOT2.1.Cl has a voltage sensitivity of 17% ΔF/F per 100 mV (Figure 1-2b and Figure 1-10d), approximately 77% of the sensitivity achieved by the parent VF2.1.Cl under similar recording conditions (Figure 1-10d and e). This decrease in voltage sensitivity may arise from improper membrane orientation of SPOT prior to uncaging[17–19] or photochemically-initiated side reactions not observed *in vitro*, and experiments are underway to determine the genesis of this effect. The small decrease in voltage sensitivity does not prevent optical recording of physiologically relevant voltage changes. Whole-field uncaging of cultured neurons loaded with SPOT, followed by field stimulation, demonstrated that activated SPOT can optically record action potentials in single trials (Figure 1-11). Photolysis of SPOT is well-tolerated by both HEK cells and neurons, as judged by analysis of MTT viability assays (Figure 1-12) and electrophysiological parameters of HEK cells treated with SPOT2.1.Cl+UV light (Figure 1-13a-e). Neurons loaded with either SPOT2.1.Cl+UV or VF2.1.Cl show no difference in action potential duration (Figure 1-13f).

We envisioned that SPOT2.1.Cl could find utility in complex neuronal contexts wherein optically orthogonal fluorescent proteins targeted to genetic subsets of neurons guide spatially-resolved photoactivation of SPOT2.1.Cl and enable sparse labeling and optical recording in neurons. We cultured rat hippocampal neurons (E18) for 14 days *in vitro* (DIV) and transfected them with mCherry localized to the inner leaflet of the cell membrane via a CAAX-mediated farnesylation sequence.[37] A small percentage of neurons displayed good expression of farnesylated mCherry (Figure 1-14a and b). These neurons were targeted for uncaging by restricting the uncaging region to a <20 μm diameter photoactivation spot centered within the soma defined by

mCherry fluorescence (Figure 1-14b and d). Photoactivation yielded bright membrane-localized fluorescence (Figure 1-14c, e, and f). Photoactivated SPOT in neurons reports on action potentials evoked by field stimulation (Figure 1-14g) with a response of 9% ΔF/F per action potential (±0.2%, *n*=29 APs from 3 cells) and a SNR of 14±4 to 1 (*n*=29 APs from 3 cells).

Precise identification of neuronal pathways and function are critical for dissecting connectivity and information processing in the brain. Current neuronal tracing methods rely on diffusion of lipophilic carbocyanine fluorescent tracers[38] and typically require invasive local delivery of dye via pipette. These tracers, while providing a structural description of neuronal projections, cannot report on the activity of labeled neurons. We envisioned that SPOT, as a voltage-sensitive dye that diffuses within membranes, could be exploited to map local circuitry. By uncaging SPOT in cellular processes and allowing diffusion of the dye to the soma, cells which were "wired" into the photoactivated region would become bright, allowing imaging of neuronal activity in the labelled cells.

To explore this, we first ascertained the ability of photoactivated SPOT to diffuse within neuronal membranes. Indeed, neurons loaded with SPOT and uncaged in the soma showed substantial diffusion of activated SPOT away from the soma into distal processes when the neurons were maintained at 37 °C (Figures 1-5 and 1-16). We then loaded cultured hippocampal neurons expressing cell membrane-localized mCherry (Figure 1-17a and b) with SPOT and photoactivated a region (Figure 1-17c, yellow circle) lacking cells bodies, but containing numerous processes, including those of an mCherry-positive cell. Following uncaging, we maintained the neurons at 37 °C to allow activated SPOT to diffuse back into cell bodies that projected processes into the uncaging region. After 30 minutes, several cell bodies were highlighted (Figure 1-17e), including the mCherry-positive cell, indicating that SPOT can be used to map local connectivity in living neurons. Upon field stimulation, uncaged SPOT clearly distinguishes action potentials in single trials from neurons labeled by retrograde tracing (Figure 1-17g and h), demonstrating that SPOT methodology can be used to report both structural and functional connectivity and dynamics within local circuits, which cannot be achieved with VF or lipophilic tracer dyes in isolation.

Concluding Remarks

In summary, we present the design, synthesis, and biological evaluation of the first member of a new class of voltage sensitive dyes—SPOTs, small photoactivatable optical sensors of trans-membrane potential. In particular, SPOT2.1.Cl, based on the VoltageFluor2.1.Cl scaffold, exhibits a large fluorescence dynamic range following near-UV photoactivation, good voltage sensitivity, staining defined by spatially-restricted illumination, and enables functional imaging of genetically specified neurons through an optically orthogonal marker—either through direct photoactivation of cells of interest, or via "back-filling" in which neuronal processes are uncaged to provide labeling in cell bodies. Current efforts are underway in our lab to apply SPOT2.1.Cl to brain tissue, as well as to explore new photocaging scaffolds with increased two-photon uncaging cross-section, improved water solubility, and enhanced targeting and retention in membranes.

Materials and Methods

General Synthetic and Analytical Methods

$Pd(OAc)_2$ was purchased from Strem Chemicals. 4,5-Dimethoxy-2-nitrobenzyl bromide was purchased from Acros Organics. All other chemicals were purchased from Sigma-Aldrich and used as received. Anhydrous solvents and reagents (DMF, Et_3N) were obtained as SureSeal bottles from Sigma-Aldrich. (E)-N,N-dimethyl-4-(4-vinylstyryl)aniline **1** and 2',7'-dichloro-5-iodosulfofluorescein **2** were synthesized according to literature procedures.[17,39]

UV absorbance and fluorescence spectra were recorded on a Shimadzu 2501 Spectrophotometer (Shimadzu) or a Quantamaster Master 4 L-format scanning spectrofluorometer (Photon Technologies International) equipped with an LPS-220B 75-W xenon lamp and power supply, A-1010B lamp housing with integrated igniter, switchable 814 photon-counting/analog photomultiplier detection unit, and MD5020 motor driver. Samples for absorption and fluorescence measurements were contained in 1-cm pathlength quartz cuvettes (Starna Cells). 1H NMR spectra were collected in d_6-DMSO (Cambridge Isotope Laboratories, Cambridge, MA) at 25 °C on a Bruker AV-600 spectrometer at the College of Chemistry NMR Facility at the University of California, Berkeley. All chemical shifts are reported in the standard δ notation of parts per million using the peak of residual proton signals of d_6-DMSO as an internal reference. Low resolution LC/ESI-MS was performed on an Advion Expression LC-MS coupled to an Agilent Infinity 1220 HPLC. Semi-preparative HPLC was performed on the same Agilent system. Luna C18(2) (Phenomenex) columns were employed for both analytical and semi-preparative separations, using water (solvent A) and acetonitrile (solvent B) with 0.05% TFA as an additive. High resolution mass spectra (HR-ESI-MS) were acquired at the QB3/Chemistry Mass Spectrometry Facility at the University of California, Berkeley.

Quantum yield of photolysis and characterization of photolysis products

The quantum yield of photolysis Φ of SPOT2.1.Cl was estimated by irradiating a 2 μM solution of SPOT2.1.Cl in PBS pH 7 + 0.01% Triton X-100 in a quartz cuvette with 365 nm light delivered from a 4W UVGL-25 (UVP) mercury lamp. At 535 nm VF2.1.Cl has an appreciable extinction coefficient, while the absorbance of SPOT2.1.CL is negligible. This permitted the determination of the relative concentrations of SPOT2.1.CL and VF2.1.Cl by reference to the absorbance at 535 nm of a 2 μM solution of pure VF2.1.Cl. Measurements were taken after irradiation for 2.5, 5, 10, 15, 20 and 25 minutes. The linear fit of $-\log\left(\frac{C}{C_0}\right)$ as a function of time *t* allows the determination of Φ according to the equation $\Phi = \frac{-\log\left(\frac{C}{C_0}\right)}{I\sigma t}$ where C is the concentration of SPOT2.1.CL at time *t*, C_0 is the initial concentration of SPOT2.1.CL, *I* is the irradiation intensity measured using ferrioxolate actinometry[40] and σ is the decadic extinction coefficient of SPOT2.1.Cl at 365 nm (10^3 times ε_{365}).[41,42] *I* was determined to be 3.44 x 10^{-9} $Ecm^{-2}s^{-1}$ and ϵ_{365} to be 3.35 x 10^4 $M^{-1}cm^{-1}$. σ has units cm^2mol^{-1}.

Photolysis products were identified by irradiating a 100 μM solution of SPOT2.1.Cl in PBS pH 7 +0.01% Triton X-100 for 20 minutes and analyzing an aliquot by analytical HPLC. Comparison to standards of pure SPOT2.1.Cl and VF2.1.Cl revealed highly selective conversion of SPOT2.1.Cl to VF2.1.Cl (Figure 1-3).

Cell culture, transfection, and dye loading

All animal procedures were approved by the UC Berkeley Animal Care and Use Committees and conformed to the NIH Guide for the Care and Use and Laboratory Animals and the Public Health Service (PHS) Policy.

Hippocampi were dissected from embryonic day 18 Sprague Dawley rats (Charles River Laboratory) in cold sterile HBSS (zero Ca^{2+}, zero Mg^{2+}). All dissection products were supplied by Invitrogen, unless otherwise stated. Hippocampal tissue was treated with trypsin (2.5%) for 15 min at 37 °C. The tissue was triturated using fire polished Pasteur pipettes, in minimum essential media (MEM) supplemented with 5% fetal bovine serum (FBS; Thermo Scientific), 2% B-27, 2% 1M D-glucose (Fisher Scientific) and 1% glutamax. The dissociated cells were plated onto 12 mm diameter coverslips (Fisher Scientific) pre-treated with poly-D-lysine (PDL; 1 mg/ml; Sigma-Aldrich) at a density of 45,000 cells per coverslip in MEM supplemented media (as above). Neurons were maintained at 37 °C in a humidified incubator with 5 % CO_2. At 3 days *in vitro* (DIV) half of the MEM supplemented media was removed and replaced with Neurobasal media containing 2% B-27 supplement and 1% glutamax. For experiments requiring the expression of a red fluorescent protein, dissociated neurons were sparsely transfected at 7 DIV with a plasmid containing mCherry-CAAX under the control of the CMV promoter using Lipofectamine 3000 (Life Technologies).

Human embryonic Kidney (HEK) cells were passaged and plated onto glass coverslips pre-coated with PDL (as above) to provide a confluency of ~15-50% for imaging. HEK cells were plated and maintained in Dulbecco's modified eagle medium (DMEM) supplemented with 4.5 g/L D-glucose, 10% FBS and 1% Glutamax.

For imaging in both HEK cells and neurons, SPOT was prepared as a 500 nM solution in HBSS with 0.01% Pluronic F-127 as an additive. Cells were incubated for 15-20 minutes at 37 °C and washed 3x with HBSS. For "optical backfilling" experiments SPOT was loaded at 2.5 µM.

For imaging cells were bathed in HBSS or, for extracellular field stimulation, with HBS (140 mM NaCl, 2.5 mM KCl, 10 mM HEPES, 10 mM D-glucose 1.3 mM MgCl2 and 2 mM CaCl2; pH 7.3 and 290 mOsmol)) supplemented with 10 µM 2,3-Dioxo-6-nitro-1,2,3,4-tetrahydrobenzo[f]quinoxaline-7-sulfonamide (NBQX; Santa Cruz Biotechnology) and 25 µM DL-2-Amino-5-phosphonopentanoic acid (APV; Sigma-Aldrich).

Epifluorescence microscopy

Epifluorescence images were acquired on an AxioExaminer Z-1 (Zeiss) equipped with a Spectra-X light engine LED light (Lumencor), all controlled with Slidebook (v6, Intelligent Imaging Innovations).

For quantification of uncaging and electrophysiology, images were acquired with a W-Plan-Apo 20x/1.0 objective (Zeiss) and focused onto either an OracFlash4.0 sCMOS camera (Hamamatsu) or Evolve 128 emCCD camera (Photometrix), respectively. Extracellular field stimulation recording images were acquired with a W-Plan-Apo 63x/1.0 water objective and Evolve 128 camera.

Uncaging was performed with 390 nm light (LED, 20 nm bandpass, 9.7W/cm2, 20x). At 20X magnification, image intensity begins to plateau at 20 s irradiation, reaching a maximum after 30 s, after which bleaching causes a net loss of signal intensity. At 63x magnification, 10 s (22.3 W/cm2) illumination is sufficient for uncaging.

For quantification of uncaging, excitation light was delivered at 542 nM (LED, 542nm, 33 nm bandpass). Emission was collected with a quadruple emission filter (430/32 nm, 508/14 nm, 586/30 nm, 708/98 nm) after passing through a quadruple dichroic mirror (432/38 nm, 509/22 nm, 586/40 nm, 654 nm LP). For electrophysiology and extracellular field stimulation excitation was delivered at 475 nM (LED, 475 nm, 34 nm bandpass). Emission was collected with a 540/50 nm bandpass filter after passing through a 510 nm longpass dichroic. 475 nm excitation maximizes net signal intensity, while fold-increase in brightness is greater with 542 nm due to better spectral separation between uncaged SPOT2.1.Cl and VF2.1.Cl. 514 nm excitation provides an excellent compromise between these two properties when imaging with a confocal microscope (See LSCM section).

For single neuron uncaging and "optical backfilling" experiments a field iris diaphragm in line with the LED light source was employed to spatially restrict the field of illumination. Under 63X magnification it was possible to uncage SPOT in a region with a < 20 µm diameter. The field diaphragm did not appear to affect the light intensity delivered within the field of illumination. When imaging single cells, field stimulation recordings (see below) were performed immediately after uncaging. When performing backfilling experiments a given region was uncaged and the imaging chamber returned to the incubator for 30 minutes. The mCherry marker permitted identification of the target region post-incubation.

Electrophysiology

Electrophysiological recordings of HEK293 cells were performed with an Axopatch 200B amplifier (Molecular Devices) at room temperature. The signals were digitized with Digidata 1332A and recorded with pCLAMP 9 software (Molecular Devices) on a PC. The intracellular solution contained (in mM) 115 potassium gluconate, 10 BAPTA tetrapotassium salt, 10 HEPES, 5 NaCl, 10 KCl, 2 ATP disodium salt, 0.3 GTP trisodium salt (pH 7.25, 275 mOsm).

Extracellular field stimulation

Extracellular field stimulation was delivered by Grass Stimulator connected to a recording chamber containing two platinum electrodes (Warner), with triggering provided through the same Digidata 1332A digitizer and pCLAMP 9 software (Molecular Devices) that ran the electrophysiology. 1 ms 80 V field potentials were delivered at 5 Hz.

Line scanning confocal microscopy

Confocal images were acquired with a Zeiss LSM710 microscope at the Molecular Imaging Center, University of California, Berkeley. Plan-Apochromat 40x/1.4 oil and 63x/1.4 oil objectives (Zeiss) were employed. Uncaging was performed with 405 nm laser diode light. For imaging SPOT2.1.Cl, excitation light was delivered at 514 nm by an argon laser. Emission was collected at 465-595 nm after passing through a MBS 458/514/594 dichroic. For imaging mCherry, excitation light was delivered at 594 nm by a helium-neon laser. Emission was collected at 594-730 nm after passing through a MBS 458/514/594 dichroic.

514 nm excitation falls quite close to the λ_{max} of VF2.1.Cl (522 nm) while still providing excellent spectral separation from uncaged SPOT2.1.Cl, excitation at 514 nm allows for both a very high fold-increase fluorescence after uncaging as well as maximizing total signal intensity. This is in contrast to epifluorescence microscopy, where a trade-off must be made between maximizing signal intensity (475 nm excitation) and maximizing fold-increase in fluorescence

(542 nm excitation). During SPOT diffusion experiments cultured neurons were maintained at 37 °C and 5% CO2 using a stage top incubator.

Data analysis

For voltage sensitivity and image intensity measurements, regions of interest were drawn around cells or neuronal processes and the mean fluorescence measured in ImageJ. For HEK cells, background fluorescence was subtracted by measuring the fluorescence where no cells grew. For experiments in neurons, both in epifluorescence and confocal microscopy, the background fluorescence was not subtracted. For field-stimulated neurons, a mean background value was subtracted from the ROI value for cellular fluorescence, and minor bleaching was corrected. In voltage clamp electrophysiology experiments, ΔF/F was calculated by dividing the fluorescence signal during a voltage step by the average fluorescence for a baseline of 15 frames prior to stimulation and 15 frames post stimulation.

Cell Viability/MTT Assay

HEK293T cells were seeded in 24 well plates at a density of 150K cells per well and allowed to grow for 36 hours under cell culture conditions described above. Cells were treated with either 1) 0.01% Pluronic-F127 2) 500 nM SPOT2.1.Cl with 0.01% Pluronic-F127 or 3) 500 nM VF2.1.Cl with 0.01% Pluronic F-127 and incubated for 20 minutes at 37 °C and 5% CO2. The final concentration of DMSO was 0.01% for all three conditions. Following incubation the media was aspirated and replaced with fresh HBSS. Experimental wells were irradiated for 5 minutes with 365 nm UV light delivered from a 4W UVGL-25 (UVP) mercury lamp. Cell viability was assessed using Cayman Chemical's MTT cell proliferation assay kit and performed according to the manufacturer's protocol. Absorbance at 570 nm was measured using a Molecular Devices SpectraMax Paradigm Multi-Mode detection platform plate reader.

Synthesis of

2-(2,7-dichloro-6-hydroxy-3-oxo-3H-xanthen-9-yl)-5-((E)-4-((E)-4-(dimethylamino)styryl)styryl)benzenesulfonic acid (VF2.1.Cl)

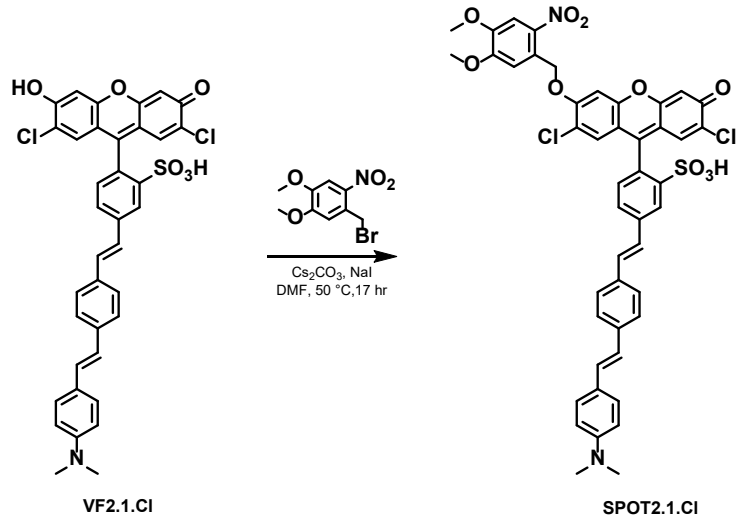

VF2.1.Cl was synthesized using a modification of the existing procedure.1 An oven-dried Schlenk flask was charged with a stir bar, 1 (111 mg, 0.442 mmol, 1 equiv.), 2 (226 mg, 0.398 mmol, 0.9 equiv.), Pd(OAc)2 (5 mg, 0.02 mmol, 0.05 equiv.), and P(o-Tol)3 (7 mg, 0.02 mmol, 0.05 equiv.). The reaction vessel was purged and backfilled with N2 three times. Solid reagents were taken up in DMF (2.0 mL) and Et3N (0.5 mL) and allowed to sir for 14 hours at 110 °C, after which the reaction was found to have gone to completion by LC-MS. The reaction was allowed to cool to room temperature, then diluted with DCM and MeOH and neutralized with 0.5 mL AcOH. The resulting solution was filtered through Celite and concentrated under reduced pressure. The crude paste was dissolved in 20 mL DCM, and precipitation induced by addition of 30 mL hexanes. The precipitate was collected by vacuum filtration and washed with Et2O. The filtrate was collected, concentrated under reduced pressure and the precipitation procedure repeated to recover additional material. A total of 164 mg (62%) of product was obtained as a brick-red powder. Characterization data was consistent with previously reported values.[17]

Synthesis of

2-(2,7-dichloro-6-((4,5-dimethoxy-2-nitrobenzyl)oxy)-3-oxo-3H-xanthen-9-yl)-5-((E)-4-((E)-4-(dimethylamino)styryl)styryl)benzenesulfonic acid (SPOT2.1.Cl)

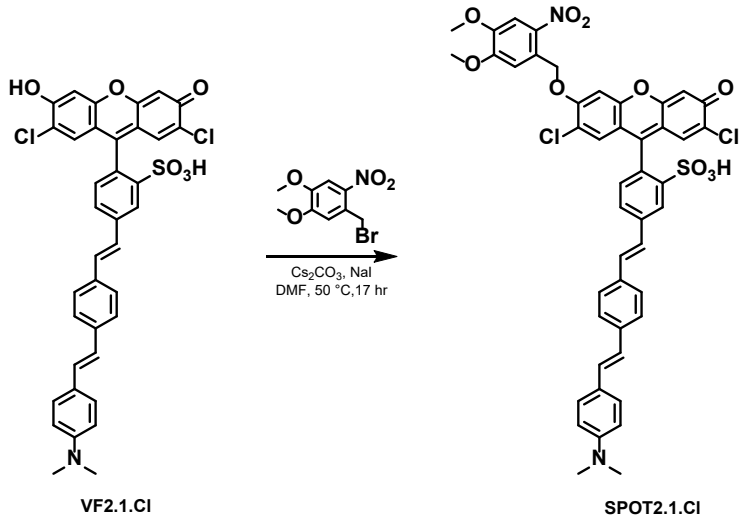

To a 20 mL vial equipped with a stir bar were added VF2.1.Cl (40 mg, 0.058 mmol, 1.0 equiv.), 4,5-Dimethoxy-2-nitrobenzyl bromide (38 mg, 0.12 mmol, 2 equiv.), cesium carbonate (42 mg, 0.13 mmol, 2.2 equiv.) and sodium iodide (1 mg, 0.006 mmol, 0.1 equiv.). Solid reagents were taken up in 1 mL of dry DMF and the reaction was stirred for 17 hours at 50 °C, after which time the reaction was found to have gone to completion by LC-MS. Solvent was removed under vacuum, and the resulting crude paste was suspended in water, acidified with AcOH and filtered. The collected precipitate was washed with water, 1:1 DCM:hexanes and Et2O to obtain SPOT2.1.Cl as a brick-red powder (49 mg, 94%). Material for characterisation and biological experiments was further purified by semi-preparative HPLC. HR-ESI-MS [M-H]- calculated 877.1395, found 877.1394. 1H NMR (600 MHz, d6-DMSO) δ: 8.17 (1H, d, J = 1.74); 7.79 (1H, dd, J1 = 8.01, J2 = 1.77); 7.75 (1H, s); 7.66 (2H, d, J = 8.04); 7.61 (1H, s); 7.57 (2H, d, J = 8.10); 7.48 (2H, d, J = 8.28); 7.44 (1H, d, J = 16.5); 7.42 (1H, s); 7.39 (1H, d, J = 16.4); 7.27 (1H, d, J = 7.8); 7.20 (1H, d, J = 16.3); 7.07 (1H, s); 7.03 (1H, d, J = 16.3); 7.00 (1H, s); 6.82 (2H, br); 6.43 (1H, s); 5.71 (2H, s); 3.88 (3H, s); 3.88 (3H, s); 2.96 (6H, s).

Scheme 1-1

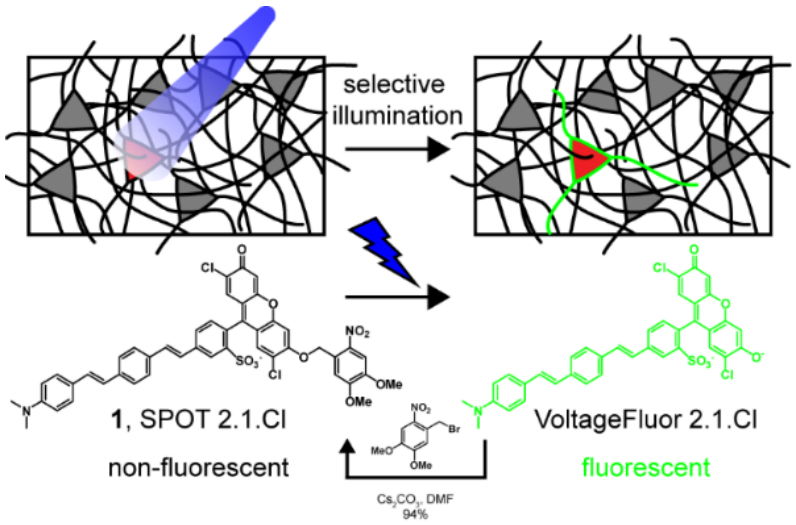
selective
illumination
1, SPOT 2.1.Cl
non-fluorescent
VoltageFluor 2.1.Cl
fluorescent
Cs2CO3, DMF
94%

Figure 1-1

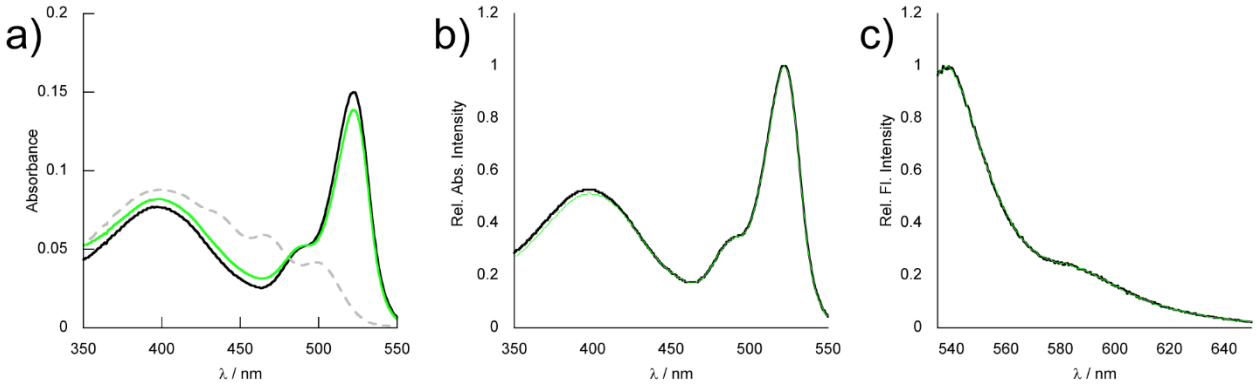

Spectroscopic characterization of SPOT2.1.Cl and VF2.1.Cl in PBS, pH 7.4. a) Absorbance profile of SPOT2.1.Cl before (grey dotted trace) and after (green trace) illumination at 365 nm. The UV-vis spectrum of photoactivated SPOT2.1.Cl is identical to a known standard of VF2.1.Cl (black trace). b) Absorbance profile of VF2.1.Cl before (black trace) and after (green trace) illumination at 365 nm as in panel (a). Emission spectrum of VF2.1.Cl before (black trace) and after (green trace) illumination at 365 nm as in panels (a) and (b). λ_{ex} is at 520 nm.

Figure 1-2

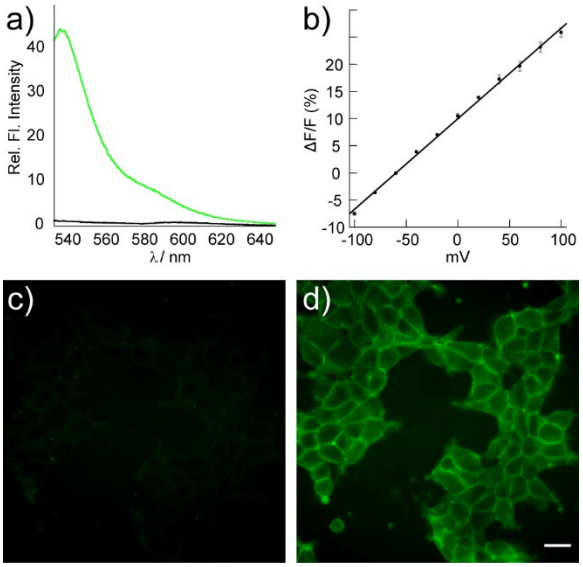

Characterization of SPOT2.1.Cl. a) Emission spectra of SPOT2.1.Cl in PBS, pH 7.4, before (black trace) and after (green trace) illumination at 365 nm (λ_{ex}=522 nm). b) Plot of ΔF/F vs mV for SPOT2.1.Cl after photoactivation in HEK cells. Error bars are ±S.E.M. for $n \geq 3$ experiments. c) HEK cells loaded with 500 nM SPOT2.1.Cl prior to illumination. d) Cells from panel (c) after illumination with 390 nm light for 30 seconds. Scale bar is 20 μm.

Figure 1-3

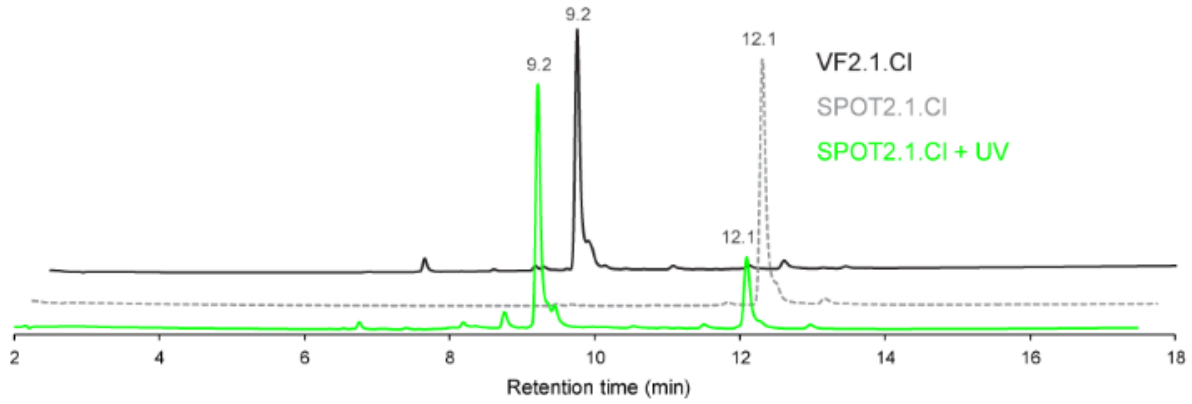

Photoactivation of SPOT2.1.Cl generates VF2.1.Cl *in vitro*. HPLC traces of SPOT2.1.Cl in PBS, pH 7.4, before (grey dotted trace) and after (green trace) illumination at 365 nm, indicating that the major photoproduct of SPOT2.1.Cl illumination is VF2.1.Cl. A standard of VF2.1.Cl is provided as a reference (black trace). Retention times are indicated above each peak.

Figure 1-4

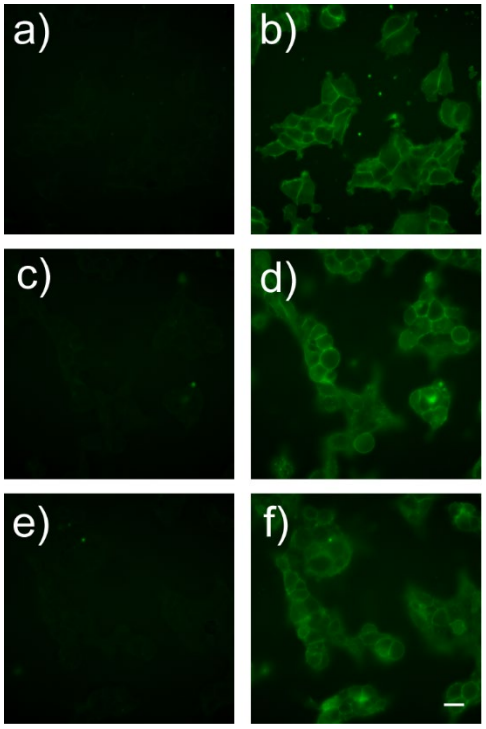

Sequential photoactivation of SPOT2.1.Cl in HEK cells. Three separate regions on the same coverslip were photoactivated with 390 nm light. Prior to uncaging, cells display negligible fluorescence (Panels a, c, e). After uncaging, cells show bright, membrane-localized fluorescence (Panels b, d, f). Scale bar is 20 μm.

Figure 1-5

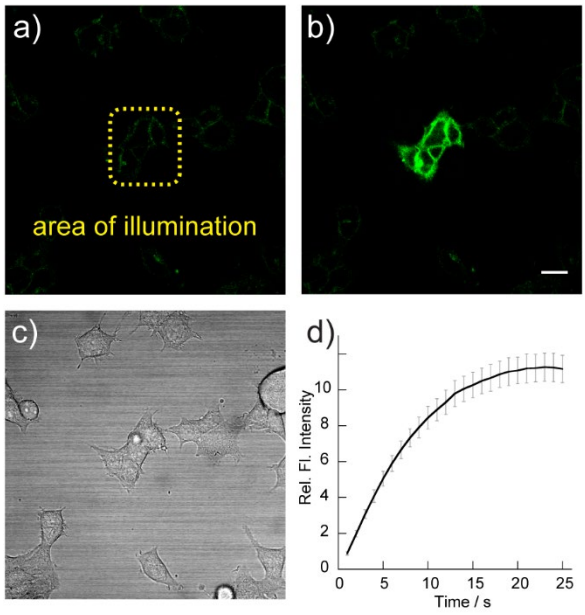

Photoactivation of SPOT2.1.Cl within defined regions using laser scanning confocal microscopy. a) Confocal fluorescence image of HEK cells loaded with 500 nM SPOT2.1.Cl prior to uncaging with 405 nm laser light. Photoactivation area is indicated in yellow. b) Cells from a) after photoactivation (25 x 1 s illuminations). c) Transmitted light image of cell from previous panels. d) Quantification of photoactivation of SPOT2.1.Cl. Relative fluorescence intensity vs. time is plotted. Error bars are ±S.E.M. for $n \geq 5$ experiments. Scale bar is 20 μm.

Figure 1-6

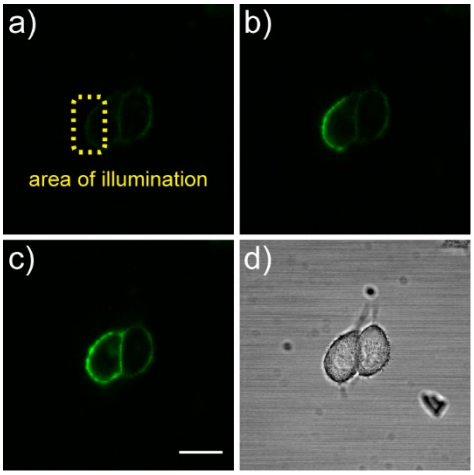

Photoactivation of SPOT2.1.Cl within a single cell. HEK cells loaded with 500 nM SPOT2.1.Cl a) prior to and b) immediately after uncaging in an area over the left side of the cell, as indicated by the yellow region of interest in panel (a). Initially, fluorescence fills only the uncaged portion of the cell (b), but after 10 min, c) the entire cell membrane appears fluorescent, while the neighboring cell remains dim. d) Transmitted light image of cells in previous panels. Scale bar is 20 μm.

Figure 1-7

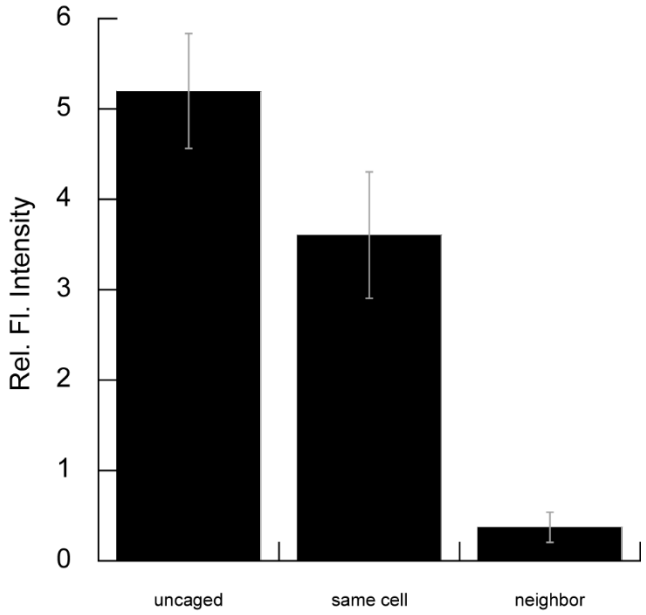

Quantification of SPOT diffusion across membranes from Figure 1-6. Values represent the relative fluorescence intensity increase 15 minutes (37 °C) after uncaging in three different regions: the directly uncaged half-cell, the un-illuminated half of the same cell, and a connected cell. Error bars are SEM for 4 separate experiments.

Figure 1-8

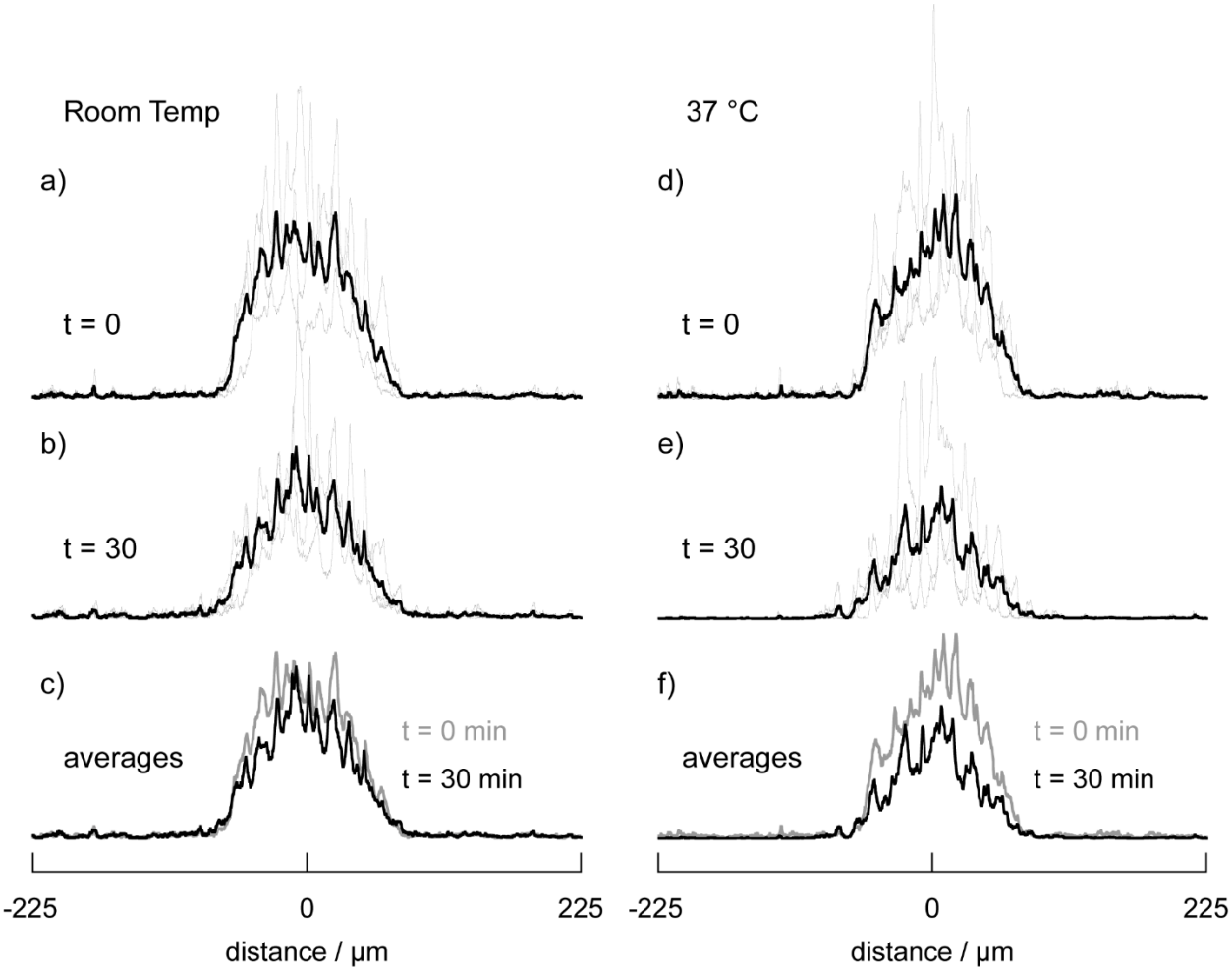

Analysis of SPOT diffusion in confluent cell monolayers following uncaging. Confluent monolayers of HEK cells loaded with SPOT2.1.Cl were photoactivated over a ~150 µm diameter circle. An intensity profile (5 µm wide) through the photoactivation region was tracked immediately (a,d) after photoactivation (t = 0) and after 30 minutes (b,e) at the indicated temperature (RT, a,b; 37 °C, d,e). Individual trials (3 separate experiments for each condition) in panels (a,b,d), and (e) are shown in grey and averages are in black. In panels (c) and (f), the averages at t = 0 (grey) and t = 30 (black) are overlaid for comparison.

Figure 1-9

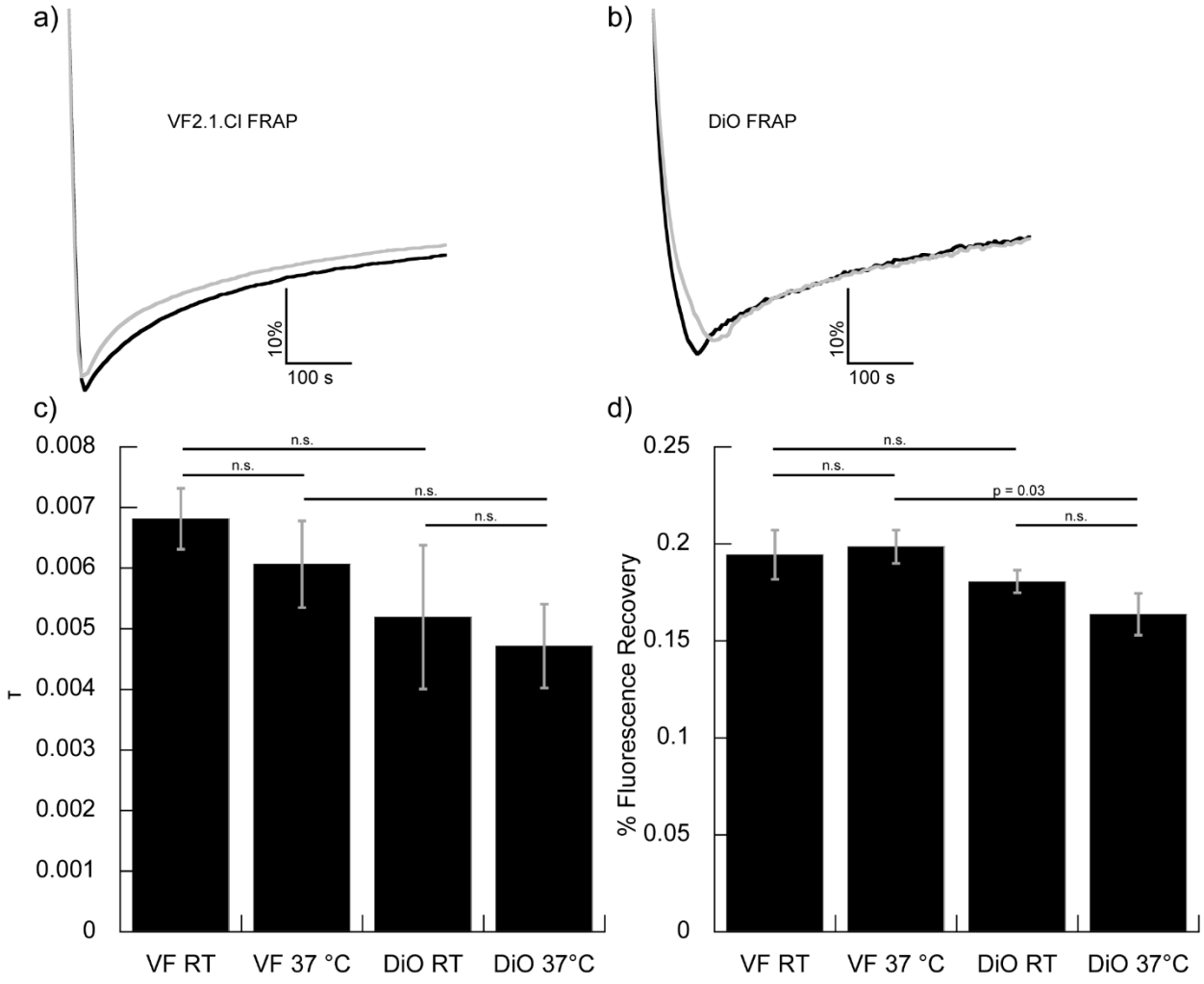

Fluorescence Recovery After Photobleaching (FRAP) comparison between VF2.1.Cl and DiO. FRAP traces of a) VF2.1.Cl at ambient, room temperature (black trace) and 37 °C (grey trace) and b) DiO at ambient, room temperature (black trace) and 37 °C (grey trace). Traces are averaged over all experiments. The fluorescence recovery was fitted to the expression $1\text{-}e^{-\tau t}$ in Kaleidagraph. Fractional recovery was calculated by subtracting the endpoint fluorescence recovery from the lowest point on the curve. c) The fitted rise time (τ) and d) fraction of fluorescence recovery for each dye at both room temperature and 37 °C. Average values are reported; error bars are SEM for n = 7, 9, 5, and 6 for VF RT, VF 37 °C, DiO RT, and DiO 37 °C, respectively. Only one condition, fractional recovery of fluorescence at 37 °C showed any significant difference (p = 0.03). All other comparisons had p values larger than 0.16 (two-tailed T-test).

Figure 1-10

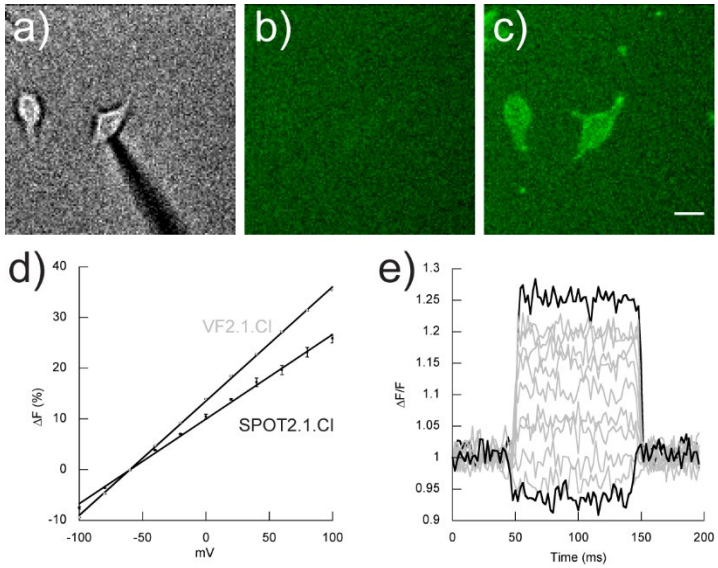

Voltage sensitivity of activated SPOT2.1.Cl. a) DIC image of HEK cell under whole-cell patch configuration. b) widefield epifluorescence image of HEK cell in panel (a), loaded with 500 nM SPOT2.1.Cl, prior to photoactivation. c) Cells in panel (b), after photoactivation. d) Fractional change in fluorescence (ΔF/F) vs. membrane potential. The HEK cell in panels a-c was subjected to depolarizing and hyperpolarizing potentials (±100 mV), starting from -60 mV, and the relative change in fluorescence was plotted. SPOT2.1.Cl shows a 16.7±0.6% ΔF/F per 100 mV, while VF2.1.Cl, under identical conditions, shows 22.5±0.04%. Error bars are ±S.E.M. for $n \geq 3$ experiments. e) Changes in fluorescence from photoactivated SPOT2.1.Cl cells vs. membrane potential in a HEK cell under voltage-clamp conditions. The cell was held at -60 mV and subsequently subjected to 20 ms depolarizing steps to the indicated potential. Panel (e) represents data used to construct panel (d).

Figure 1-11

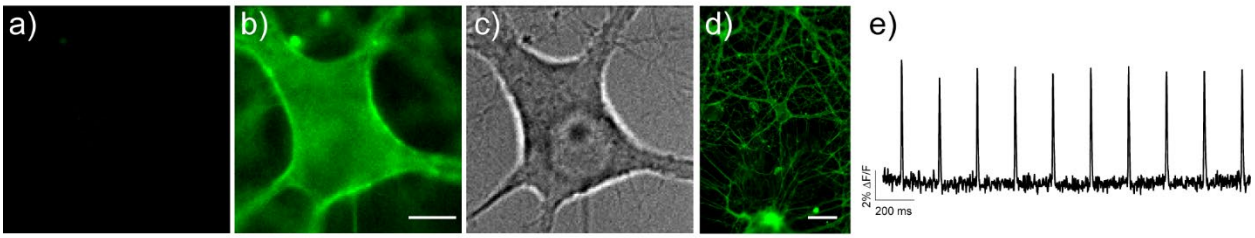

Voltage sensing in neurons with activated SPOT2.1.Cl. Rat hippocampal neurons were stained with 500 nM SPOT2.1.Cl. a) Widefield epifluorescence image of neurons stained with SPOTl2.1.Cl, prior to photoactivation with light. b) Widefield epifluorescence image of cell in panel (b), after photoactivation with light. c) DIC images of neurons stained with SPOT2.1.Cl. Panels (a)-(c) are at 63x magnification. d) Demagnified image of cells in panels (a)-(c) (20x), indicating the area of photoactivation. The optically recorded neuron is located in the center of the field. e) Plot of ΔF/F vs. time (ms) for the neuron in panel (b). Action potentials evoked by field stimulation of neurons at 5 Hz and recorded optically at 500 Hz. Scale bar is 10 μm for (a), (b), and (c), and 40 μm for (d).

Figure 1-12

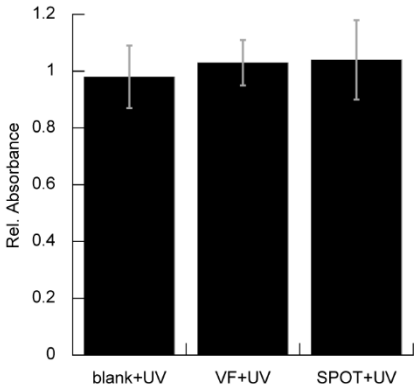

Viability of HEK cells treated with VF2.1.Cl or SPOT2.1.Cl and UV light and analyzed by MTT assay. Cells were loaded with 500 nM VF2.1.Cl, SPOT2.1.Cl or DMSO and Pluronic F127 alone and then irradiated for 5 minutes. Following this treatment, cells were incubated with MTT and analyzed as described in the supporting information. The absorbance was normalized to VF2.1.Cl + UV treated cells; higher absorbance indicates higher cellular viability. Error bars represent S.E.M. for $n = 6$ independent experiments. Differences are not statistically significant (two-tailed T-test, $p > 0.53$ for all comparisons).

Figure 1-13

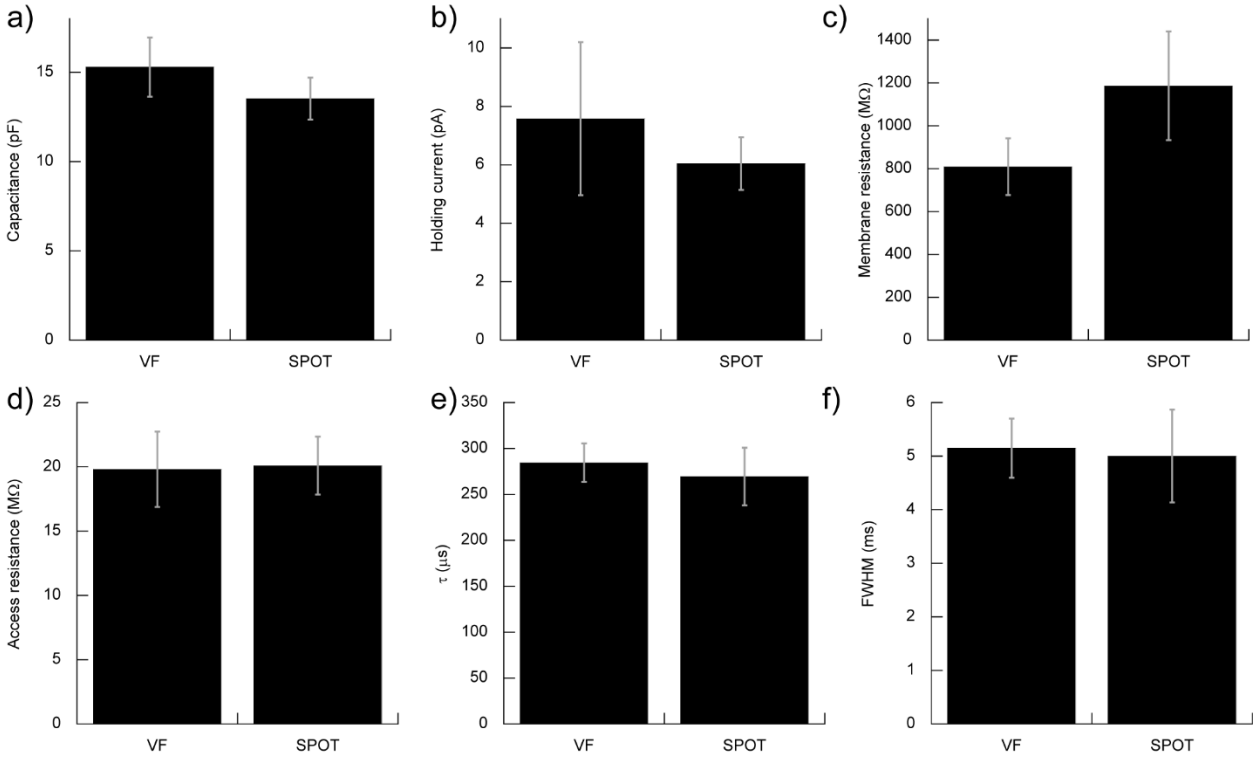

Comparison of cellular parameters in HEK cells or neurons loaded with VF2.1.Cl or SPOT2.1.Cl. a-e) Comparison of electrophysiological parameters associated with HEK cells loaded with VF2.1.Cl or SPOT2.1.Cl + UV photoactivation. Each value represents the average of at least 9 independent cells. a) Cell capacitance, b) holding current, c) membrane resistance, d) access resistance, and e) τ for membrane charging. f) Action potential duration in neurons loaded with VF2.1.Cl or SPOT+UV photoactivation. Neurons were stimulated with an extracellular field stimulator at a rate of 5 Hz and optically recorded at 500 Hz (see Figure 1-14 for examples). The full width at half-maximum values for evoked action potentials were measured from the optical response of either VF or SPOT. Data in panel f represent data from $n = 3$ cells for each, with each cell representing the average of 10 action potentials (30 APs, 3 cells each). For all cases, $p > 0.25$ (two-tailed t-test), indicating non-significant differences.

Figure 1-14

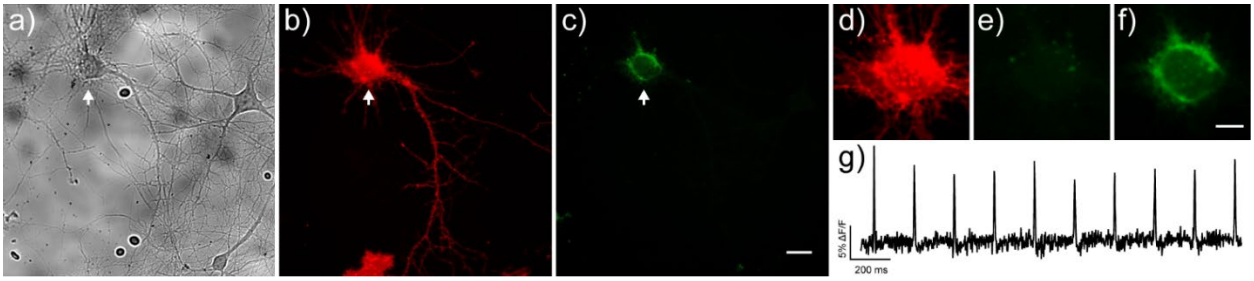

SPOT2.1.Cl uncaging in single neurons. Dissociated, cultured rat neurons (a) were transiently transfected with CAAX-mCherry for use as a fiducial marker for illumination. Panels (a) and (b) show DIC and mCherry fluorescence images, respectively. Cells were loaded with 500 nM SPOT2.1.Cl and then photoactivated (390 nm, 10 s, 22.3 W/cm2) over a region defined by the somatic staining of the mCherry signal (white arrow). (c) Following photoactivation, VF fluorescence appears to be membrane-localized. d-f) EMCCD image of indicated cell, showing mCherry fluorescence. VF dye fluorescence from the mCherry-positive neuron, e) prior to SPOT photoactivation and f) immediately after. g) Field stimulation of the SPOT-stained neuron at 5 Hz produced a train of optically recorded action potentials, which were captured in a single trial at 500 Hz with an EMCCD camera. Scale bars are 20 μm for panels a-c and 10 μm for panels d-f.

Figure 1-15

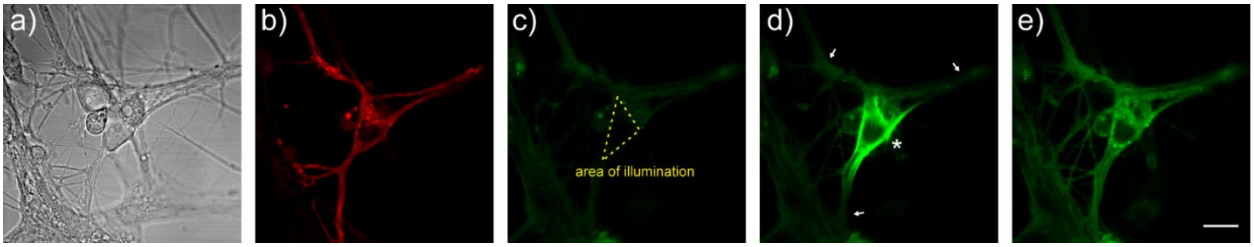

SPOT2.1.Cl uncaging in neurons. Dissociated, cultured rat neurons (a) were transiently transfected with CAAX-mCherry for use as a fiducial marker for illumination. Panels (a) and (b) show DIC and and mCherry fluorescence images, respectively. Cells were loaded with SPOT2.1.Cl and then photoactivated with 405 nm laser light over a region defined by the somatic staining of the mCherry signal. Prior to photoactivation, SPOT2.1.Cl is only weakly fluorescent, as shown in panel (c). Following photoactivation over the indicated area in panel (c), somatic fluorescence increases dramatically, as shown in panel (d). After a period of 15 min, fluorescence decreases at the soma (white star) and increases in distal processes (white arrows), as shown in panel (e). All SPOT2.1.Cl images were acquired and processed with identical settings. Scale bar = 20 μm.

Figure 1-16

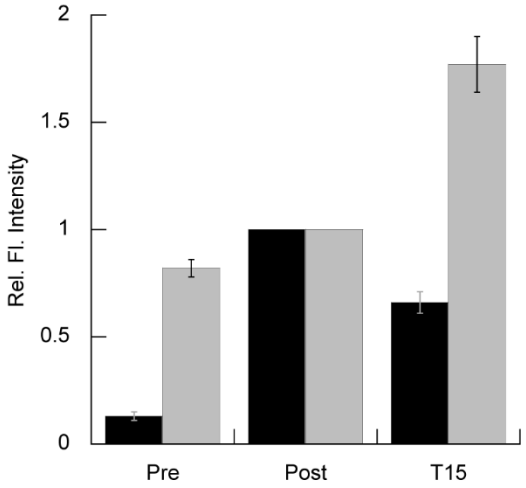

Quantification of SPOT2.1.Cl diffusion in neurons. Data represent regions of interest in the soma (black) or processes (grey) before, immediately and 15 minutes post uncaging with UV light. Relative values are normalized to fluorescence immediately following uncaging. Error bars are +/- SEM for $n \geq 4$ cells.

Figure 1-17

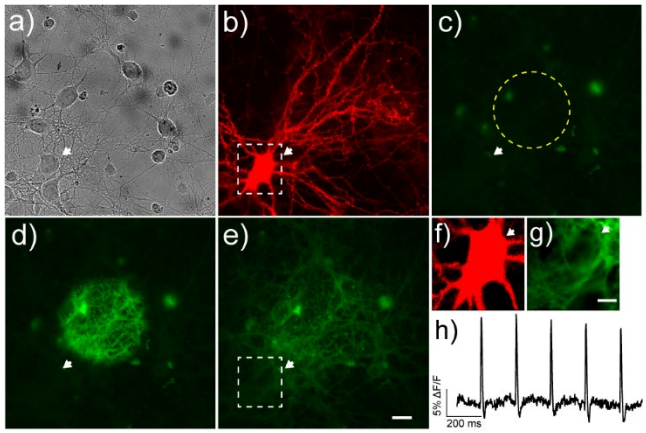

Voltage sensing in neurons identified by SPOT retrograde tracing. Neurons were stained with 2.5 μM SPOT2.1.Cl. a) DIC image of neurons stained with SPOT2.1.Cl. b) Widefield epifluorescence image of neurons in panel (a), demonstrating labeling with mCherry-CAAX. c) Green fluorescence image of same cells, prior to SPOT2.1.Cl photoactivation. Area of photoactivation is indicated by yellow dotted circle. d) Cells in panel (c) immediately after photoactivation. e) Diffusion of photoactivated SPOT2.1.Cl away from uncaging area after 30 min. at 37 °C. f) mCherry-positive neuron from panel (b) within the region in dotted white box. g) Image of SPOT-traced neuron used to generate functional imaging data, after photoactivation and diffusion. h) Action potentials evoked by field stimulation of neurons at 5 Hz and recorded optically in the indicated cell—white arrow—in a single trial at 500 Hz. Scale bar is 20 μm (a-e) and 10 μm (f and g).

References

(1) Alivisatos, A. P.; Chun, M.; Church, G. M.; Greenspan, R. J.; Roukes, M. L.; Yuste, R. *Neuron* **2012**, *74* (6), 970–974.

(2) Alivisatos, A. P.; Chun, M.; Church, G. M.; Deisseroth, K.; Donoghue, J. P.; Greenspan, R. J.; McEuen, P. L.; Roukes, M. L.; Sejnowski, T. J.; Weiss, P. S.; Yuste, R.; Alivisatos, A. P.; Andrews, A. M.; Weiss, P. S.; Koch, C.; Reid, R. C.; Lozano, A. M.; Hochberg, L. R. *Science* **2013**, *339* (6125), 1284–1285.

(3) Insel, T. R.; Landis, S. C.; Collins, F. S. *Science (80-.).* **2013**, *340* (6133), 687–688.

(4) Jin, L.; Han, Z.; Platisa, J.; Wooltorton, J. R. a; Cohen, L. B.; Pieribone, V. a. *Neuron* **2012**, *75* (5), 779–785.

(5) St-Pierre, F.; Marshall, J. D.; Yang, Y.; Gong, Y.; Schnitzer, M. J.; Lin, M. Z. *Nat. Neurosci.* **2014**, *17* (6), 884–889.

(6) Akemann, W.; Sasaki, M.; Mutoh, H.; Imamura, T.; Honkura, N.; Knöpfel, T. *Sci. Rep.* **2013**, *3*, 1–7.

(7) Hochbaum, D. R.; Zhao, Y.; Farhi, S. L.; Klapoetke, N.; Werley, C. a; Kapoor, V.; Zou, P.; Kralj, J. M.; Maclaurin, D.; Smedemark-Margulies, N.; Saulnier, J. L.; Boulting, G. L.; Straub, C.; Cho, Y. K.; Melkonian, M.; Wong, G. K.-S.; Harrison, D. J.; Murthy, V. N.; Sabatini, B. L.; Boyden, E. S.; Campbell, R. E.; Cohen, A. E. *Nat. Methods* **2014**, No. May.

(8) González, J. E.; Tsien, R. Y. *Biophys. J.* **1995**, *69* (4), 1272–1280.

(9) Yan, P.; Acker, C. D.; Zhou, W.-L.; Lee, P.; Bollensdorff, C.; Negrean, A.; Lotti, J.; Sacconi, L.; Antic, S. D.; Kohl, P.; Mansvelder, H. D.; Pavone, F. S.; Loew, L. M. *Proc. Natl. Acad. Sci.* **2012**, *109* (50), 20443–20448.

(10) Fink, A. E.; Bender, K. J.; Trussell, L. O.; Otis, T. S.; DiGregorio, D. A. *PLoS One* **2012**, *7* (8).

(11) Bradley, J.; Luo, R.; Otis, T. S.; DiGregorio, D. A. *J. Neurosci.* **2009**, *29* (29), 9197–9209.

(12) Fromherz, P.; Hübener, G.; Kuhn, B.; Hinner, M. J. *Eur. Biophys. J.* **2008**, *37* (4), 509–514.

(13) Fluhler, E.; Burnham, V. G.; Loew, L. M. *Biochemistry* **1985**, *24* (21), 5749–5755.

(14) Wang, D.; McMahon, S.; Zhang, Z.; Jackson, M. B. *J. Neurophysiol.* **2012**, *108* (11), 3147–3160.

(15) Sjulson, L.; Miesenbock, G. *J. Neurosci.* **2008**, *28* (21), 5582–5593.

(16) Chanda, B.; Blunck, R.; Faria, L. C.; Schweizer, F. E.; Mody, I.; Bezanilla, F. *Nat. Neurosci.* **2005**, *8* (11), 1619–1626.

(17) Miller, E. W.; Lin, J. Y.; Frady, E. P.; Steinbach, P. a; Kristan, W. B.; Tsien, R. Y. *Proc. Natl. Acad. Sci. U. S. A.* **2012**, *109* (6), 2114–2119.

(18) Woodford, C. R.; Frady, E. P.; Smith, R. S.; Morey, B.; Canzi, G.; Palida, S. F.; Araneda, R. C.; Kristan, W. B.; Kubiak, C. P.; Miller, E. W.; Tsien, R. Y. *J. Am. Chem. Soc.* **2015**, *137* (5), 1817–1824.

(19) Li, L. *Nano Lett.* **2007**.

(20) Ellis-Davies, G. C. R. *Nat. Methods* **2007**, *4* (8), 619–628.

(21) Klán, P.; Šolomek, T.; Bochet, C. G.; Blanc, A.; Givens, R.; Rubina, M.; Popik, V.; Kostikov, A.; Wirz, J. *Chem. Rev.* **2013**, *113* (1), 119–191.

(22) Patchornik, A.; Amit, B.; Woodward, R. B. *J. Am. Chem. Soc.* **1970**, *92* (21), 6333–6335.

(23) Engels, J.; Schlaeger, E. J. *J. Med. Chem.* **1977**, *20* (7), 907–911.

(24) Kaplan, J. H.; Forbush, B.; Hoffman, J. F. *Biochemistry* **1978**, *17* (10), 1929–1935.

(25) Griepenburg, J. C.; Ruble, B. K.; Dmochowski, I. J. *Bioorganic Med. Chem.* **2013**, *21* (20), 6198–6204.

(26) Adams, S. R.; Kao, J. P. Y.; Grynkiewicz, G.; Minta, A.; Tsien, R. Y. *J. Am. Chem. Soc.* **1988**, *110* (10), 3212–3220.

(27) Ellis-Davies, G. C.; Kaplan, J. H. *Proc. Natl. Acad. Sci. U. S. A.* **1994**, *91* (1), 187–191.

(28) Ciesienski, K. L.; Haas, K. L.; Dickens, M. G.; Tesema, Y. T.; Franz, K. J. *J. Am. Chem. Soc.* **2008**, *130* (37), 12246–12247.

(29) Gwizdala, C.; Kennedy, D. P.; Burdette, S. C. *Chem. Commun.* **2009**, No. 45, 6967–6969.

(30) Chalmers, S.; Caldwell, S. T.; Quin, C.; Prime, T. A.; James, A. M.; Cairns, A. G.; Murphy, M. P.; McCarron, J. G.; Hartley, R. C. *J. Am. Chem. Soc.* **2012**, *134* (2), 758–761.

(31) Matsuzaki, M.; Ellis-Davies, G. C. R.; Nemoto, T.; Miyashita, Y.; Iino, M.; Kasai, H. *Nat. Neurosci.* **2001**, *4* (11), 1086–1092.

(32) Miller, E. W.; Taulet, N.; Onak, C. S.; New, E. J.; Lanselle, J. K.; Smelick, G. S.; Chang, C. J. *J. Am. Chem. Soc.* **2010**, *132* (48), 17071–17073.

(33) Ryu, K. A.; Stutts, L.; Tom, J. K.; Mancini, R. J.; Esser-Kahn, A. P. *J. Am. Chem. Soc.* **2014**, *136* (31), 10823–10825.

(34) Hemphill, J.; Borchardt, E. K.; Brown, K.; Asokan, A.; Deiters, A. *J. Am. Chem. Soc.* **2015**, *137* (17), 5642–5645.

(35) Kobayashi, T.; Urano, Y.; Kamiya, M.; Ueno, T.; Kojima, H.; Nagano, T. *J. Am. Chem. Soc.* **2007**, *129* (21), 6696–6697.

(36) Wysocki, L. M.; Grimm, J. B.; Tkachuk, A. N.; Brown, T. a; Betzig, E.; Lavis, L. D. *Angew. Chem. Int. Ed. Engl.* **2011**, *50* (47), 11206–11209.

(37) Hancock, J. F.; Cadwallader, K.; Paterson, H.; Marshall, C. J. *EMBO J.* **1991**, *10* (13), 4033–4039.

(38) Godement, P.; Vanselow, J.; Thanos, S.; Bonhoeffer, F. *Development* **1987**, *101*, 697–713.

(39) Jiao, G.; Han, J.; Burgess, K. *J. Org. Chem.* **2003**, *3012* (10), 8264–8267.

(40) Montalti, M.; Credi, A.; Prodi, L.; Gandolfi, M. T. *Handbook of Photochemistry*, 3rd ed.; Taylor & Francis, 2006.

(41) Tsien, R. Y.; Li, W.; Llopis, J.; Whitney, M.; Zlokarnik, G. *Nature* **1998**, *392* (6679), 936–941.

(42) Zhao, Y.; Zheng, Q.; Dakin, K.; Xu, K.; Martinez, M. L.; Li, W.-H. *J. Am. Chem. Soc.* **2004**, *126* (14), 4653–4663.

Chapter 2

Additional Photocaged VoltageFluors

Portions of this work were completed in collaboration with others:

Compounds in this chapter were synthesized in collaboration with Wootack Hong.

Introduction

Chapter 1 described the synthesis, characterization and application of a photoactivatable caged VoltageFluor, SPOT2.1.Cl.[1] SPOT2.1.Cl showed a 12-fold fluorescence turn-on upon illumination with near-UV light in HEK cells, remained voltage sensitive after uncaging and reported evoked action potentials in neurons with good signal to noise. Although SPOT2.1.Cl met our criteria for a proof-of-principle photoactivatable voltage sensitive dye, the design space for future small molecule photoactivatable optical reporters of transmembrane potential (SPOTs) remains largely unexplored. We sought to improve the performance of SPOTs on two fronts: i) increasing the voltage sensitivity of the released VSD by caging improved voltage indicators[2,3] and ii) increasing the uncaging efficiency of SPOTs by swapping the dimethoxynitrobenzyl cage for an alternate photolabile protecting group.[4–6] To that end we synthesized a panel of new SPOTs (Scheme 2-1) caging VoltageFluors VF2.1.Cl, VF2.1(OMe).Cl or VFiso2.2(OMe).Cl with either the previously employed dimethoxynitrobenzyl (DMNB) cage or the related α-carboxy-6-nitroveratryl (CNV) cage,[7,8] a variant of DMNB bearing a carboxylic acid at the benzylic position.

Results and Discussion

DMNB-caged VoltageFluors were synthesized as reported in Chapter 1. The resting properties and uncaging behaviors of different DMNB-caged VoltageFluors were strikingly different. When loaded at 1 μM in HEK293T cells DMNB-VF2.1(OMe).Cl was found to have a resting fluorescence intensity 2.7-fold higher than that of DMNB-VF2.1.Cl (SPOT2.1.Cl) (Figure 2-1a, n = 8 and 12 single cells or small rafts, respectively). This is the opposite of the relative fluorescence intensities of the free VoltageFluors – VF2.1(OMe).Cl is dimmer than VF2.1.Cl when bath applied to cells.[2] DMNB-VF2.(OMe).Cl showed a substantial increase in cellular fluorescence intensity upon irradiation with 390 nm light (3.7 ±0.9X), which was nonetheless less than that observed with DMNB-VF2.1.Cl under identical imaging conditions (6.7 ±2.2X) We had previously attributed quenching in DMNB-VF2.1.Cl to be driven largely by capping of the phenolic oxygen in the xanthene fluorophore, which prevents access to the highly fluorescent anionic form of the dye.[9,10] While this mechanism is undoubtedly in place, it clearly cannot account for the full extent of quenching observed with DMNB-VF2.1.Cl. Photoinduced electron transfer (PeT) between fluorophores and nitro groups is a well-known quenching process in fluorescent probes[11] and this mechanism appears to play an important roles in SPOTs as well. The voltage-sensing mechanism of VoltageFluors also operates through PeT, wherein electron transfer from the electron-rich aniline group on the molecular wire quenches the fluorescence of dichlorofluorescein. It therefore appears that in our three-chromophore systems (photolabile cage, fluorophore and molecular wire) competing electron-transfer processes may play an important role in governing the baseline fluorescence of caged VoltageFluor. DMNB-VFiso2.2(OMe).Cl also possessed the relatively high fluorescence of DMNB-VF2.1(OMe).Cl (Figure 2-1a), but unlike both DMNB-VF2.1.Cl or DMNB-VF2.1(OMe).Cl did not exhibit an appreciable increase in cellular fluorescence upon irradiation with 390 nm light (1.6 ±0.5X, n = 11 single cells or small rafts, Figure 2-1c, Figure 2-2). I propose the following hypothesis for this effect: At 390 nm the extinction co-efficient of a phenylene-vinylene molecular wire[2,12] is over an order-of-magnitude greater than that of a typical nitrobenzyl photolabile group.[4] Accordingly, the mechanism of uncaging in SPOT dyes most likely involves excitation of the molecular wire followed by an intramolecular energy transfer to the dimethoxynitrobenzyl cage, followed by rearrangement of the caging group and release of the free VoltageFluor. In the case of DMNB-isoVF2.2(OMe).Cl the electronics of the system are poorly matched and this electron transfer process is inoperative,

preventing the release of VFiso2.2(OMe).Cl. Such a "co-operative uncaging" mechanism has previously been described in the literature,[13] and has been exploited to sensitize nitrobenzyl cages to 2P excitation via energy transfer from a molecular-wire like structure with a high 2P cross-section.[14]

The CNV cage[7,8] has high structural similarity to the DMNB cage, making it likely that it could also serve as a useful trigger for a photoactivatable VoltageFluor, but we hoped that the additional carboxylic acid would improve the solubility of an extremely lipophilic class of dyes and provide enhanced uncaging kinetics. CNV-caged tyrosine and carboxylic acids[7,8,15] show excellent release kinetics, and a CNV-caged naloxone[15] has been employed to study opioid signaling. Analogously to the dimethoxy derivatives, carboxynitrobenzyl is a popular alternative to the simple nitrobenzyl cage due its rapid "dark" reaction following excitation.[16] Synthesis of CNV-VF2.1.Cl (Scheme 2-2) was modeled on the syntheses of CNV-tyrosine reported by Snaith and co-workers[7] and begins with commercially available dimethoxynitrobenzyl precursor **1**. Esterification of the carboxylic acid gave protected intermediate **2** in good yield. Regitz diazo-transfer with tosyl azide and halogenation of diazo compound **3** with HBr in acetic acid provided **4** in 60% yield across two steps. **3** and **4** decompose over time, and should be stored at or below 4 °C and shielded from light. **4** served as a substrate for addition of the protected photocage to VF2.1.Cl. CNV-VF2.1.Cl-methyl ester **5** was deprotected via alkaline hydrolysis with dilute lithium hydroxide to yield CNV-VF2.1.Cl. We discovered that deprotection of **4** led to the formation of two products with the correct product mass but which were fully resolved by HPLC (Figure 2-3). We surmised that racemic substitution at the benzylic position, in combination with hindered rotation about the xanthene-meso ring bond led to a pair of diastereomers possessing axial chirality. We successfully isolated each product by semi-preparative HPLC and characterized their uncaging properties independently. In the absence of further structural information, they will be referred to as "CNV-VF2.1.Cl isomer 1" and "CNV-VF2.1.Cl isomer 2". When bath applied to HEK293T cells isomer 1 and isomer 2 were both found to be approximately 12-fold brighter than DMNB-VF2.1.Cl (Figure 2-4a). Both isomers 1 and 2 could be effectively photoactivated with 390 nm light, but displayed only 2.5 ±0.1X (isomer 1, n = 10 single cells or small rafts) and 3.3 ±0.1X (isomer 2, n = 14 single cells or small rafts) fold turn-on responses (Figure 2-4b-c, Figure 2-5), substantially less than the 6.5-fold turn-on observed with DMNB-VF2.1.Cl under the same imaging conditions. Tantalizingly, the turn-on response, but not starting fluorescence, between the two diastereomers was found to be statistically significant. This raises the possibility of a stereochemical influence on either the energy transfer from the molecular wire to the nitrobenzyl cage (presuming this mechanism is operative) or the dark reaction which follows excitation of the cage and leads to release of the free VSD.

In addition to CNV-VF2.1.Cl, we sought to synthesize CNV-VF2.1(OMe).Cl and CNV-VFiso2.2(OMe).Cl, but these compounds were not successfully isolated with acceptable purity. Synthetically, there remains substantial room for improvement in the synthesis of CNV-caged VoltageFluors. Although the methyl ester protected caging group is easily accessible, **5** is susceptible to decomposition during alkaline hydrolysis and alternate protecting groups should be investigated if this project is to be pursued further.

Concluding Remarks

While the additional probes reported in this Appendix failed to exceed the performance of DMNB-VF2.1.Cl as a functional probe, they nevertheless hint at interesting photochemical processes occurring in SPOT dyes. Variations in baseline fluorescence intensity between DMNB-VF2.1.Cl and DMNB-VF2.1(OMe).Cl and DMNB-VF2.1.Cl and CNV-VF2.1.Cl make it clear that the quenching effect of the nitrobenzyl is heavily influenced by a PeT-mechanism between the fluorophore and nitrobenzyl cage. The wide variation in fluorescence turn-on response observed across the DMNB series suggests that a co-operative uncaging effect involving an intramolecular energy transfect may be at play. Finally, the different uncaging responses of the two isomers of CNV-VF2.1.Cl have little precedent in the literature, and the possibility of a stereochemical effect on the photolysis of nitrobenzyl cages deserves follow-up beyond these preliminary results.

General Synthetic and Analytical Methods

^{1}H NMR spectra were collected in $CDCl_3$ or acetone-d_6 (Cambridge Isotope Laboratories, Cambridge, MA) at 25 °C on a Bruker AV-300 or AVQ-400 spectrometer at the College of Chemistry NMR Facility at the University of California, Berkeley. All chemical shifts are reported in the standard δ notation of parts per million using the peak of residual proton signals of $CDCl_3$ or acetone -d_6 as an internal reference. Low resolution LC/ESI-MS was performed on an Advion Expression LC-MS coupled to an Agilent Infinity 1220 HPLC. Semi-preparative HPLC was performed on the same Agilent system. Luna C18(2) (Phenomenex) columns were employed for both analytical and semi-preparative separations, using water (solvent A) and acetonitrile (solvent B) with 0.05% TFA as an additive. All reactions were performed under N_2 in oven-dried glassware, shielded from light.

Cell culture, transfection, and dye loading

Human embryonic Kidney (HEK) cells were passaged and plated onto glass coverslips pre-coated with PDL to provide a confluency of ~15-50% for imaging. HEK cells were plated and maintained in Dulbecco's modified eagle medium (DMEM) supplemented with 4.5 g/L D-glucose, 10% FBS and 1% Glutamax.

For imaging in HEK cells, dyes were prepared as a 1 μM solution in HBSS with 0.01% Pluronic F-127 as an additive. Cells were imaged approximately 16 hours after plating on poly-D-lysine coated 12 mm coverslips. Cells were incubated for 20 minutes at 37 °C and washed 3x with HBSS.

Epifluorescence microscopy

Epifluorescence images were acquired on an AxioExaminer Z-1 (Zeiss) equipped with a Spectra-X light engine LED light (Lumencor), all controlled with Slidebook (v6, Intelligent Imaging Innovations). Images were acquired with a W Plan-Apochromat 20x/1.0 objective (Zeiss) and focused onto a OracFlash4.0 sCMOS camera (Hamamatsu) camera.

Uncaging was performed with 390 nm light (LED, 20 nm bandpass, 13.5 mW/mm^2) delivered in 1 second intervals. For quantification of uncaging, excitation light was delivered at 542 nM (LED, nm bandpass, 11.9 mw/mm^2, 50 ms exposure). Emission was collected with a quadruple emission filter (430/32 nm, 508/14 nm, 586/30 nm, 708/98 nm) after passing through a quadruple dichroic mirror (432/38 nm, 509/22 nm, 586/40 nm, 654 nm LP).

Data analysis

Regions of interest were drawn around cells and the mean fluorescence measured in Fiji (ImageJ). All values are background subtracted. Turn-on response was calculated by dividing cellular fluorescence intensity after 30 seconds of UV irradiation by the cellular fluorescence intensity measured prior to UV illumination. In cases where the starting fluorescence of an ROI was measured as being below that of background, the fluorescence intensity of the ROI was manually set to 0.

Synthetic Methods

Synthesis of **methyl 2-(4,5-dimethoxy-2-nitrophenyl)acetate (2**):

In a round bottom flask dissolved **1** (250 mg, 1.04 mmol) in 5 mL of anhydrous methanol. Added 3 drops of concentrated H_2SO_4 and refluxed overnight. The reaction was cooled to room temperature and solvent removed under reduced pressure. Crude product was recrystallized in methanol to yield **2** in 70% yield as a fluffy white solid. ^{1}H NMR (400 MHz, Acetone-d_6) δ 7.74 (s, 1H), 7.12 (s, 1H), 4.05 (s, 2H), 3.96 (s, 3H), 3.96 (s, 3H), 3.65 (s, 3H).

Synthesis of **methyl 2-diazo-2-(4,5-dimethoxy-2-nitrophenyl)acetate (3):**

To a solution of **2** (200 mg, 784 μmol) in 4 mL anhydrous DCM was added 1,8-Diazabicyclo[5.4.0]undec-7-ene (DBU) (130 mg, 862 μmol). After stirring for 5 minutes freshly prepared tosyl azide (170 mg, 862 μmol) was added and the reaction stirred for three hours. The reaction was diluted to a total volume of 20 mL DCM and washed with 20 mL water. The organic phase was dried over $MgSO_4$, decanted, and concentrated under reduced pressure. Product was purified by flash column chromatography (30% EtOAc/hexanes) to obtain **3** in 81% yield as a yellow oil. ^{1}H NMR (300 MHz, $CDCl_3$) δ 7.72 (s, 1H), 7.01 (s, 1H), 3.97 (s, 3H), 3.97 (s, 3H), 3.83 (s, 3H).

Synthesis of **methyl 2-bromo-2-(4,5-dimethoxy-2-nitrophenyl)acetate (4):**

0.1 mL HBr (33% in AcOH) was added to a solution of **3** (70 mg, 249 μmol) in 2.5 mL anhydrous DCM. After stirring for 30 minutes the reaction was diluted to 10 mL DCM and washed with 10 mL saturated $NaHCO_3$. The organic phase was dried over $MgSO_4$, decanted and concentrated under reduced pressure. Crude material was purified by flash column chromatography (30% EtOAc/hexanes) to obtain **4** in 74% yield as a yellow oil. ^{1}H NMR (300 MHz, $CDCl_3$) δ 7.61 (s, 1H), 7.42 (s, 1H), 6.24 (s, 1H), 4.02 (s, 3H), 3.96 (s, 3H), 3.81 (s, 3H).

Synthesis of **CNV-VF2.1.Cl methyl ester (5):**

To a solution of VF2.1.Cl (75 mg, 122 μmol) and Cs_2CO_3 (75 mg, 230 μmol) in 2 mL anhydrous DMF added **4** (105 mg, 314 μmol). After stirring overnight at room temperature solvent was removed under vacuum, and the resulting crude paste was suspended in water, acidified with AcOH and filtered. The collected red precipitate was washed with water, 1:1 DCM:hexanes and Et_2O to obtain 70 mg (67%) of CNV-VF2.1.Cl methyl ester which was used without further purification.

Synthesis of **CNV-VF2.1.Cl:**

5 (10 mg) was dissolved in 4:2:1 MeOH:DCM:0.2 M aqueous LiOH. After stirring for 30 minutes the reaction was acidified by dropwise addition of acetic acid, diluted with methanol, filtered through a 0.22 μm filter and purified by semi-preparative HPLC. Two well resolved peaks with the desired product mass $[M+H]^+$ 868.2, presumably a pair of diastereomers, were collected in 6% (0.58 mg) and 10% yield (1.02 mg) for a combined yield of 16%. See Figure 2-3 for characterization data.

Scheme 2-1 SPOTs characterized in this Appendix

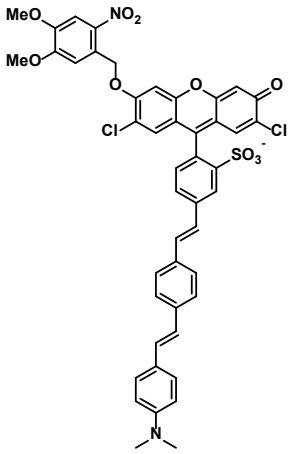

DMNB-VF2.1.Cl
(SPOT2.1.Cl)

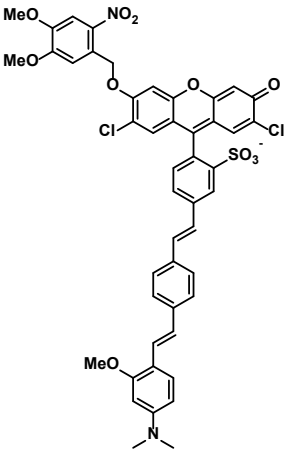

DMNB-VF2.1(OMe).Cl

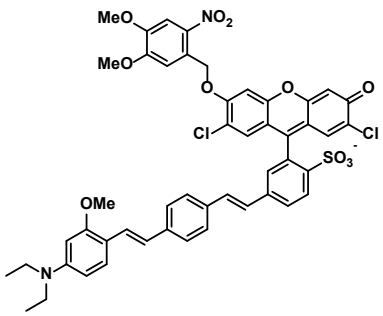

DMNB-VFiso2.2(OMe).Cl

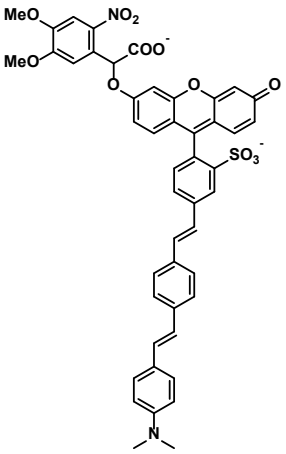

CNV-VF2.1.Cl

Figure 2-1

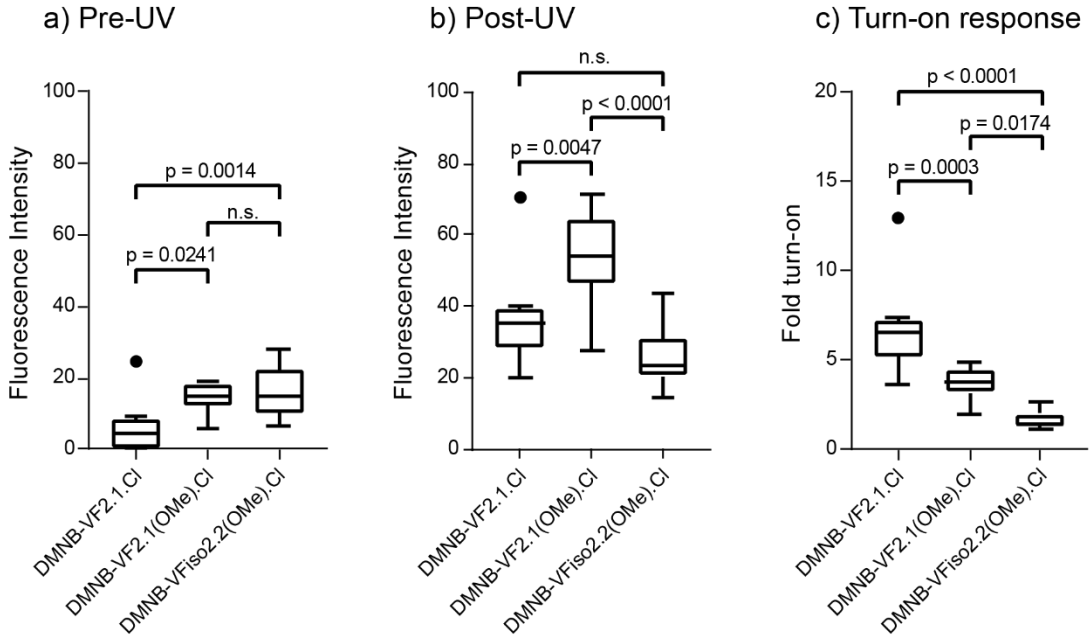

Dimethoxynitrobenzyl caged VoltageFluors show important differences in cellular fluorescence intensity and uncaging response. a) Tukey boxplot of cellular fluorescence intensity of HEK cells with the indicated dyes at 1 µM prior to UV exposure. b) Cellular fluorescence intensity of the same cells after 30 seconds with 13.5 mW/mm^2 390 nm light. c) Ratio of post to pre-UV fluorescence intensity. Data are from 8 (DMNB-VF2.1.Cl), 12 (DMNB-VF2.1(OMe).Cl) and 11 (DMNB-VFiso2.2(OMe).Cl) single cells or small rafts. Statistics are one-way ANOVA followed by Tukey's test.

Figure 2-2

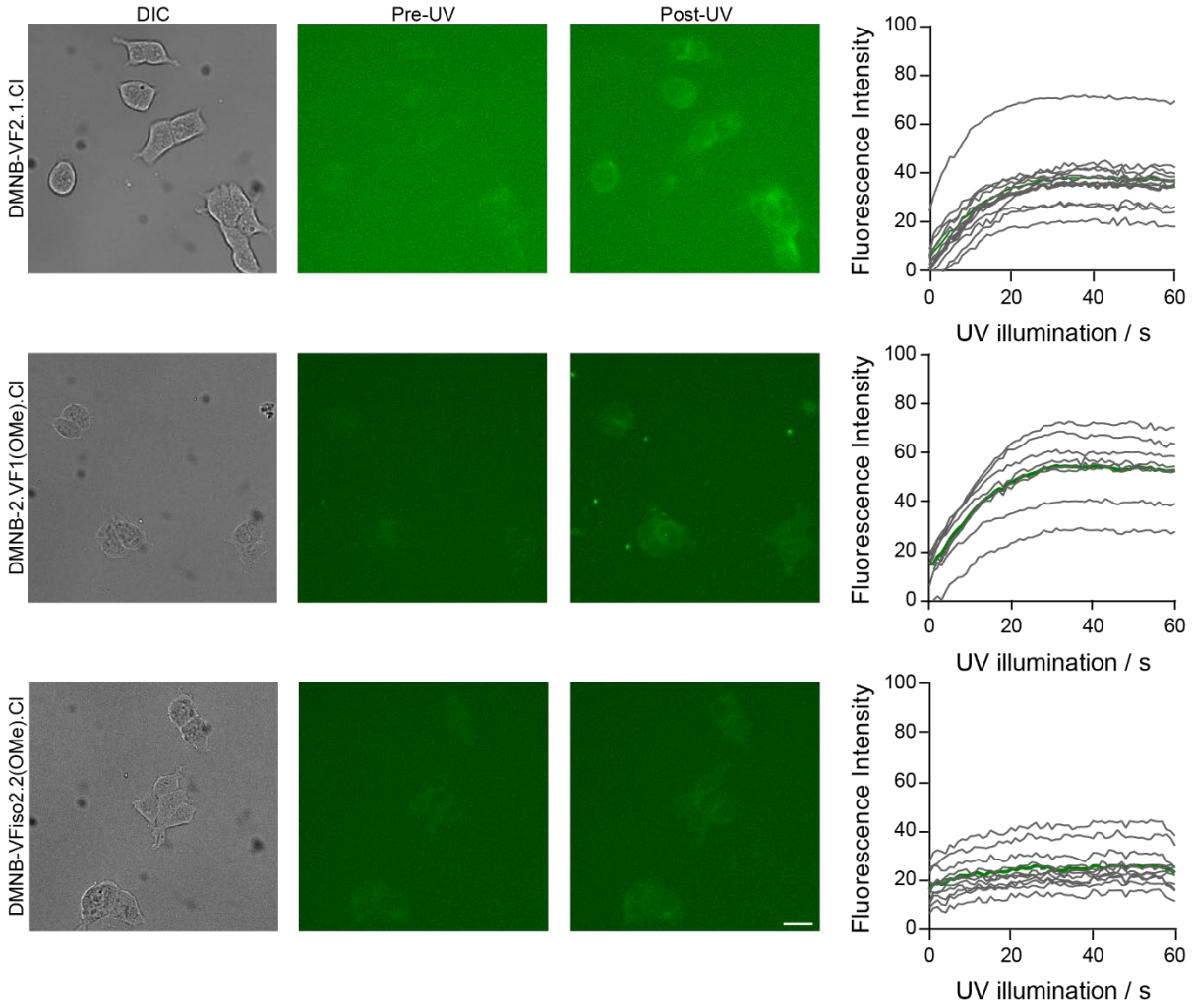

Widefield (DIC and fluorescence) images from cells analyzed in Figure 2-1. Uncaging traces indicate raw fluorescence values from individual ROIs in grey, and the mean trace in green. Scale bar is 20 µm.

Scheme 2-2 Synthesis of CNV-VF2.1.Cl

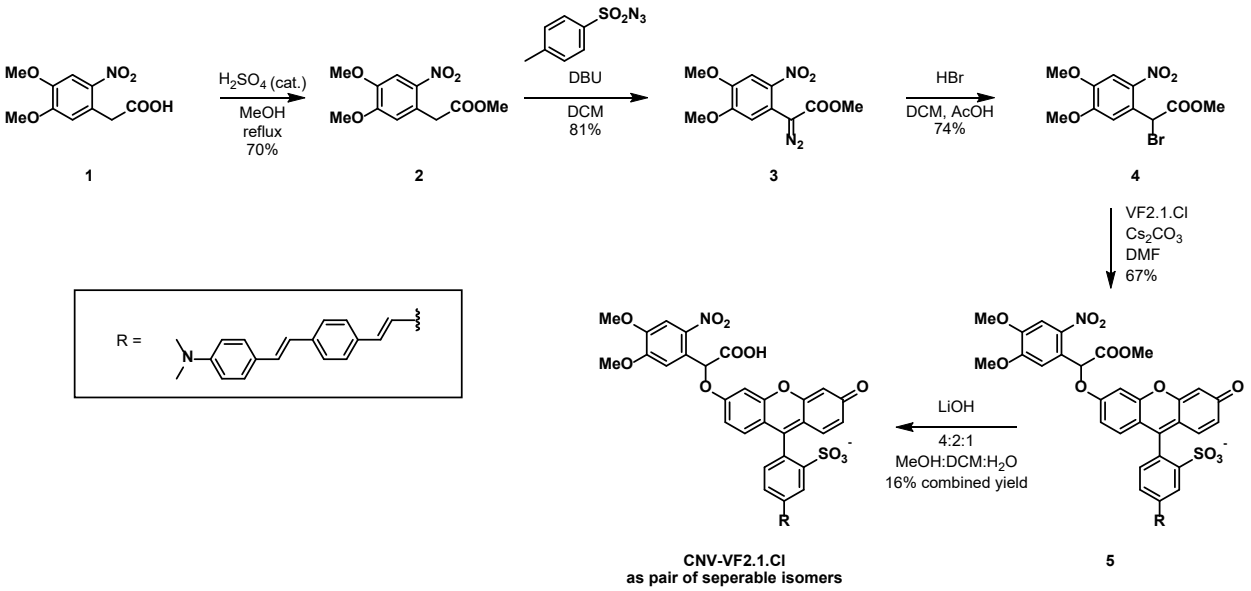

Figure 2-3 LC-MS trace of isolated CNV-VF2.1.Cl diastereomers

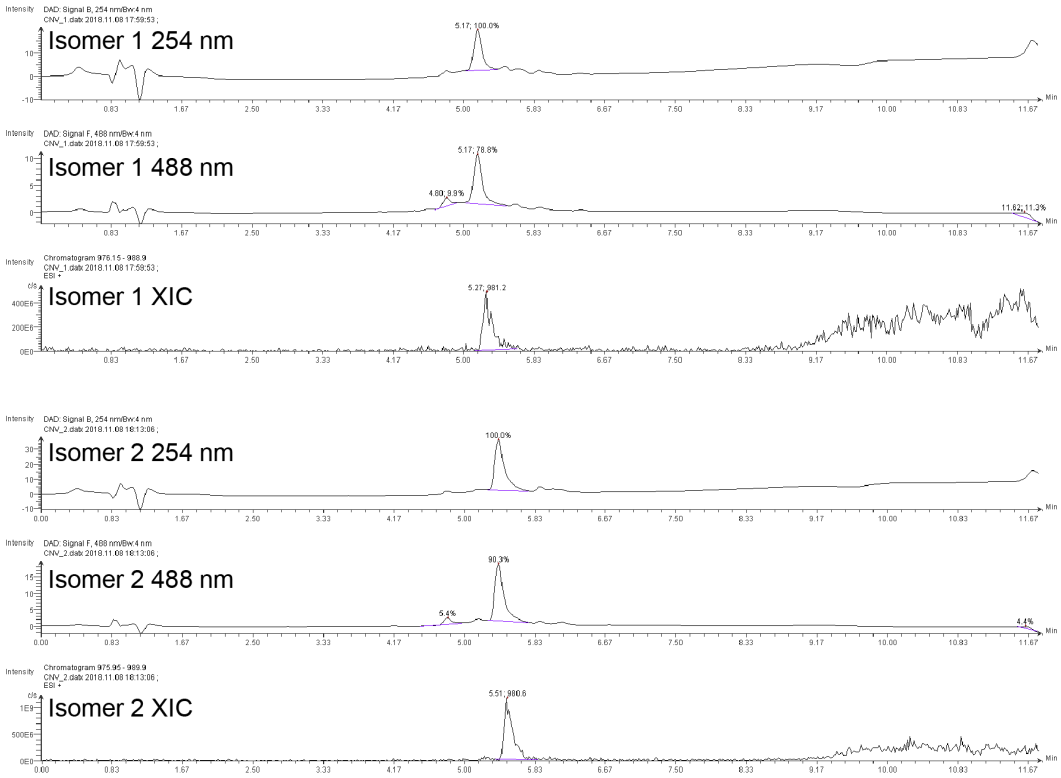

Figure 2-4

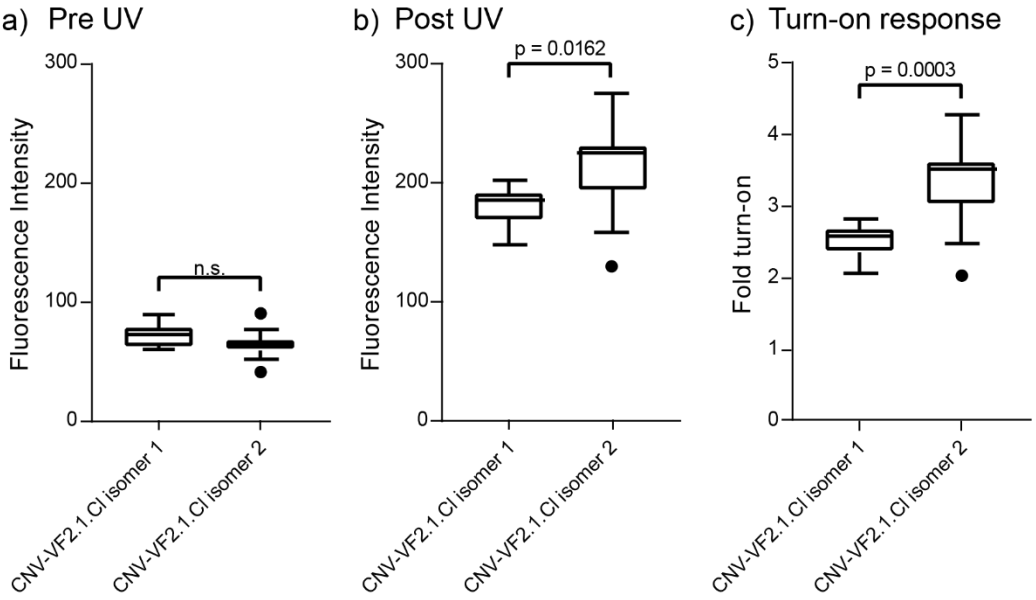

The two isolated isomers of CNV-VF2.1.Cl show different uncaging behaviors. a) Tukey boxplot of cellular fluorescence intensity of HEK cells with the indicated dyes at 1 μM prior to UV exposure. b) Cellular fluorescence of the same cells after 30 seconds with 13.5 mW/mm^2 390 nm light. c) Ratio of post to pre-UV fluorescence intensity. Data are from 10 (isomer 1) or 14 (isomer 2) single cells or small rafts. Statistics are one-way ANOVA followed by Tukey's test.

Figure 2-5

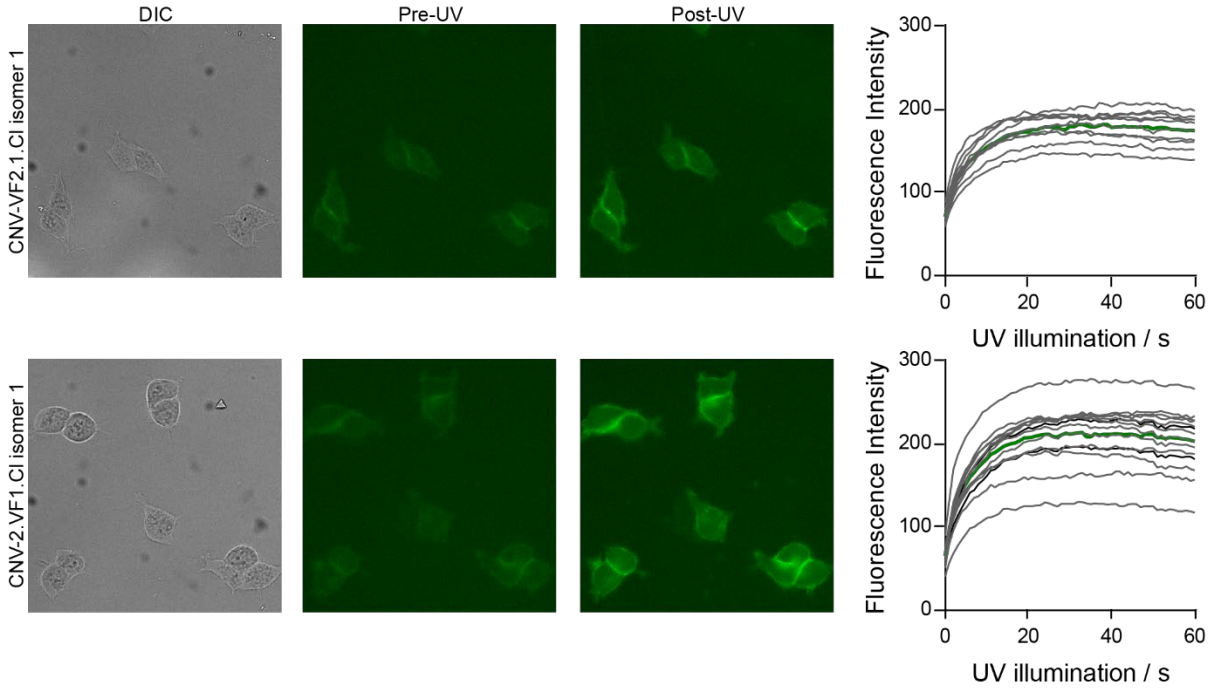

Widefield (DIC and fluorescence) images from cells analyzed in Figure 4-2. Uncaging traces indicate raw fluorescence values from individual ROIs in grey, and the mean trace in green. Scale bar is 20 μm.

References

(1) Grenier, V.; Walker, A. S.; Miller, E. W. *J. Am. Chem. Soc.* **2015**, *137* (34), 10894–10897.

(2) Woodford, C. R.; Frady, E. P.; Smith, R. S.; Morey, B.; Canzi, G.; Palida, S. F.; Araneda, R. C.; Kristan, W. B.; Kubiak, C. P.; Miller, E. W.; Tsien, R. Y. *J. Am. Chem. Soc.* **2015**, *137* (5), 1817–1824.

(3) Kulkarni, R. U. Design and Application of Photoinduced-Electron Transfer-Based Voltage-Sensitive Dyes to Biological Imaging, University of Califoria, Berkeley, 2018.

(4) Ellis-Davies, G. C. R. *Nat. Methods* **2007**, *4* (8), 619–628.

(5) Li, W.; Zheng, G. *Photochem. Photobiol. Sci.* **2012**, *11* (3), 460–471.

(6) Lee, H.-M.; Larson, D. R.; Lawrence, D. S. *ACS Chem. Biol.* **2009**, *4* (6), 409–427.

(7) Russell, A. G.; Sadler, M. J.; Laidlaw, H. J.; Gutiérrez-Loriente, A.; Wharton, C. W.; Carteau, D.; Bassani, D. M.; Snaith, J. S. *Photochem. Photobiol. Sci.* **2012**, *11* (3), 556.

(8) Russell, A. G.; Ragoussi, M.-E.; Ramalho, R.; Wharton, C. W.; Carteau, D.; Bassani, D. M.; Snaith, J. S. *J. Org. Chem.* **2010**, *75* (13), 4648–4651.

(9) Kobayashi, T.; Urano, Y.; Kamiya, M.; Ueno, T.; Kojima, H.; Nagano, T. *J. Am. Chem. Soc.* **2007**, *129* (21), 6696–6697.

(10) Sjöback, R.; Nygren, J.; Kubista, M. *Spectrochimica Acta Part A: Molecular and Biomolecular Spectroscopy*. 1995, pp L7–L21.

(11) Ueno, T.; Urano, Y.; Kojima, H.; Nagano, T. *J. Am. Chem. Soc.* **2006**, *128* (33), 10640–10641.

(12) Miller, E. W.; Lin, J. Y.; Frady, E. P.; Steinbach, P. a; Kristan, W. B.; Tsien, R. Y. *Proc. Natl. Acad. Sci. U. S. A.* **2012**, *109* (6), 2114–2119.

(13) Zhao, Y. R.; Zheng, Q.; Dakin, K.; Xu, K.; Martinez, M. L.; Li, W. H. *J. Am. Chem. Soc.* **2004**, *126* (14), 4653–4663.

(14) Jose, E.; Cueto, D.; Chevasson, V.; Daniel, J.; Hugues, V.; Mongin, O.; Genin, E.; Blanchard-desce, M. **2015**, 8–11.

(15) Banghart, M. R.; Williams, J. T.; Shah, R. C.; Lavis, L. D.; Sabatini, B. L. *Mol. Pharmacol.* **2013**, *84* (5), 687–695.

(16) Corrie, J. E. T.; Munasinghe, V. R. N.; Trentham, D. R.; Barth, A. *Photochem. Photobiol. Sci.* **2008**, *7* (1), 84–97.

Chapter 3

Synthesis of Enzyme-Activatable Fluorogenic Voltage Sensitive Dyes

Portions of this work have been published in the Journal of the American Chemical Society:

Liu, P.; Grenier, V.; Hong, W.; Muller, V.R.; Miller, E.W. *J. Am. Chem. Soc.*, **2017**, *139* (48), 17334-17340.

Portions of this work were completed in collaboration with others:

HPLC uncaging studies were performed in collaboration with Pei Liu. UV-Vis and fluorescence spectroscopy experiments were performed by Pei Liu.

Introduction

The successful synthesis and proof-of-principle application of a photocaged VoltageFluor (SPOT2.1.Cl, described in Chapter 1 of this thesis) raised the possibility that masking the phenolic oxygen of VF2.1.Cl could serve a general design strategy for creating fluorogenic voltage sensitive dyes (VSDs). In principal, any cleavable moiety capable of releasing a phenol under physiological conditions could serve as a candidate masking system. The chemical literature is rich with such systems, most prominently enzymatically cleavable groups which can respond to enzymes such as monoamine oxidases, nitroreductases, phosphatases, glycosidases, β-lactamases and esterases to release fluorophores, fluorescent probes, or metabolically active compounds (comprehensively reviewed by Chyan and Raines, see ref. 1).[1–5]

The development of a fluorogenic VoltageFluor seeks to address a number of related limitations of untargeted VSDs. First, the mammalian brain is densely packed with cell bodies. Application of a dye which labels all plasma membranes can make it difficult to isolate the signal from a single cell when they are adjacent and their individual plasma membranes poorly resolved.[6] In this context, it is highly desirable to achieve sparse labeling of cells. Second, the electrical properties of subcellular structures of neurons are of great interest in neuroscience, and their study is an area of application that is particularly amenable to the use of optical tools,[7–10] as they are largely inaccessible through electrophysiology.[11] However, the dense labeling of all membranes can obscure these structures, both in tissue and culture. Finally, it can be of interest to separate the signal of functionally and genetically distinct populations of cells, e.g. excitatory and inhibitory neurons in the hippocampus, as these may respond differently to disease processes and pharmacological agents.[12]

SPOT2.1.Cl, in combination with the expression of a genetically encoded fluorescent protein "target", can address many of these issues. However, it suffers from important drawbacks which have hampered its further development. The absolute fluorescence intensity of released functional dye remains low, as a concomitant photobleaching effect likely competes with uncaging in cells. Despite the fact that released VF dye will diffuse out of the soma after uncaging, total signal in axons and dendrites is far too low for imaging of action potentials at these sites. In addition, it is not possible to deliver single-photon illumination with sufficient spatial control to uncage single cells in a three-dimensional matrix, as light from a traditional widefield or confocal microscope invariably exits the objective as a cone, resulting in out-of-plane uncaging of VF2.1.Cl in the z-axis. While 2-photon activation could potentially deliver the spatial precision necessary for such an experiment, nitrobenzyl cages have very small 2-photon cross-sections.[13,14]

It therefore appears evident that an enzyme activated fluorogenic probe might be a useful method of circumventing the problems encountered when using light as a trigger. Ester-esterase pairs are perhaps the most widely-employed strategy for the release of fluorophores. Acetoxymethyl esters,[2] which may be cleaved by native esterases, are widely used for the delivery of otherwise cell impermeable substrates into cells. A more selective strategy, based on 1-methylcyclopropyl esters and ethers, which do not react with native human esterases but can be cleaved by exogenously expressed pig liver esterase (PLE),[3] could allow selective activation of a masked VoltageFluor in neurons expressing PLE at their cell surface (Scheme 3-1). Accordingly,

I set out to synthesize a 1-methylcyclopropyl ether capped VF dye (VoltageFluor activated by esterase expression, VF-EX1, Scheme 3-2).

Results and Discussion

VF-EX1 is accessible in a single step from VF2.1.Cl and iodomethyl 1-methylcyclopropanecarboxylate in *N,N*-dimethylformamide (DMF), with diisopropylethylamine (DIPEA) as a base. Unexpectedly, addition of excess iodoalkane was found to lead to the formation of the sulfonate ester VF-EX2. VF-EX1 or VF-EX2 could be selectively formed by addition of stoichiometric or excess iodoalkane, and were isolated in 16 and 32% percent yield, respectively, following purification by semi-preparative HPLC. VG-299c, an analog of VF-EX1 lacking the aniline moiety of the molecular wire (Scheme 3-1), was also synthesized through this route – interestingly, despite using an excess of iodoalkane no formation of the sulfonyl ester was observed when using the electron deficient VF2.0.Cl as starting material. An alternative method, using Ag_2O as a Lewis acid, can be used to selectively generate VF-EX1,[2,3] but unless the solvent has been carefully degassed leads to formation of a side-product with mass $[M+H]^+$-14 (low resolution ESI-MS), which we attributed to *N*-demethylation of the molecular wire fragment.

To isolate the effects of the sulfonate ester modification I synthesized VF-EX0, where the phenolic oxygen of the xanthene fluorophore remains unmodified. The three step synthesis of VF-EX0 begins with the bis-protection of VF2.1.Cl with para-methoxybenzyl bromide, yielding intermediate **1**. Selective cleavage of the para-methoxybenzyl sulfonate ester with dilute lithium hydroxide (0.25 M in 3:1 DMF:H_2O) provided VF2.1.Cl-PMB in 77% yield over two steps. One-pot installation of the methycyclopropyl moiety and cleavage of the para-methoxybenzyl ether yielded VF-EX0 in 47% yield. This synthesis is the first reported use of para-methoxybenzyl group as a protecting group for sulfonates.

The three VF-EX compounds were characterized by NMR spectroscopy, HPLC, and mass spectrometry. Both VF-EX1 and VF-EX2 display optical properties consistent with *O*-alkylated fluoresceins:[15] a weak absorbance at λ = 500 nm (Figure 3-1a, c). VF-EX1 and VF-EX2 are minimally fluorescent, with quantum yields of 0.004 and 0.013, respectively (in Hank's balanced salt solution, pH 7.4). Compared with VF2.1.Cl, which has a quantum yield of 0.08 under identical conditions, these represent 19- and 6.7-fold decreases in fluorescence intensity, respectively (Figure 3-1b,d). VF-EX0, in which only the sulfonic acid is esterified, has a quantum yield of 0.24, consistent with a 3-fold increase in quantum efficiency for sulfonate esters (VF-EX0, VF-EX2) compared with their cognate acids (VF2.1.Cl, VF-EX1).

We confirmed that purified PLE (Sigma, E2884) hydrolyzes VF-EX1 and VF-EX2 *in vitro*. The action of PLE on VF-EX1 or VF-EX2 results in a 53- or 11-fold increase in fluorescence, respectively, after 3 hours. The fluorescence increase is accompanied by the restoration of a fluorescein-like absorption and emission profile (Figure 3-1a-d) HPLC analysis revealed VF2.1.Cl as the product of PLE-mediated hydrolysis reactions (Figure 3-2).

VF-EX2 proved to be an effective fluorogenic voltage sensitive dyes, and was used to probe the neuromodulatory effect of serotonin in cultured mammalian neurons. This work was completed by Pei Liu and is further described in our publication.

Materials and Methods

General Synthetic and Analytical Methods

Anhydrous sodium iodide and diisopropylethylamine were purchased from Sigma-Aldrich. Anhydrous solvents (acetonitrile, dichloromethane and N,N-dimethylformamide) were purchased from Acros Organics. VF2.1.Cl and chloromethyl 1-methylcyclopropanecarboxylate were synthesized according to literature procedures.[17–19]

^{1}H and ^{13}C NMR spectra were collected in $(CD_3)_2SO$ (anhydrous, Alfa Aesar, Ward Hill, MA or Cambridge Isotope Laboratories, Cambridge, MA) or $CDCl_3$ (Cambridge Isotope Laboratories, Cambridge, MA) at 25 °C on a Bruker AV-600 spectrometer at the College of Chemistry NMR Facility at the University of California, Berkeley, or at the QB3 Central California 900 MHz NMR Facility. All chemical shifts are reported in the standard δ notation of parts per million using the peak of residual proton signals of $(CD_3)_2SO$ or $CDCl_3$ as an internal reference. Low resolution LC/ESI-MS was performed on an Advion Expression LC-MS coupled to an Agilent Infinity 1220 HPLC, with a Phenomenex Luna 5 µm C18(2) 75 x 4.6 mm column. Semi-preparative HPLC was performed on a Perkin Elmer Series 200 HPLC, with a Phenomonex Luna 5 µm C18(2) 150 x 10 mm column. In both cases water (eluent A) and acetonitrile (eluent B) were employed as the mobile phase, with 0.05% trifluoroacetic acid as an additive, with the exception of VG-299c, which was purified with 10 mM ammonium acetate as HPLC modifier. For analytical HPLC the mobile phase was ramped from 10 to 100% eluent B over eight minutes, then held at 100% B for two minutes at a flow rate of 1.0 mL/minute. For semi-preparative HPLC the mobile phase was ramped from 10 to 100% eluent B over twenty minutes at 5.0 mL/minute. High resolution mass spectra (HR-ESI-MS) were acquired at the QB3/Chemistry Mass Spectrometry Facility at the University of California, Berkeley.

Spectroscopic studies

Stock solutions of dyes were prepared in DMSO (2 mM) and diluted with HBSS (zero Ca^{2+}, zero Mg^{2+}, no phenol red, pH 7.4). UV-Vis absorbance and fluorescence spectra were recorded using a Shimadzu 2501 Spectrophotometer (Shimadzu) and a Quantamaster Master 4 L-format scanning spectrofluorometer (Photon Technologies International). The fluorometer is equipped with an LPS-220B 75-W xenon lamp and power supply, A-1010B lamp housing with integrated igniter, switchable 814 photon-counting/analog photomultiplier detection unit, and MD5020 motor driver. Samples were measured in 1-cm path length quartz cuvettes (Starna Cells). All measurements were done at room temperature.

In vitro PLE reactions and characterization

Commercially purified pig liver esterase (PLE, MW = 168 kDa) was obtained from Sigma-Aldrich (E2884) as a suspension in 3.2 M $(NH_4)_2SO_4$, and was diluted from a stock solution of 28.1 mg/mL to appropriate concentrations in HBSS, pH 7.4. For the enzymatic reaction, 1 µL dyes (final concentration of 50 µM) were incubated with 1 µL PLE (final concentration of 0.7025 mg/mL) and 1 µL Pluronic F-127 (20% solution in DMSO) in 40 µL HBSS at 37 °C for ~ 3 h. The enzymatic products were characterized by spectroscopy and HPLC and compared with the starting

materials. Absorbance was collected from 300 nm to 700 nm. For emission scans, the samples were excited at 520 nm and emission was collected from 525 nm to 700 nm.

Synthetic Methods

Example preparation of iodomethyl 1-methylcyclopropanecarboxylate

In a 4 mL dram vial chloromethyl 1-methylcyclopropanecarboxylate (205 mg, 1.38 mmol) and sodium iodide (221 mg, 1.47 mmol) were dissolved in 1 mL of anhydrous acetonitrile. The reaction was stirred under N_2 for 23 hours, at which time a small aliquot was drawn and the reaction was found to have reached completion by ^{1}H NMR. The reaction was diluted with 2 mL of anhydrous dichloromethane and filtered through a cotton plug. Solvents were removed under reduced pressure at 25 °C to yield a golden liquid over residual salts. The supernatant was carefully pipetted into a tared vial to obtain 228 mg (0.706 mmol) of pure iodomethyl 1-methylcyclopropanecarboxylate. The reagent was then employed neat, or as a 1.00 M solution in anhydrous *N*,*N*-dimethylformamide for use in subsequent reactions. ^{1}H NMR (600 MHz, $CDCl_3$) δ 5.90 (s, 2H), 1.29 (s, 3H), 1.27 (dd, J = 7.5, 3.9 Hz, 2H), 0.73 (dd, J = 7.6, 4.0 Hz, 2H). ^{13}C NMR (151 MHz, $CDCl_3$) δ 173.86, 31.36, 31.34, 18.98, 17.00.

Synthesis of

((2,7-dichloro-9-(4-((E)-4-((E)-4-(dimethylamino)styryl)styryl)phenyl)-3-oxo-3H-xanthen-6-yl)oxy)methyl-1-methylcyclopropane-1-carboxylate (VF-EX1)

In a 4 mL dram vial VF2.1.Cl (25.1 mg, 36.7 µmol, 1 equivalent) was dissolved in 175 µL of anhydrous *N,N*-dimethylformamide and 25.6 µL of diisopropylethylamine (147 µmol, 4 equivalents), followed by addition of 36.6 uL of a 1.00 M solution of iodomethyl 1-methylcyclopropanecarboxylate in anhydrous N,N-dimethylformamide (36.6 µmol, 1 equivalent). The reaction was stirred under N2 at room temperature and monitored by LC-MS. After one hour approximately 50% of the starting material had been consumed. An additional 0.75 equivalents of iodomethyl 1-methylcyclopropanecarboxylate were added. One hour later approximately 15% VF2.1.Cl remained and the reaction was neutralized with 50 µL acetic and diluted with 2 mL of dimethylsulfoxide. The diluted reaction was purified by semi-preparative HPLC without further workup to obtain 4.77 mg of product (5.99 µmol) following evaporation of the mobile phase at a bath temperature of 60 °C and drying under high vacuum. ^{1}H NMR (900 MHz, $(CD_3)_2SO$) δ 8.17 (s, 1H), 7.80 (d, J = 7.8 Hz, 1H), 7.67 (d, J = 7.8 Hz, 2H), 7.59 (s, 1H), 7.57 (d, J = 7.9 Hz, 2H), 7.48 (d, J = 8.0 Hz, 2H), 7.44 (s, 1H), 7.40 (d, J = 16.6 Hz, 1H), 7.28 (d, J = 7.7 Hz, 1H), 7.21 (d, J = 16.3 Hz, 1H), 7.07 (s, 1H), 7.03 (d, J = 16.3 Hz, 1H), 6.98 (s, 1H), 6.80 (s, 2H), 6.47 (s, 1H), 6.00 (s, 2H), 2.96 (s, 6H), 1.25 (s, 3H), 1.18 – 1.14 (m, 2H), 0.84 – 0.82 (m, 2H). ^{13}C NMR (226 MHz, $(CD_3)_2SO$) δ 176.25, 173.74, 158.18, 158.02, 157.86, 157.75, 155.20, 151.41, 151.07, 147.36, 138.54, 137.63, 135.19, 132.45, 130.08, 130.06, 129.75, 129.74, 128.82, 128.81, 127.65, 127.62, 127.27, 127.19, 126.63, 126.52, 126.25, 125.31, 118.41, 118.22, 117.07, 104.15, 102.84, 84.99, 54.90, 18.65, 18.29, 16.79, 16.76. Analytical HPLC retention time: 6.36 minutes. HR-ESI-MS $[M-H]^-$ calculated 794.1388, found 794.1381.

Synthesis of

((9-(4-((E)-4-((E)-4-(dimethylamino)styryl)styryl)-2-((((1-methylcyclopropane-1-carbonyl)oxy)methoxy)sulfonyl)phenyl)-3-oxo-3H-xanthen-6-yl)oxy)methyl 1-methylcyclopropane-1-carboxylate (VF-EX2)

In a 4 mL vial VF2.1.Cl (23.2 mg, 33.89 μmol, 1 equivalent) was dissolved in 203 μL of a 1.00 M solution of iodomethyl 1-methylcyclopropanecarboxylate in anhydrous *N,N*-dimethylformamide (203 μmol, 6 equivalents) and 35.4 μL of diisopropylethylamine (203 μmol, 6 equivalents). The reaction was stirred under N_2 at room temperature and monitored by LC-MS. After two and a half hours VF-EX2 and VF-EX1 were present in an approximately 1:1 ratio. An additional 4 equivalents of iodomethyl 1-methylcyclopropanecarboxylate were added. Two hours later the reaction was found to have reached completion. The reaction was neutralized with 50 μL of acetic acid and diluted with 2 mL of dimethylsulfoxide. The diluted reaction was purified by semi-preparative HPLC without further workup to obtain 9.83 mg of product (10.8 μmol) following evaporation of the mobile phase at a bath temperature of 60 °C and drying under high vacuum. ^{1}H NMR (900 MHz, $(CD_3)_2SO$) δ 8.20 (s, 1H), 7.93 (d, J = 8.4 Hz, 2H), 7.86 (d, J = 8.3 Hz, 2H), 7.81 (d, J = 7.7 Hz, 1H), 7.75 (d, J = 7.8 Hz, 2H), 7.68 (d, J = 7.8 Hz, 2H), 7.59 (s, 1H), 7.51 (d, J = 16.5 Hz, 1H), 7.49 (d, J = 16.4 Hz, 1H), 7.44 (d, J = 16.4 Hz, 1H), 7.40 (d, J = 16.4 Hz, 1H), 7.29 (d, J = 7.6 Hz, 1H), 7.07 (s, 1H), 6.98 (s, 1H), 6.46 (s, 1H), 6.00 (s, 2H), 5.72 (s, 2H), 3.64 (s, 6H), 1.24 (s, 3H), 1.18 – 1.14 (m, 2H), 1.11 (s, 3H), 0.95 (m, 2H), 0.83 (m, 2H), 0.78 – 0.75 (m, 2H). ^{13}C NMR (226 MHz, $(CD_3)_2SO$) δ 176.23, 173.73, 172.35, 158.15, 157.98, 157.73, 155.20, 151.41, 150.97, 147.38, 141.41, 139.18, 138.35, 136.79, 136.16, 132.45, 130.98, 130.09, 129.80, 129.71, 127.63, 127.51, 127.46, 127.27, 127.23, 126.64, 126.20, 125.45, 122.02, 118.41, 118.20, 117.03, 104.16, 102.83, 84.98, 84.01, 51.01, 18.64, 18.28, 18.24, 17.97, 17.01, 16.78, 16.75. Analytical HPLC retention time: 6.29 minutes. HR-ESI-MS $[M+H]^+$ calculated 908.2057, found 908.2079.

A minor peak (5.5% peak area by integration at 254 nm) with retention time 6.67 minutes can be observed eluting after the main product peak. This minor peak also has the correct product mass. It has been our experience that installing bulky esters at the 3 position of xanthene-based VoltageFuors leads to the formation of conformational isomers, and we believe that this is the case here.[20]

Synthesis of

2-(2,7-dichloro-6-((4-methoxybenzyl)oxy)-3-oxo-3H-xanthen-9-yl)-5-((E)-4-((E)-4-(dimethylamino)styryl)styryl)benzenesulfonic acid (VF2.1.Cl-PMB)

In a 20 mL scintillation vial dissolved VF2.1.Cl (107 mg, 156 μmol) and cesium carbonate (112 mg, 343 μmol) in 1 mL anhydrous *N,*N-dimethylformamide, followed by addition of 109 μL of 4-methoxybenzyl bromide (780 μmol). After stirring for 4 hours the reaction was diluted with 10 mL of H_2O which resulted in the precipitation of intermediate **1** as an orange solid. The precipitate was recovered by vacuum filtration and washed with approximately 5 mL of diethyl ether and employed without further purification.

1 was collected and dissolved in 4.5 mL of *N,N*-dimethylformamide and 1.5 mL of 1.0 M aqueous lithium hydroxide. The solution was stirred under N2 for five hours at 50 °C. The reaction was then diluted with 20 mL of H_2O and acidified with 1.75 mL of 1.0 M aqueous HCl. The aqueous solution was extracted with 40 mL of 10% isopropanol in dichloromethane. The organic phase was collected and washed twice with 10 mL of H_2O. The organic phase was dried over magnesium sulfate and solvents removed under reduced pressure. The resulting gum was then dissolved in 5 mL of dichloromethane. Addition of an equal volume of hexanes led to precipitation of an orange solid and solvents were again removed under reduced pressure. Obtained VF2.1.Cl-PMB (96.1 mg, 77%) as an orange solid. ^{1}H NMR (900 MHz, $(CD_3)_2SO$) δ 8.17 (s, 1H), 7.79 (d, J = 7.6 Hz, 1H), 7.66 (d, J = 7.8 Hz, 2H), 7.58 – 7.54 (m, 3H), 7.48 – 7.41 (m, 5H), 7.41 – 7.38 (m, 2H), 7.25 (d, J = 7.9 Hz, 1H), 7.19 (d, J = 16.5 Hz, 1H), 7.06 (s, 1H), 7.04 (d, J = 8.5 Hz, 1H), 7.01 (d, J = 8.5 Hz, 1H), 7.00 – 6.95 (m, 3H), 6.42 (s, 1H), 5.33 (s, 2H), 3.75 (s, 3H), 2.94 (s, 6H). ^{13}C NMR (226 MHz, $(CD_3)_2SO$) δ 176.08, 160.56, 159.32, 157.79, 157.63, 151.95, 151.62, 147.35, 138.49, 137.71, 135.10, 134.47, 132.45, 132.15, 130.04, 129.66, 129.36, 128.94, 127.60, 127.36, 127.18, 126.57, 126.46, 126.19, 125.34, 119.72, 118.46, 117.46, 115.62, 114.26, 114.21, 114.02, 113.61, 103.90, 101.64, 55.26, 55.09. Analytical HPLC retention time: 6.68 minutes. HR-ESI-MS $[M-H]^-$ calculated 802.1439, found 802.1411.

Synthesis of

(((2-(2,7-dichloro-6-hydroxy-3-oxo-3H-xanthen-9-yl)-5-((E)-4-((E)-4-(dimethylamino)styryl)styryl)phenyl)sulfonyl)oxy)methyl 1-methylcyclopropane-1-carboxylate (VF-EX0)

In a 20 mL scintillation vial dissolved VF2.1.Cl-PMB (83.9 mg, 104 µmol) and iodomethyl 1-methylcyclopropanecarboxylate (108 mg, 417 µmol) in 1 mL of anhydrous *N,N*-dimethylformamide, followed by addition of 72.6 µL of diisopropylethylamine (417 µmol). After stirring for 16 hours at room temperature the reaction was diluted with water and concentrated under reduced pressure at a bath temperature of 60 °C. The resulting gum was dissolved in approximately 1 mL of dichlorometane and precipitation induced by addition of approximately 3 mL of hexanes. The flocculent precipitate was collected by vacuum filtration to obtain VF-EX0 (45.3 mg, 47% crude yield) as an orange solid. Workup was accompanied by concomitant hydrolysis of the phenolic *p*-methoxybenzyl protecting group. A small aliquot for characterization was purified by semi-preparative HPLC. ^{1}H NMR (900 MHz, $(CD_3)_2SO$) δ 8.19 (s, 1H), 7.93 (d, J = 8.4 Hz, 2H), 7.86 (d, J = 8.3 Hz, 2H), 7.80 (d, J = 7.9 Hz, 1H), 7.75 (d, J = 7.8 Hz, 2H), 7.69 (d, J = 7.9 Hz, 2H), 7.51 (d, J = 16.6 Hz, 1H), 7.49 (d, J = 16.6 Hz, 1H), 7.43 (d, J = 16.4 Hz, 1H), 7.40 (d, J = 16.5 Hz, 1H), 7.26 (d, J = 7.8 Hz, 1H), 7.13 (s, 1H), 7.08 (s, 1H), 7.02 (s, 1H), 5.72 (s, 2H), 3.64 (s, 6H), 1.12 (s, 3H), 0.95 (s, 2H), 0.77 (s, 2H). ^{13}C NMR (226 MHz, $(CD_3)_2SO$) δ 172.83, 158.12, 157.99, 152.35, 147.80, 141.87, 139.65, 138.66, 137.34, 137.29, 136.61, 131.46, 130.57, 130.26, 130.24, 130.20, 130.18, 128.27, 128.13, 127.92, 127.74, 127.69, 127.02, 126.65, 125.97, 122.50, 84.47, 51.45, 18.71, 18.44, 17.47. Analytical HPLC retention time: 5.19 minutes. HR-ESI-MS $[M+H]^+$ calculated 796.1533, found 796.1526.

Synthesis of

2-(2,7-dichloro-6-(((1-methylcyclopropane-1-carbonyl)oxy)methoxy)-3-oxo-3H-xanthen-9-yl)-5-((E)-4-((E)-styryl)styryl)benzenesulfonic acid (VG-299c)

In a 20 mL dram vial dissolved VF2.0.Cl (18.0 mg, 28.06 µmol, 1 equiv.) in 500 µL *N,N*-dimethylformamide, then added iodomethyl 1-methylcyclopropanecarboxylate (39.6 µL, 281 µmol, 10 equiv.) and diisopropylethylamine (29.3 µL, 168 µmol, 6 equiv.). Precipitation was induced by addition of H_2O. Obtained 12.8 mg of crude product after vacuum filtration. Obtained 4.3 mg of red solid after purification by semi-preparative HPLC. ^{1}H NMR (600 MHz, $(CD_3)_2SO$) δ 7.96 (d, J = 8.2 Hz, 1H), 7.86 – 7.82 (m, 1H), 7.59 (m, J = 8.9, 3.8 Hz, 7H), 7.53 (s, 1H), 7.40 – 7.32 (m, 4H), 7.25 (m, J = 17.4, 11.0 Hz, 3H), 7.07 (s, 1H), 6.97 (s, 1H), 6.48 (s, 1H), 6.00 (d, J = 2.2 Hz, 2H), 3.31 (s, 6H), 1.24 (s, 3H), 1.17 – 1.14 (m, 2H), 0.83 (m, J = 3.3 Hz, 2H).

Scheme 3-1 Neuron-specific targeting with ester/esterase pairs (VF-EX)

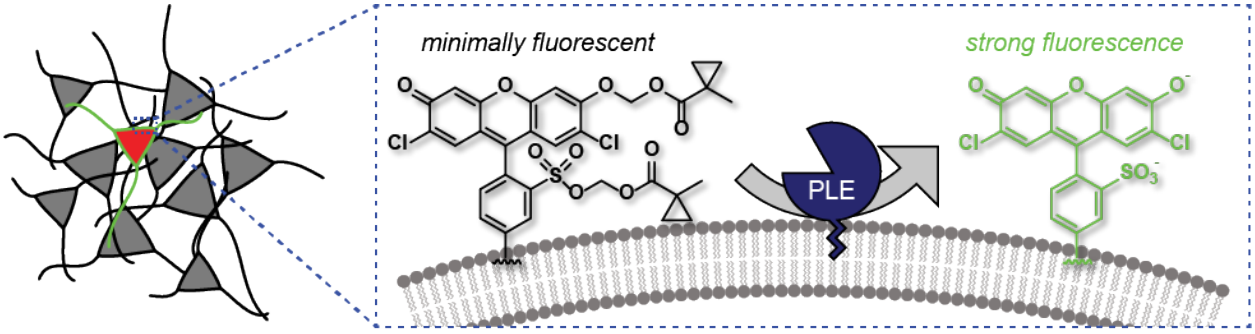

Scheme 3-1 Synthesis of VF-EX dyes and VG-299C

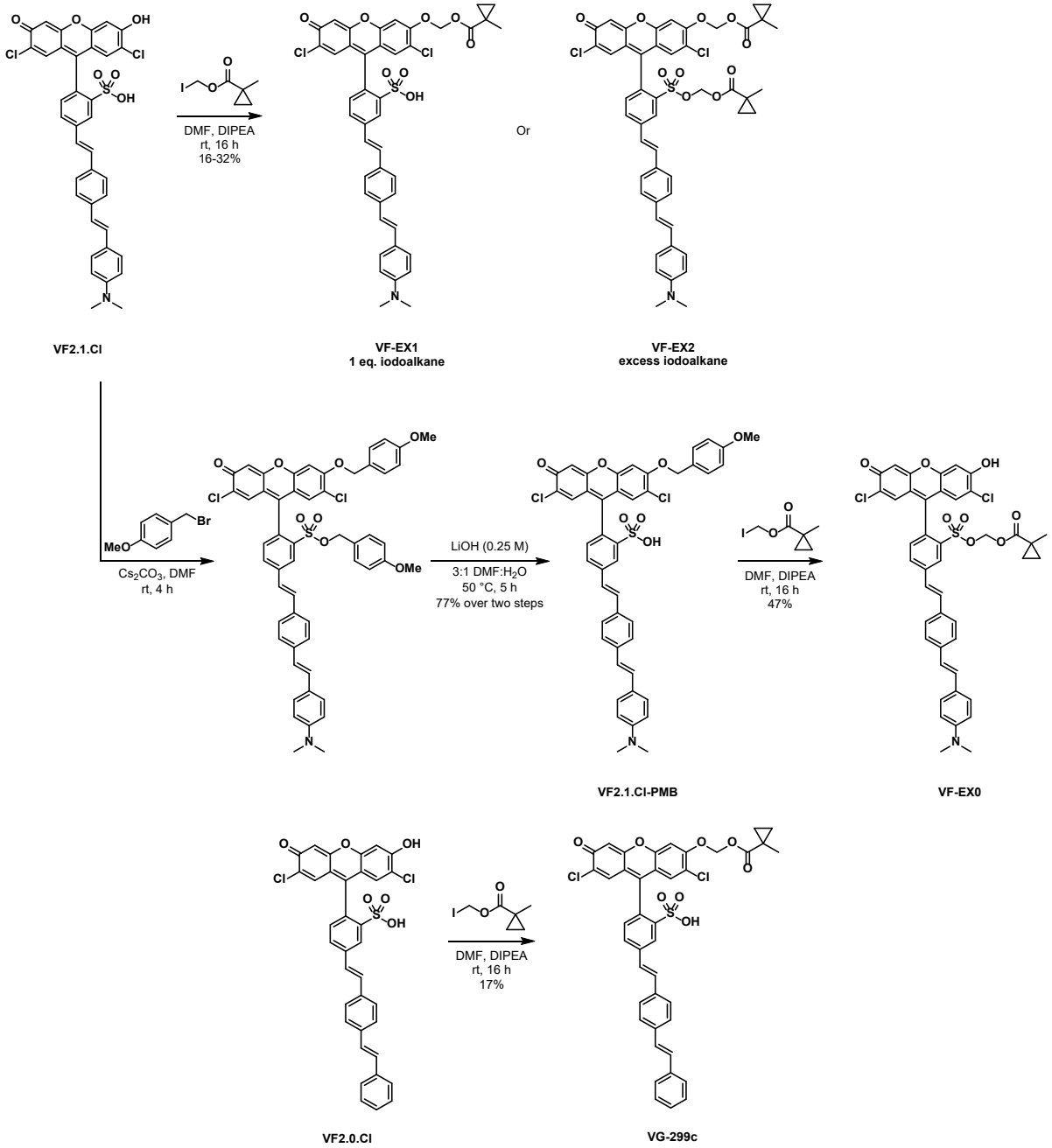

Figure 3-1 HPLC analysis of PLE reaction with VF-EX1 and VF-EX2

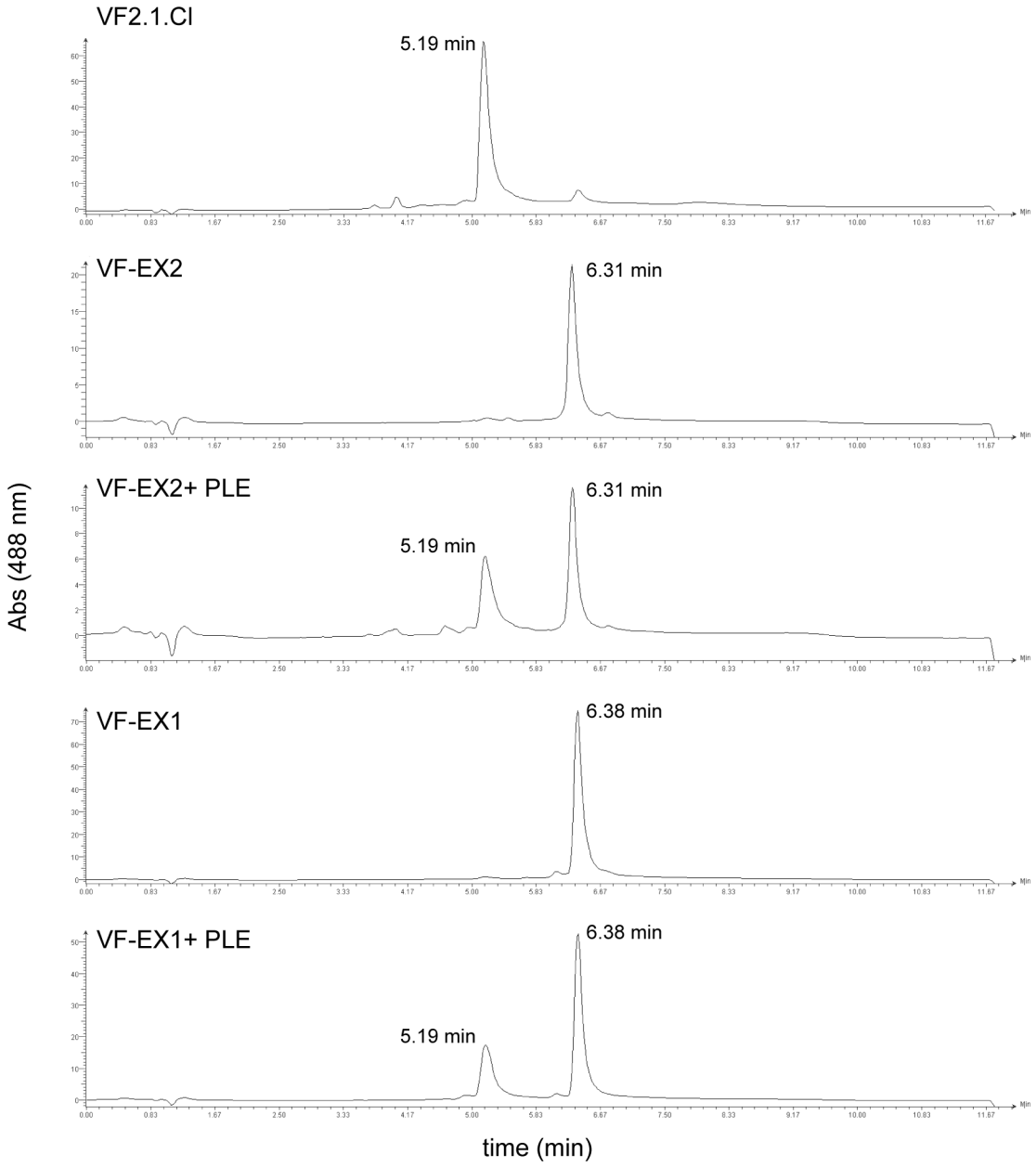

Figure 3-2 UV-Vis and fluorescence spectra of VF-EX dyes

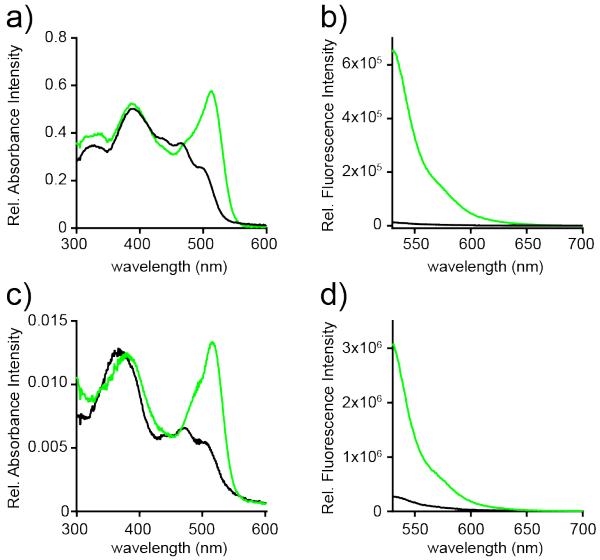

Spectroscopic characterization of VoltageFluor-EX 1 and 2. a,c) UV/vis absorption and b,d) fluorescence emission spectra of VF-EX1 (a,b) or VF-EX2 (d,e) in the absence (black line) or presence (green line) of purified porcine liver esterase (PLE, 0.7 mg/mL, 3 h). Excitation provided at 520 nm.

References

(1) Chyan, W.; Raines, R. T. *ACS Chem. Biol.* **2018**.

(2) Lavis, L. D.; Chao, T.-Y.; Raines, R. T. *Chem. Sci.* **2011**, *2* (3), 521–530.

(3) Tian, L.; Yang, Y.; Wysocki, L. M.; Arnold, A. C.; Hu, A.; Ravichandran, B.; Sternson, S. M.; Looger, L. L.; Lavis, L. D. *Proc. Natl. Acad. Sci. U. S. A.* **2012**, *109* (13), 4756–4761.

(4) Gao, W.; Xing, B.; Tsien, R. Y.; Rao, J. *J. Am. Chem. Soc.* **2003**, *125* (37), 11146–11147.

(5) Zlokarnik, G.; Negulescu, P. A.; Knapp, T. E.; Mere, L.; Burres, N.; Feng, L.; Whitney, M.; Roemer, K.; Tsien, R. Y. *Science (80-.).* **1998**, *279* (5347), 84–88.

(6) Kulkarni, R. U.; Kramer, D. J.; Pourmandi, N.; Karbasi, K.; Bateup, H. S.; Miller, E. W. *Proc. Natl. Acad. Sci.* **2017**, 201610791.

(7) Nuriya, M.; Jiang, J.; Nemet, B.; Eisenthal, K. B.; Yuste, R. *Proc. Natl. Acad. Sci. U. S. A.* **2006**, *103* (3), 786–790.

(8) Cartailler, J.; Kwon, T.; Yuste, R.; Holcman, D. *Neuron* **2018**, 1–11.

(9) Araya, R.; Andino-Pavlovsky, V.; Yuste, R.; Etchenique, R. *ACS Chem. Neurosci.* **2013**, *4* (8), 1163–1167.

(10) Hoppa, M. B.; Gouzer, G.; Armbruster, M.; Ryan, T. A. *Neuron* **2014**, *84* (4), 778–789.

(11) Beaulieu-Laroche, L.; Harnett, M. T. *Neuron* **2017**, 1–8.

(12) Hoyer, D.; Hannon, J. P.; Martin, G. R. *Pharmacol. Biochem. Behav.* **2002**, *71* (4), 533–554.

(13) Warther, D.; Gug, S.; Specht, a; Bolze, F.; Nicoud, J.-F.; Mourot, a; Goeldner, M. *Bioorg. Med. Chem.* **2010**, *18* (22), 7753–7758.

(14) Bort, G.; Gallavardin, T.; Ogden, D.; Dalko, P. I. *Angew. Chem. Int. Ed. Engl.* **2013**, *52* (17), 4526–4537.

(15) Kawaguchi, M.; Okabe, T.; Okudaira, S.; Hanaoka, K.; Fujikawa, Y.; Terai, T.; Komatsu, T.; Kojima, H.; Aoki, J.; Nagano, T. *J. Am. Chem. Soc.* **2011**, *133* (31), 12021–12030.

(16) Torii, S.; Tanaka, H.; Taniguchi, M.; Kameyama, Y. *Society* **1991**, No. 1 mL, 3633–3637.

(17) Miller, E. W.; Lin, J. Y.; Frady, E. P.; Steinbach, P. a; Kristan, W. B.; Tsien, R. Y. *Proc. Natl. Acad. Sci. U. S. A.* **2012**, *109* (6), 2114–2119.

(18) Tian, L.; Yang, Y.; Wysocki, L. M.; Arnold, A. C.; Hu, A.; Ravichandran, B.; Sternson, S. M.; Looger, L. L.; Lavis, L. D. **2012**, 2–7.

(19) Yamawaki, K.; Nomura, T.; Yasukata, T.; Tanimoto, N.; Uotani, K.; Miwa, H.; Yamano, Y.; Takeda, K.; Nishitani, Y. *Bioorganic Med. Chem.* **2008**, *16* (4), 1632–1647.

(20) Deal, P. E.; Kulkarni, R. U.; Al-Abdullatif, S. H.; Miller, E. W. *J. Am. Chem. Soc.* **2016**, *138* (29), 9085–9088.

Chapter 4

Spying on Neuronal Membrane Potential with Genetically Targetable Voltage Indicators

Portions of this work are available on the *ChemRxiv* preprint server, and are under review for publication in a scientific journal.

Grenier, V.; Daws, B. R.; Liu, P; Miller, E. W.; Spying on neuronal membrane potential with genetically tar-getable voltage indicators. *ChemRxiv*. **2018**, Preprint. DOI: 10.26434/chemrxiv.7313657.v1.

Portions of this work were completed in collaboration with others:

Brittany R. Daws synthesized VoltageSpy PEG_{11} (compound 20). Spectroscopic measurements were acquired in collaboration with Brittany R. Daws. Pei Liu provided Ace-2N-mNeon and ASAP2f plasmids, as well as the pcDNA3-synapsin vector.

Introduction

Cellular membrane potential, or voltage, is a key physiological parameter critically important to all aspects of life, but especially to excitable cells, like neurons. Optical methods to image voltage promise to relieve our dependence on classic electrode-based methods, which are highly invasive, often limited to single cells, and extremely low-throughput. Voltage-sensitive fluorescent indicators – either chemically synthesized or genetically encoded – offer an attractive solution for the direct observation of voltage dynamics in a minimally invasive, highly parallel, and high throughput manner.[1-2]

Pioneering work showed that many commercially available dyes possess voltage-sensitive optical properties.[3-5] Targeted synthesis of voltage-sensitive compounds yielded dyes with voltage sensitivity arising from an electrochromic interaction between the fluorophore and the electric field across the membrane, or Stark-effect.[6-7] These electrochromic dyes offer incredibly fast responses, but at the expense of relatively small shifts in their excitation/emission spectra. More recent versions display improved sensitivity but require torturous chemical syntheses.[8-9] Other chemical indicators include oxonol dyes which partition on the outer or inner leaflet of the plasma membrane in a voltage-dependent fashion. These dyes can give larger fractional changes in fluorescence, but oftentimes do not possess the required response kinetics to enable resolution of action potentials.[10-12] To address challenges associated with speed and sensitivity of chemical dyes, we were inspired by elegant theoretical models[13] and early experimental examples,[14] to explore photoinduced electron transfer (PeT) through molecular wires as a modality for voltage sensing. These voltage-sensitive fluorophores, or VoltageFluors, developed in our lab are amenable to voltage sensing across a wide range of colors, afford high voltage sensitivities (60% $\Delta F/F$ per 100 mV, in HEK cells), and maintain response times capable of clearly resolving action potential spikes in mammalian neurons.[15-19]

Completely genetically encoded approaches to voltage imaging offer a complementary method for voltage imaging.[20-21] Genetically encoded platforms for voltage imaging cluster into three groups: fluorescent proteins coupled to voltage sensing domains from ion channels and/or enzymes,[22-27] opsin-based indicators,[28-32] or hybrid opsin-fluorescent protein fusions.[33-35] Improved trafficking[36-37] of fluorescent protein-based indicators enabled considerable improvement over early, pioneering protein-based voltage indicators.[22-24] Yet despite progress in recent years, significant challenges remain regarding proper trafficking of heterologous proteins to the cell membrane, response speed, low brightness, added capacitance, and/or light induced ion pumping.

Hybrid chemical and genetic approaches to voltage imaging combine the speed and sensitivity of chemical indicators with the cell-type specificity of genetic model systems. Previous hybrid chemical-genetic methods for voltage sensing include hVOS indicators, in which an exogenously added, lipophilic anion partitions between inner and outer leaflets of the membrane in a voltage-dependent fashion to quench fluorescent protein fluorescence;[38-42] enzymatic localization in which genetically encoded phosphatases on the cell surface improve the membrane accumulation of a modified electrochromic dye;[43-45] electrochromic-FRET (eFRET), in which a fluorophore is selectively attached to an unnatural amino acid encoded on a voltage-sensitive opsin via Cu-mediated click chemistry;[46] and a fluorogenic approach from our lab in which a genetically encoded esterase unmasks a caged VF dye in defined neurons (VoltageFluor activated by esterase Expression, VF-EX).[47] These approaches suffer variously from the use of capacitance-adding

anions like dipicrylamine; low selectivity in cell uptake and difficult chemical syntheses; toxicity associated with Cu-mediated catalysis on neuronal surfaces and the requirement for expanded genetic codes; and/or low contrast between cells which express the targeting enzyme and the wild-type cells.

We hypothesized that we could address some of the shortcomings of our VF-EX targeting approach – specifically the low contrast between expressing and non-expressing cells – by covalently tethering VF dyes to a cell of interest (Scheme 4-1). A number of excellent approaches exist for the covalent labeling of modified enzymes.[48-52] All rely on a modified enzyme that will label itself with a small, chemical ligand. We envisioned that one of these self-labeling enzymes could be targeted to the cell surface of a neuron of interest to direct covalent capture of a VF dye modified with the cognate ligand. We were specifically attracted to the SpyTag/SpyCatcher system[52] that employs an engineered cell adhesion molecule from *Streptococcus pyogenes*. The SpyTag fragment is a small peptide (13 amino acid residues) that interacts with the SpyCatcher enzyme to form an isopeptide bond. We hoped that by linking the SpyTag peptide to a VF dye via a flexible polyethyleneglycol (PEG) linker, we could direct selective localization of VF dye only to those cells which express SpyCatcher on the cell surface. We additionally reasoned that use of the SpyTag peptide on VF would limit the amount of VF dye that passed through cell membranes, thus improving the membrane localization of the VF dye. Here, we show that SpyTag/SpyCatcher can be applied to a new VF scaffold to achieve fast and sensitive voltage imaging in genetically-defined neurons.

Results

Synthesis of sarcosine VoltageFluor dyes

The structure of the prototypical green VoltageFluor VF2.1.Cl (Scheme 4-1) does not lend itself to further synthetic modification. We recently reported a family of rhodamine-based voltage reporters (RhoVRs) which have a sarcosine amide at the 3 position of the meso aromatic ring, rather than an aryl sulfonate as in VF2.1.Cl.18,[53] The resultant free carboxylic acid offers a convenient handle for synthetic modification, maintains cellular impermeability, and is largely decoupled from the conjugated system of the phenylenevinylene molecular wire, making it a logical site for installing a targeting moiety (Scheme 4-1). We synthesized and characterized a new series of sarcosine-containing VoltageFluor dyes (**11-14**) (Scheme 4-2). Starting from isomerically pure 5- and 6-bromo-2',7'-dichlorofluorescein (**1**, **2**),[18,54] HATU-mediated amide couplings yielded *tert*-butyl ester protected intermediates **3** and **4** in 72 and 87% yield, respectively. Heck couplings with molecular wire fragments **5** or **6**[18] gave four *tert*-butyl ester protected VF-sarcosine compounds **7-10** in yields ranging from 53 to 83%. Removal of the *tert*-butyl ester with TFA gave sarcosinyl-VoltageFluors **11-14** in moderate to good yield (40%-99%) after purification by preparative TLC. We confirmed sarcosinyl-VoltageFluors and their synthetic precursors form stable rotamer pairs using VT-NMR (Figure 4-1). All four sarcosine VF dyes (Table 4-1) displayed similar optical properties, with absorption and emission maxima centered at 525 and 540 nm respectively. Quantum yields ranged from 0.008 (**12**) to 0.055 (**14**), in line with typical values for fluorescein-type VoltageFluors.[18-19]

Cellular characterization of sarcosine VoltageFluors

All the newly synthesized sarcosine VoltageFluors clearly labeled the plasma membranes of HEK cells (Figure 4-2, Figure 4-3) with variable fluorescence intensity. The brightest VF dye

was **13**, displaying cellular fluorescence 40-fold greater than the dimmest indicator, **12** (Table 4-1, Figure 4-3). The voltage sensitivity of VoltageFluor-sarcosine probes was determined by dual optical and electrophysiology in HEK cells (Figure 4-2). We delivered voltage steps from +100 to -100 mV volts in 20 mV increments to HEK293T in whole-cell voltage clamp while recording concomitant changes in fluorescence intensity over the cell body. Sarcosine VF **14** displayed the greatest voltage sensitivity, at 29% ΔF/F per 100 mV. The least sensitive was sarcosine VF **12**, at 12% ΔF/F. Because sarcosine VF **13** possessed high cellular brightness, good voltage sensitivity, and superior signal to noise ratios (SNR) for detecting depolarizing voltage steps in HEK cells (Table 4-1, Figure 4-2, Figure 4-3), we thought it a promising candidate for covalent attachment to cell surfaces via SpyTag/SpyCatcher interaction.

Design and synthesis of VoltageSpy Indicators

We envisioned that sarcosine VF **13** could be linked to the SpyTag peptide via a flexible PEG linker. The linker should be long enough to allow incorporation of the VF dye into the cell membrane. Because proper orientation of VF-type dyes in the cell membrane is critical for optimal voltage sensitivity,[17] the linker should ideally allow the dye to freely orient in the membrane. At the same time, a linker that is too long may increase the entropic penalty for incorporation of the VF dye into the membrane. To assess this, we coupled sarcosine VF **13** to PEG linkers of lengths ranging from 14 to 128 Å (PEG$_X$; X = 3, 11, 23, or 35, Scheme 4). Amide coupling of sarcosine VF **13** with heterobifunctional PEG linkers terminating with amino and azido groups provided VF-PEG$_X$-N$_3$ intermediates **15-18** in 59 to 99% yields. PEGylation of **13** resulted in a small, linker-length dependent redshift in the emission spectra, as well as an increase in quantum yield (Table 4-1, Figure 4-4). Copper catalyzed azide-alkyne cyclization of compounds **15-18** with SpyTag-alkyne, in which the native SpyTag 13-mer peptide (AHIVMVDAYKPTK) is modified to contain propargyl glycine (Pra) on the C-terminus, resulting in the 14-residue peptide, AHIVMVDAYKPTK-Pra (SpyTag-Pra), gave VF-PEG$_X$-SpyTags **19-22** in 3 to 22% yield after purification by reversed-phase, semi-preparative HPLC (Scheme 2-3).

Evaluation of VoltageSpy dyes in HEK cells

In order to evaluate the performance of the new VF-PEG$_X$-SpyTags (VoltageSpy dyes), we expressed SpyCatcher on the surface of HEK cells. The SpyCatcher protein, originally engineered from the second immunoglobulin-like collagen adhesion domain (CnaB2) from the fibronectin binding protein FbaB of *Streptococcus pyogenes*, forms a stable isopeptide bond with SpyTag.[52] We hypothesized that the new VF-PEG$_X$-SpyTag dyes would be dependent on the presence of cell-surface SpyCatcher for effective membrane staining. We fused the original SpyCatcher protein to an N-terminal PAT3-derived signal peptide[55] for efficient export from the cell and appended a C-terminal glycophosphatidyl inositol (GPI) anchor sequence derived from decay accelerating factor (DAF) (Figure 4-5).

SpyCatcher expression in HEK cells was confirmed by immunofluorescence directed against the hemagglutinin tag (HA) that was included at the N-terminus of the Spy-Catcher protein (Figure 4-6a-d). To readily identify living cells expressing SpyCatcher, we included a nuclear-localized mCherry on the same gene, linked through the self-cleaving T2A linker to provide stoichiometric expression of nuclear mCherry alongside cell-surface SpyCatcher (Figure 4-5, Figure 4-7). VF-PEG$_X$-SpyTag conjugates **19-22** all show membrane labeling, with high selectivity for SpyCatcher expressing HEK293T cells over neighboring, non-expressing cells (Figure 4-7, Figure 4-8). SpyCatcher permits the use of other signal peptides and transmembrane

domains; plasmids employing a signal peptide from immunoglobulin κ (IgK) and platelet-derived growth factor receptor (PDGFR) also showed good surface expression of SpyCatcher in HEK293T cells (Figure 4-6e-k). The inclusion of the SpyTag peptide is essential for membrane localization: azido-PEG precursors **15-18** all show some degree of cellular internalization (Figure 4-9).

SpyCatcher-mediated labeling of HEK cells

VoltageSpy labeling of live HEK293T cells provides good contrast between SpyCatcher-expressing and non-expressing cells (Figure 4-7a-h, Figure 4-8). At concentrations as low as 5 nM, dyes of all PEG lengths gave mean contrast ratios ranging from 5.6 (± 3.8, S.D., n = 77, PEG_3, VoltageSpy **19**) to 35 (± 29, S.D., n = 50, PEG_{35}, VoltageSpy **22**). At a higher concentration of VoltageSpy, 25 nM, contrast ratios decreased, ranging from 3.9 (± 1.9, S.D., n = 40, PEG_3, VoltageSpy **19**) to 13 (± 8.8, S.D., n = 87, PEG_{35}, VoltageSpy **22**). At 100 nM VoltageSpy, contrast ratios decreased further to 3 (±1.9, S.D., n = 41, PEG_{11}, VoltageSpy **20**) and 7 (± 4.1, S.D., n = 38, PEG_{35}, VoltageSpy **22**). The decrease in contrast ratio is driven by increasing amounts of non-specific VoltageSpy labeling at higher dye concentrations. This non-specific labeling is worse for short PEG linkers (x = 3, 11, VoltageSpy **19** and **20**) and is near negligible for the longer PEG linkers (x = 23, 35, VoltageSpy **21** and **22**) (Fig. S5b). The fluorescence intensities of SpyCatcher-expressing cells do not substantially increase with addition of more VoltageSpy dye, indicating near-saturation of available SpyCatcher binding sites, even at 5 nM VoltageSpy treatment (Figure 4-8a).

VoltageSpy dependence on SpyCatcher

VoltageSpy labeling depends on the expression of cell-surface SpyCatcher. Cellular VoltageSpy labeling could be blocked by preincubation of SpyCatcher-expressing cells with unlabeled SpyTag-peptide[52] (Figure 4-10). When VoltageSpy **20** (PEG_{11}) was applied to SpyCatcher-expressing cells pre-treated with 10 μM SpyTag-Pra[52], we observed a 62 % decrease in membrane-associated fluorescence (Figure 4-10). The large excess of unlabeled SpyTag-Pra[52] required to block nM concentrations of VoltageSpy suggests that the presence of a lipophilic molecular wire increases the labeling speed of VoltageSpy dyes. We find that SpyTag conjugated to a simple dichlorofluorescein (Fig. S8, DCF-PEG_{11}-SpyTag, **24**) applied at 100 nM gave only poor labeling of HEK cells, where μM concentrations of **24** were required to achieve appreciable labeling of SpyCatcher-expressing cells (Figure 4-11). However, in the absence of the lipophilic molecular wire, almost no off-target labeling was observed.

VoltageSpy labels extracellular membrane surfaces

The majority of the cellular fluorescence is associated with the extracellular face of the membrane. Treatment of VoltageSpy-labeled HEK cells (**22**, PEG_{35}, 5 nM) with Trypan Blue (0.1%) to quench extracellularly-associated fluorescence[56] results in a 79% decrease in fluorescence intensity (Figure 4-12). In contrast, Trypan Blue treatment does not substantially decrease the fluorescence of a cytosolic fluorescent indicator, Oregon Green BAPTA (Figure 4-12), establishing that the majority of VoltageSpy fluorescence is associated with the external face of the plasma membrane. In this regard, VoltageSpy circumvents a common problem observed with genetically encoded voltage indicators; the presence of a substantial intracellular pool of improperly-trafficked fluorophores which contribute a non-responsive background signal.[36-37] Poor trafficking stymied the wide adoption of first-generation GEVIs,[22-24, 36-37] and improvements

to the trafficking and sub-cellular targeting of GEVIs continue to advance the usefulness of fluorescent GEVIs.[32]

VoltageSpy dyes are voltage-sensitive after labeling SpyCatcher expressing cells (Figure 4-7). VoltageSpy dyes **19-22** are all equally voltage sensitive, with a response of 12% ΔF/F per 100 mV (Table 4-1, Figure 4-13). We hypothesize that the small size of the SpyCatcher protein and the conformational flexibility of the C-terminus of SpyCatcher[57] enables even a PEG_3 linker (approximately 14 Å) to allow a VF dye to insert into the plasma membrane. Additionally, the final 3 amino acid residues of SpyTag project away from and do not form hydrogen bonds with SpyCatcher in the crystal structure,[57] providing additional flexibility for a tethered VF to reach the membrane.

VoltageSpy in Neurons

In neurons, VoltageSpy dyes recapitulate the selective staining observed in HEK293T cells. Using immunocytochemistry, we verified that the PAT3 signal sequence and the GPI sequence from DAF under control of the human synapsin promoter gave good cell surface expression of SpyCatcher in cultured rat hippocampal neurons (Figure 4-14). A combination of live-cell imaging followed by fixation and immunocytochemistry confirm the high specificity of the VoltageSpy/SpyCatcher interaction in neurons (Figure 4-14). Following live-cell staining with VoltageSpy **20** (PEG_{11}), membrane-associated VoltageSpy fluorescence survived fixation Figure 4-14e,f) to establish good correlation between VoltageSpy localization and HA-epitope staining of SpyCatcher (Figure 4-14g-j). Live-cell imaging in neurons stained with VoltageSpy dyes (PEG_{11}, VoltageSpy **20**, Figure 4-15a-d; and PEG_{35}, VoltageSpy **22**, Figure 4-15e-h) showed good selectivity for SpyCatcher-expressing neurons over non-expressing cells, with contrast ratios of approximately 5, across PEG lengths and concentrations (Figure 4-16). The contrast in neurons varied widely, owing to differences in SpyCatcher expression. The brightest neurons stained with VoltageSpy indicators possessed contrast ratios of approximately 25-fold over non-transfected cells, a 5-fold increase over contrast we achieved using fluorogenic VF dyes (~4-fold in neurons).[47] We selected the brightest cells for subsequent imaging analysis.

Functional imaging with VoltageSpy in neurons

VoltageSpy dyes clearly report on action potentials from neurons expressing SpyCatcher. Under low-light illumination conditions (8 mW/mm^2) we successfully recorded spontaneous activity in cultured neurons with good signal to noise (Figure 4-15i). Both VoltageSpy **20** (PEG_{11}) and VoltageSpy **22** (PEG_{35}) readily recorded action potential spikes, with sensitivities of 11.6 ±1.3% and 11.1 ±1.4% ΔF/F, respectively (Figure 4-15i, values are for n = 15 neurons and represent mean ± standard deviation, recorded at 500 Hz). The selectivity of targeting, lack of linker-length dependence on voltage sensitivity, and ΔF/F values in neurons match well with VoltageSpy performance in HEK cells. Dual optical and electrophysiological recordings of VoltageSpy **22** (PEG_{35}) reveal that targeted indicators faithfully report underlying action potential dynamics with no lag time (Figure 4-15j-l). Additionally, we established that the presence of either SpyCatcher alone or SpyCatcher + VoltageSpy did not alter neuronal membrane properties; we saw no difference in membrane capacitance, resting membrane potential, or action potential kinetics (Figure 4-17).

VoltageSpy **22** (PEG_{35}) performs well in neurons, compared to other genetically encoded voltage indicators. VoltageSpy dyes possessed excellent sensitivity, detecting evoked action

potential with 9.7 ± 1.5% ΔF/F, compared to -2.7 ± 0.6% for ASAP2f,[58] a fluorescent protein-based indicator, and -3.4 ± 0.9% for Ace2N-mNeon,[59] an electrochromic FRET-based indicator (Figure 4-18) when all three indicators were imaged under identical conditions. Both ASAP2f and Ace2N-mNeon displayed negative-going responses to membrane depolarization, as a result of their sensing mechanism.[59-60] The SNR of VoltageSpy **22** for action potentials is 7.7 ± 1.9, comparable to Ace2N-mNeon (7.1 ± 1.1) and substantially larger than ASAP2f (4.4 ± 0.5) (Figure 4-18f). Much of the fluorescence of the genetically encoded indicators comes from fluorescence associated with internal structures – not the plasma membrane (Figure 4-18a-c, Figure 4-19). This highlights again a unique advantage of a hybrid approach in which a voltage-sensitive fluorophore is appended to a non-fluorescent genetically-encoded membrane target: in the hybrid case of VoltageSpy/SpyCatcher, poorly-trafficked proteins are invisible and do not contribute to unproductive background fluorescence.

Imaging sub-cellular voltage dynamics

Measurements of the electronic properties of pre- and post-synaptic sites in neurons have been a tremendous, long-standing experimental challenge in neuroscience. Patching pre-synaptic boutons is difficult, and dendritic spines are inaccessible to electrophysiology. These structures therefore provide a unique opportunity where optical tools are the only viable existing method for interrogating their biology. The electric properties of dendrites have previously been probed with VSDs, but requires laborious internal loading of dyes via patch pipette.[61-65] GEVIs have been also been employed to interrogate pre- and post-synaptic biology, but the slow kinetics and low brightness of GEVIs make these experiments challenging.[66]

By employing the speed and sensitivity of VF dyes with genetic targeting of the SpyTag/SpyCatcher system, we can readily image sub-cellular voltage dynamics in cultured hippocampal neurons. Application of 5 nM VoltageSpy **22** (PEG_{35}) results in clear, membrane-associated fluorescent restricted to SpyCatcher-expressing neurons indicated by nuclear mCherry (Figure 4-20a). VoltageSpy labeling discriminates sub-cellular dendritic morphology – peripheral regions of dendrites are brighter than the internal cytosolic component (Figure 4-20b) – and micron-sized structures, dendritic spines, are visible (Figure 4-20b). Single-trial (no stimulus-timed averaging used) optical recordings of a train of 25 evoked action potentials imaged at dendritic sites (purple, green, and blue ROIs, Figure 4-20c) reveal clear action potentials (Figure 4-20d). VoltageSpy dyes enable remote monitoring of voltage dynamics in sub-cellular regions 60 to 90 μm away from neuronal soma, the site of traditional electrophysiological recordings (Figure 4-20d). In this way, genetically targeted VoltageSpy circumvents space clamp errors[67] associated with measuring voltage changes in structures that are not close to the neuronal cell body. In a complementary fashion, VoltageSpy **20** (PEG_{11}) can also image voltage dynamics in pre-synaptic structures associated with axon terminals (Figure 4-20e-g). The cellular specificity of the VoltageSpy/SpyCatcher interaction enables tracing of extensive axonal tracks (Figure 4-20e). Zooming in on the boxed region reveals the fine structure of an axon, several hundred microns distant from the nearest cell body (Figure 4-20f). Single-trial, high speed imaging of 25 evoked action potentials clearly resolves fast voltage dynamics in a micron-sized axonal terminal hundreds of micrometers away from the neuronal soma (Figure 4-20g).

Conclusion

In conclusion, we show that voltage-sensitive fluorescent dyes can be covalently appended to the cell surface of mammalian cells and neurons, affording the opportunity for voltage imaging

in genetically-defined cells or in sub-cellular regions of interest. The best of the newly-synthesized, sarcosine-containing VoltageFluors is readily functionalized with a PEG linker terminating with the SpyTag ligand. Localization of this VoltageSpy is determined by the expression of the SpyCatcher protein on cell surfaces. In this way, the speed and sensitivity of fluorescein-based voltage-sensitive fluorophores can be coupled with a genetically encoded component. This hybrid approach readily detects voltage changes in cultured cells and mammalian neurons. VoltageSpy performs well in cultured neurons, displaying up to 25-fold increase in staining in SpyCatcher-expressing cells, and reporting on action potentials with higher sensitivity than commonly used genetically encoded voltage indicators. Using VoltageSpy, voltage dynamics in sub-cellular structures are readily observable in single trial experiments. Looking forward, we aim to expand the palette of available VoltageSpy dyes by engaging carboxylate-containing rhodamine-based voltage reporters (RhoVRs),[53] develop new chemistries to target far-red dyes,[15] apply next-generation SpyTag/SpyCatcher constructs,[68] and mix and match complementary covalent targeting strategies[48-52] with our existing palette of voltage-sensitive dyes for multiplexed imaging in complex neural tissue.

General Synthetic and Analytical Methods

Chemical reagents and solvents were purchased from commercial suppliers and used without further purification. Synthesis of 5-bromo-2',7'-dichlorofluorescein **1**, 6-bromo-2',7'-dichlorofluorescein **2**, and molecular wires **5** and **6** were adapted from existing procedures.[18,54] SpyTag-Pra was purchased from Genscript. Thin layer chromatography (TLC) and preparative thin layer chromatography (PTLC) was performed on glass backed plates pre-coated with silica gel (Silicyle, F254, 250 μm (TLC) or 1000 μm (PTLC)). Plates were visualized by fluorescence quenching under UV light. Flash column chromatography was performed on Silicycle Silica Flash F60 (230–400 Mesh) using a forced flow of air at 0.5–1.0 bar.

^{1}H spectra were collected in DMSO-d_6 at 25 °C on a Bruker AV-600 spectrometer at the College of Chemistry NMR Facility at the University of California, Berkeley, or at the QB3 Central California 900 MHz NMR Facility, with assistance from Dr. Jeffrey Pelton. Variable temperature NMR data was measured on a DRX-500 spectrometer at the College of Chemistry NMR Facility. All chemical shifts are reported in the standard δ notation of parts per million using the peak of residual proton signals of DMSO-d_6 as an internal reference. High resolution mass spectra (HR-ESI-MS) were acquired at the QB3/Chemistry Mass Spectrometry Facility at the University of California, Berkeley. Low resolution LC/ESI-MS was performed on an Advion Expression LC-MS coupled to an Agilent Infinity 1220 HPLC, with a Phenomenex Luna 5 μm C18(2) 75 x 4.6 mm column. Semi-preparative HPLC was performed on a Perkin Elmer Series 200 HPLC, with a Phenomonex Luna 5 μm C18(2) 150 x 10 mm column. In both cases water (eluent A) and acetonitrile (eluent B) were employed as the mobile phase, with 0.05% trifluoroacetic acid present as an additive. For analytical HPLC the mobile phase was ramped from 10 to 100% eluent A over eight minutes, then held at 100% A for two minutes at a flow rate of 1.0 mL/minute. For semi-preparative HPLC the mobile phase was ramped from 10 to 100% eluent A over twenty minutes at 5.0 mL/minute.

Spectroscopic studies

Stock solutions of dyes were prepared in DMF or DMSO and diluted with HBSS (zero Ca^{2+}, zero Mg^{2+}, no phenol red, pH 7.4). UV-Vis absorbance and fluorescence spectra were recorded using a Shimadzu 2501 Spectrophotometer (Shimadzu) and a Quantamaster Master 4 L-

format scanning spectrofluorometer (Photon Technologies International). The fluorometer is equipped with an LPS-220B 75-W xenon lamp and power supply, A-1010B lamp housing with integrated igniter, switchable 814 photon-counting/analog photomultiplier detection unit, and MD5020 motor driver. Samples were measured in 1-cm path length quartz cuvettes (Starna Cells). All measurements were done at room temperature.

Cell culture, transfection, and dye loading

All animal procedures were approved by the UC Berkeley Animal Care and Use Committees and conformed to the NIH Guide for the Care and Use of Laboratory Animals and the Public Health Service (PHS) Policy.

Human embryonic kidney 293T (HEK) cells were maintained in Dulbecco's modified eagle medium (DMEM) supplemented with 4.5 g/L D-glucose, 10% fetal bovine serum (FBS; Thermo Scientific) and 1% GlutaMax (Invitrogen) at 37 °C in a humidified incubator with 5 % CO_2. Cells were plated in either high glucose DMEM (as above) or low glucose DMEM (1 g/L D-glucose, 10% FBS, 1% GlutaMax, for electrophysiology) at a density of 50 000 to 75 000 cells per well on 12 mm coverslips pre-coated with Poly-D-Lysine (PDL; 1 mg/mL; Sigma-Aldrich) in a 24-well plate. Transfection of plasmids was carried out using Lipofectamine 3000 (with P3000 reagent) 1 to 4 hours after plating.

Hippocampi were dissected from embryonic day 19 Sprague Dawley rats (Charles River Laboratory) in cold, sterile HBSS (zero Ca^{2+}, zero Mg^{2+}, phenol red). All dissection products were supplied by Invitrogen, unless otherwise stated. Hippocampal tissue was treated with trypsin (2.5%) for 15 min at 37 °C. The tissue was triturated using fire polished Pasteur pipettes, in minimum essential media (MEM) supplemented with 5% FBS, 2% B-27, 2% 1M dextrose (Fisher Scientific) and 1% GlutaMax. The dissociated cells were plated onto 12 mm diameter coverslips (Fisher Scientific) pre-treated with PDL (as above) at a density of 25-30,000 cells per coverslip in MEM supplemented media (as above). Neurons were maintained at 37 °C in a humidified incubator with 5 % CO_2. At 1 day *in vitro* (DIV) half of the MEM supplemented media was removed and replaced with Neurobasal media containing 2% B-27 supplement and 1% GlutaMax. Transfection of plasmids was carried out using Lipofectamine 3000 (without P3000 reagent) at 6-7 DIV. Imaging was performed on mature neurons 12-16 DIV.

Unless stated otherwise, for loading of HEK cells and hippocampal neurons, DMF or DMSO stock solutions of dyes were diluted in HBSS to working concentrations. All imaging experiments were performed in HBSS at room temperature.

Epifluorescence microscopy

Imaging was performed on an AxioExaminer Z-1 (Zeiss) equipped with a Spectra-X Light engine LED light (Lumencor), controlled with Slidebook (v6, Intelligent Imaging Innovations) or μManager (Open Imaging). Images were acquired with a W-Plan-Apo 20x/1.0 water objective (20x; Zeiss). Images were focused onto either an OrcaFlash4.0 sCMOS camera (sCMOS; Hamamatsu) or an eVolve 128 EMCCD camera (EMCCD; Photometrix. For imaging VoltageFluor dyes, excitation light was delivered at 475 nM (LED, 475 nm, 34 nm bandpass) and emission was collected with a 540/50 nm bandpass filter after passing through a 510 nm longpass dichroic. For imaging mCherry, excitation was delivered at 542 nm (LED, 542 nm, 33 nm

bandpass) and emission was collected with a 650/50 bandpass filter after passing through a 594 nm longpass dichroic.

Electrophysiology

For electrophysiological experiments, pipettes were pulled from borosilicate glass (Sutter Instruments, BF150-86-10), with a resistance of 5–6 MΩ, and were filled with an internal solution; 125 mM potassium gluconate, 1 mM EGTA tetrasodium salt, 10 mM HEPES, 5 mM NaCl, 10 mM KCl, 2 mM ATP disodium salt, 0.3 mM GTP trisodium salt (pH 7.25, 275 mOsm). Recordings were obtained with an Axopatch 200B amplifier (Molecular Devices) at room temperature. The signals were digitized with a Digidata 1440A, sampled at 50 kHz and recorded with pCLAMP 10 software (Molecular Devices) on a PC. Fast capacitance was compensated in the on-cell configuration. For all electrophysiology experiments, recordings were only pursued if series resistance in voltage clamp was less than 15 MΩ for HEK293T cells, or 30 MΩ for cultured neurons.

For whole-cell, voltage clamp recordings in HEK 293T cells, cells were held at -60 mV and hyper- and de- polarizing steps applied from -100 to +100 mV in 20 mV increments. Optical traces were acquired under 21 mW/mm^2 illumination, and captured on an eVolve 128 EMCCD with 4x4 binning at a framerate of 500 Hz.

For whole-cell, current clamp experiments in cultured neurons, we delivered 10 successive 50 ms, 0.05 pA current injection. Resting membrane potential, action potential amplitude and kinetic parameters were extracted in Clampfit 10 (Molecular Devices). For cells labeled with VF-PEG$_{35}$-SpyTag **22,** recordings were acquired under constant 8 mW/mm^2 illumination at 475 nm. Optical traces were acquired at 1 kHz on an OrcaFlash4.0 sCMOS camera, with 4x4 binning.

Extracellular field stimulation and imaging spontaneous activity

Extracellular field stimulation was delivered by a SD9 Grass Stimulator connected to a recording chamber containing two platinum electrodes (Warner), with triggering provided through the same Digidata 1440A digitizer and pCLAMP 10 software (Molecular Devices) that ran the electrophysiology. To prevent recurrent activity the HBSS bath solution was supplemented with synaptic blockers 10 μM 2,3-Dioxo-6-nitro-1,2,3,4-tetrahydrobenzo[f]quinoxaline-7-sulfonamide (NBQX; Santa Cruz Biotechnology) and 25 μM DL-2-Amino-5-phosphonopentanoic acid (APV; Sigma-Aldrich). Optical recordings of evoked activity from VoltageSpy dyes and genetically encoded voltage indicators were captured on an OrcaFlash4.0 sCMOS camera at 500 Hz, in a restricted 2048x400 imaging window, with 4x4 binning and 15 mW/mm^2 illumination. To enable imaging at 1.2 kHz in subcellular regions of interest, optical traces were captured on an OrcaFlash4.0 sCMOS in a restricted 2048x400 imaging window, with 4x4 binning, 150 mW/mm^2 illumination, controlled in μManager (Slidebook does not support sub-millisecond imaging with the OrcaFlash4.0).

Optical recordings of spontaneous activity were captured on an OrcaFlash4.0 sCMOS camera at 500 Hz, in a restricted 2048x400 imaging window, with 4x4 binning and 8 mW/mm^2 illumination.

Image analysis

For fluorescence intensity measurements, images were corrected for uneven illumination through pseudo flat-field correction by subtracting a Gaussian-blurred version of an image from the original using the BioVoxxel Toolbox in FIJI.. Regions of interest were drawn around cells or neuronal cell bodies and the mean fluorescence was calculated in ImageJ (FIJI, NIH). Background fluorescence was subtracted by measuring the fluorescence where no cells grew. Contrast was calculated by dividing the fluorescence intensity of transfected, VoltageSpy labeled, cells by the median fluorescence intensity of untransfected cells on the same coverslip, both background subtracted. In cultured neurons, data was accumulated across three different preparations.

Analysis of voltage sensitivity in HEK cells was performed using ImageJ (FIJI). A region of interest (ROI) was selected and applied as a mask to all image frames. Fluorescence intensity values were calculated at known baseline and voltage step epochs. For analysis of voltage responses in neurons, regions of interest encompassing cell bodies (all of approximately the same size) were drawn in ImageJ and the mean fluorescence intensity for each frame extracted. ΔF/F values were calculated by first subtracting a mean background value from all raw fluorescence frames to give a background subtracted trace. A least squares linear regression was fit to the background subtracted trace and a bleaching curve, derived from the slope of the regression, was used to correct for photobleaching. A baseline fluorescence value (F_{base}) was calculated from the median of all the frames and was subtracted from each timepoint of the bleach corrected trace to yield a ΔF trace. The ΔF was then divided by F_{base} to give ΔF/F traces. No averaging was applied to any voltage traces.

Trypan Blue quenching of extracellular fluorescence

HEK293T cells were plated in at a density of 125 000 cells per dish in 35 mm glass bottom gridded dishes (Ibidi). Imaging was performed on an AxioObserver Z-1 (Zeiss) equipped with a Spectra-X Light engine LED light (Lumencor), controlled with μManager. Images were acquired with a Plan-Achromat 20X/0.8 water objective (Zeiss). Images were focused onto a OrcaFlash4.0 sCMOS camera (sCMOS; Hamamatsu). Excitation light was delivered at 475 nM (LED, 475 nm, 34 nm bandpass) and emission was collected with a 540/50 nm bandpass filter after passing through a 510 nm longpass dichroic. Cells were imaged immediately after replacing HBSS with 0.1% Trypan Blue in HBSS (diluted from 0.4% Trypan Blue in PBS (Gibco)).

Plasmid construction

For expression in HEK cells, SpyCatcher with a PAT3 signal peptide, N-terminal HA tag and C-terminal decay accelerating factor (DAF) was subcloned into a pCAGS vector. For expression in neurons SpyCatcher was subcloned into a pCDNA3 vector with a human synapsin promoter (Syn) and a regulatory element from the woodchuck hepatitis virus (WPRE). Nuclear-targeted mCherry (NLS-mCherry) was inserted downstream of SpyCatcher, separated by a self-cleaving T2A sequence. The following sequences were used (5' to 3'):

PAT3

ATGCCACCTTCTACTAGTCTTTTGTTGCTTGCTGCACTTCTCCCCTTCGCTCTTCCCGC
TTCAGATTGGAAGACAGGAGAAGTCACC

HA

TATCCATATGATGTTCCAGATTATGCT

His6-SpyCatcher

ATGTCGTACTACCATCACCATCACCATCACGATTACGACATCCCAACGACCGAAAAC
CTGTATTTTCAGGGCGCCATGGTTGATACCTTATCAGGTTTATCAAGTGAGCAAGGT
CAGTCCGGTGATATGACAATTGAAGAAGATAGTGCTACCCATATTAAATTCTCAAAA
CGTGATGAGGACGGCAAAGAGTTAGCTGGTGCAACTATGGAGTTGCGTGATTCATCT
GGTAAAACTATTAGTACATGGATTTCAGATGGACAAGTGAAAGATTTCTACCTGTAT
CCAGGAAAATATACATTTGTCGAAACCGCAGCACCAGACGGTTATGAGGTAGCAAC
TGCTATTACCTTTACAGTTAATGAGCAAGGTCAGGTTACTGTAAATGGCAAAGCAAC
TAAAGGTGACGCTCATATT

DAF

CCAAATAAAGGAAGTGGAACCACTTCAGGTACTACCCGTCTTCTATCTGGGCACACG
TGTTTCACGTTGACAGGTTTGCTTGGGACGCTAGTAACCATGGGCTTGCTGACTTAG

T2A

GAGGGTCGGGGCTCTCTGCTCACATGTGGCGACGTCGAGGAGAATCCCGGACCGGC
CCCGGGGTCGACA

NLS-mCherry

ATGGTGCCCAAGAAGAAGAGGAAAGTCGTGAGCAAGGGCGAGGAGGACAACATGG
CCATCATCAAGGAGTTCATGCGCTTCAAGGTGCACATGGAGGGCTCCGTGAACGGC
CACGAGTTCGAGATCGAGGGCGAGGGCGAGGGCCGCCCCTACGAGGGCACCCAGA
CCGCCAAGCTGAAGGTGACCAAGGGCGGCCCCCTGCCCTTCGCCTGGGACATCCTGT
CCCCTCAGTTCATGTACGGCTCCAAGGCCTACGTGAAGCACCCCGCCGACATCCCCG
ACTACTTGAAGCTGTCCTTCCCCGAGGGCTTCAAGTGGGAGCGCGTGATGAACTTCG
AGGACGGCGGCGTGGTGACCGTGACCCAGGACTCCTCCCTGCAGGACGGCGAGTTC
ATCTACAAGGTGAAGCTGCGCGGCACCAACTTCCCCTCCGACGGCCCCGTAATGCA
GAAGAAGACCATGGGCTGGGAGGCCTCCTCCGAGCGGATGTACCCCGAGGACGGCG
CCCTGAAGGGCGAGATCAAGCAGAGGCTGAAGCTGAAGGACGGCGGCCACTACGA
CGCCGAGGTCAAGACCACCTACAAGGCCAAGAAGCCCGTGCAGCTGCCCGGCGCCT
ACAACGTCAACATCAAGCTGGACATCACCTCCCACAACGAGGACTACACCATCGTG
GAACAGTACGAGCGCGCCGAGGGCCGCCACTCCACCGGCGGCATGGACGAGCTGTA
CAAG

WPRE

GCTTATCGATAATCAACCTCTGGATTACAAAATTTGTGAAAGATTGACTGGTATTCT
TAACTATGTTGCTCCTTTTACGCTATGTGGATACGCTGCTTTAATGCCTTTGTATCAT
GCTATTGCTTCCCGTATGGCTTTCATTTTCTCCTCCTTGTATAAATCCTGGTTGCTGTC
TCTTTATGAGGAGTTGTGGCCCGTTGTCAGGCAACGTGGCGTGGTGTGCACTGTGTT
TGCTGACGCAACCCCCACTGGTTGGGGCATTGCCACCACCTGTCAGCTCCTTTCCGG
GACTTTCGCTTTCCCCCTCCCTATTGCCACGGCGGAACTCATCGCCGCCTGCCTTGCC
CGCTGCTGGACAGGGGCTCGGCTGTTGGGCACTGACAATTCCGTGGTGTTGTCGGGG

AAATCATCGTCCTTTCCTTGGCTGCTCGCCTGTGTTGCCACCTGGATTCTGCGCGGGA
CGTCCTTCTGCTACGTCCCTTCGGCCCTCAATCCAGCGGACCTTCCTTCCCGCGGCCT
GCTGCCGGCTCTGCGGCCTCTTCCGCGTCTTCGCCTTCGCCCTCAGACGAGTCGGAT
CTCCCTTTGGGCCGCCTCCCCGCATCGATACCG

Synapsin Promoter

GTGTCTAGACTGCAGAGGGCCCTGCGTATGAGTGCAAGTGGGTTTTAGGACCAGGA
TGAGGCGGGGTGGGGGTGCCTACCTGACGACCGACCCCGACCCACTGGACAAGCAC
CCAACCCCCATTCCCCAAATTGCGCATCCCCTATCAGAGAGGGGGAGGGGAAACAG
GATGCGGCGAGGCGCGTGCGCACTGCCAGCTTCAGCACCGCGGACAGTGCCTTCGC
CCCCGCCTGGCGGCGCGCGCCACCGCCGCCTCAGCACTGAAGGCGCGCTGACGTCA
CTCGCCGGTCCCCCGCAAACTCCCCTTCCCGGCCACCTTGGTCGCGTCCGCGCCGCC
GCCGGCCCAGCCGGACCGCACCACGCGAGGCGCGAGATAGGGGGGCACGGGCGCG
ACCATCTGCGCTGCGGCGCCGGCGACTCAGCGCTGCCTCAGTCTGCGGTGGGCAGC
GGAGGAGTCGTGTCGTGCCTGAGAGCGCAGTCGAGA

Immunocytochemistry

To detect expression and localization of SpyCatcher, HEK cells or neurons were fixed with 4% paraformaldehyde in PBS for 10 min and permeabilized (if required) with 0.3% v/v Triton-X100 (Sigma Aldrich) in PBS for 2 min. Blocking was done in 5% w/v bovine serum albumin (BSA; Sigma Aldrich) in PBS for 1 h. Primary antibody was incubated at 4 °C overnight, followed by AlexaFluor secondary antibody (Life Technologies) at room temperature for 2 h. All antibodies were used at 1:1000 dilution.

Name	Primary/Secondary	Manufacturer	Catalog #	Isotype
Anti-HA	Primary	CST	3724S	Rabbit IgG
Anti-rabbit 647	Secondary	Life Technologies	A21244	Goat IgG

Synthetic Methods

Synthesis of **3:**

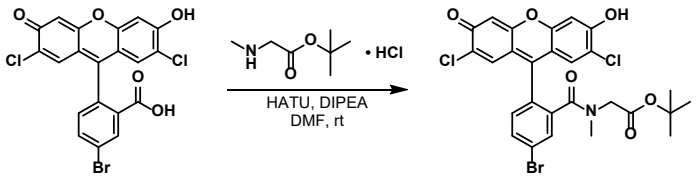

4

5-bromo-2',7'-dichlorofluorescein (1.00 g, 2.08 mmol), sarcosine *tert*-butyl ester hydrochloride (415 mg, 2.28 mmol) and HATU (872 mg, 2.29 mmol) were dissolved in 10 mL anhydrous DMF, followed by addition of 1.81 mL (10.4 mmol) DIPEA. After stirring for 7 hours the reaction for was found to have reached completion by LC-MS. The deep-red solution was acidified with acetic acid (2 mL), then concentrated under reduced pressure. The resulting gum was then diluted with 100 mL 10% *i*PrOH/DCM and washed three with 50 mL H_2O. The organic phase was dried over magnesium sulfate, and solvent removed under reduced pressure. The crude material was purified

by flash chromatography (dry-loading, 50 g SiO_2, 10% MeOH/DCM isocratic). Obtained 0.9084 g (72% yield) of product as an orange powder. ^{1}H NMR (600 MHz, DMSO-d_6) δ 7.93 (dd, J = 8.2, 2.1 Hz, 1H), 7.78 (d, J = 2.0 Hz, 1H), 7.51 (d, J = 8.2 Hz, 1H), 7.12 (s, 2H), 6.70 (s, 2H), 3.79 (s, 2H), 2.80 (s, 3H), 1.25 (s, 9H). Analytical HPLC retention time: 7.20 minutes. HR-ESI-MS $[M+H]^+$ calculated 606.0080, found 606.0084.

Synthesis of **4:**

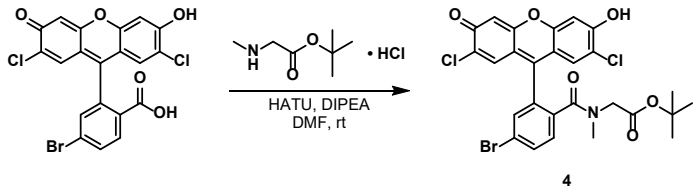

6-bromo-2',7'-dichlorofluorescein (201 mg, 419 µmol), sarcosine *tert*-butyl ester hydrochloride (81.0 mg, 446 µmol) and HATU (173 mg, 455 µmol) were dissolved in 2 mL anhydrous DMF, followed by addition of 363 µL DIPEA (2.08 mmol). After stirring for 18 hours the reaction was found to have reached completion by LC-MS. The reaction was acidified with 500 uL AcOH, and precipitation induced by addition of 5 mL H_2O. The flocculent orange precipitate was collected by vacuum filtration. Crude **1** was purified by flash chromatography (dry-loading, 25 g SiO_2, 5% MeOH/DCM isocratic). Obtained 147 mg (58%) of product as an orange powder. ^{1}H NMR (600 MHz, DMSO-d_6) δ 7.94 (dd, J = 8.3, 2.0 Hz, 1H), 7.86 (d, J = 2.0 Hz, 1H), 7.55 (d, J = 8.3 Hz, 1H), 7.13 (s, 2H), 6.74 (br s, 2H), 3.79 (s, 2H), 2.81 (s, 3H), 1.24 (s, 9H). Analytical HPLC retention time: 7.02 minutes. HR-ESI-MS $[M+H]^+$ calculated 606.0080, found 606.0084.

Synthesis of **7**:

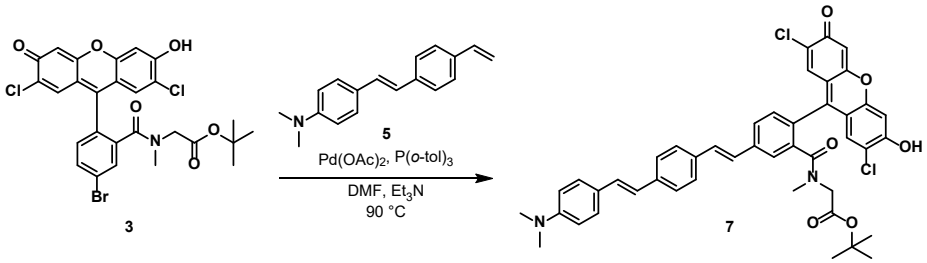

A 25 mL Schlenk flask was charged with fluorophore **3** (49.8 mg, 82.0 µmol), molecular wire **5** (25.0 mg, 100 µmol), $Pd(OAc)_2$ (1.65 mg, 7.35 µmol) and P(*o*-Tol)$_3$ (4.77 mg, 15.7 µmol). The flask was evacuated and backfilled with N_2 three times. Solid reagents were dissolved in 1 mL anhydrous DMF and 0.5 mL anhydrous Et_3N, and the reaction stirred at 90 °C for 12 hours. After cooling the reaction was diluted with 25 mL DCM and filtered through a pad of celite. The filtrate was washed with 20 mL 1 M HCl, then washed three times with 20 mL portions of water. The organic phase was dried over magnesium sulfate, decanted, and solvents removed under reduced pressure. The resulting crude was purified by preparative TLC (7.5% MeOH/DCM) to obtain 39.7 mg of **7** (62%). ^{1}H NMR (900 MHz, DMSO-d_6) δ 7.94 (dd, J = 8.0, 1.7 Hz, 1H), 7.79 (d, J = 1.7 Hz, 1H), 7.64 (d, J = 8.2 Hz, 2H), 7.58 (d, J = 7.9 Hz, 2H), 7.54 (d, J = 7.8 Hz, 1H), 7.51 (d, J = 16.7 Hz, 1H), 7.47 – 7.43 (m, 3H), 7.20 (d, J = 16.3 Hz, 1H), 7.14 (s, 2H), 7.00 (d, J = 16.3 Hz, 1H), 6.73 (d, J = 8.3 Hz, 2H), 6.69 (br s, 2H), 3.83 (s, 2H), 2.94 (s, 6H), 2.84 (s, 3H), 1.27 (s, 9H). Analytical HPLC retention time: 6.65 min. HR-ESI-MS $[M+H]^+$ calculated 775.2342, found 775.2345.

Synthesis of **8**:

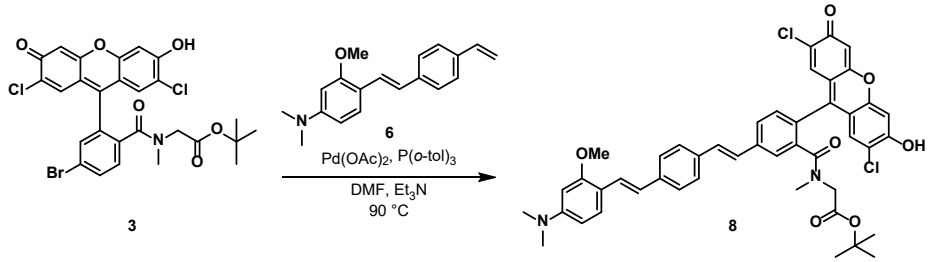

A 25 mL Schlenk flask was charged with fluorophore **3** (75.4 mg, 124 µmol), molecular wire **6** (40.38 mg, 144 µmol), $Pd(OAc)_2$ (2.18mg, 9.71 µmol) and P(*o*-Tol)$_3$ (9.08 mg, 29.8 µmol). The flask was evacuated and backfilled with N_2 three times. Solid reagents were dissolved in 2 mL anhydrous DMF and 1 mL anhydrous Et_3N, and the reaction stirred at 90 °C for 24 hours. After cooling the reaction was diluted with 100 mL DCM and filtered through a pad of celite. The filtrate was washed with 50 mL 1 M HCl, then washed three times with 50 mL portions of water. The organic phase was dried over magnesium sulfate, decanted, and solvents removed under reduced pressure. The resulting crude was purified by preparative TLC (7.5% MeOH/DCM) to obtain 39.7 mg of **8** (82%). ^{1}H NMR (900 MHz, DMSO-d_6) δ 7.94 (dd, J = 8.0, 1.8 Hz, 1H), 7.78 (d, J = 1.7 Hz, 1H), 7.63 (d, J = 7.6 Hz, 2H), 7.55 – 7.47 (m, 7H), 7.42 (d, J = 16.3 Hz, 1H), 7.37 (d, J = 16.4 Hz, 1H), 7.12 (s, 2H), 7.00 (d, J = 16.4 Hz, 1H), 6.65 (s, 2H), 6.35 (dd, J = 8.7, 2.3 Hz, 1H), 6.29 (d, J = 2.4 Hz, 1H), 3.87 (s, 3H), 3.83 (s, 2H), 2.97 (s, 6H), 2.84 (s, 3H), 1.27 (s, 9H). Analytical HPLC retention time: 6.92 min. HR-ESI-MS $[M-H]^-$ calculated 803.2296, found 803.2274.

Synthesis of **9**:

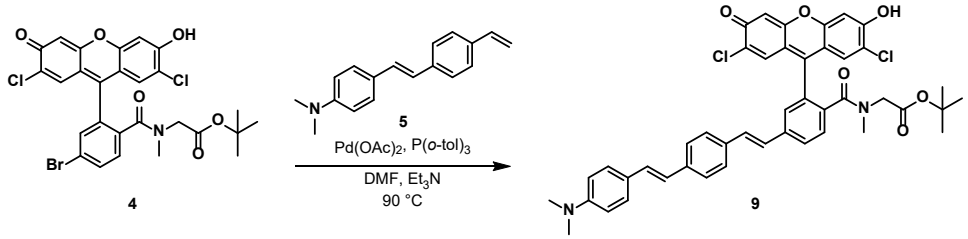

A 50 mL Schlenk flask was charged with fluorophore **4** (252 mg, 415 µmol), molecular wire **5** (124 mg, 497 µmol), $Pd(OAc)_2$ (2.4 mg, 11 µmol) and P(*o*-Tol)$_3$ (6.4 mg, 35 µmol). The flask was evacuated and backfilled with N_2 three times. Solid reagents were dissolved in 4 mL anhydrous DMF and 2 mL anhydrous Et_3N, and the reaction stirred at 90 °C for 13 hours. After cooling the reaction was diluted with 125 mL DCM and filtered through a pad of celite. The filtrate was washed with 50 mL 1 M HCl, then washed three times with 50 mL portions of water. The organic phase was dried over magnesium sulfate, decanted, and solvents removed under reduced pressure. The resulting crude was purified by flash column chromatography (2.5 to 10% MeOH/DCM). Fractions containing the product were pooled and solvent removed under reduced pressure to obtain 169 mg of **9** (52%). ^{1}H NMR (900 MHz, DMSO-d_6) δ 7.93 (dd, J = 8.1, 1.7 Hz, 1H), 7.78 (d, J = 1.7 Hz, 1H), 7.60 (d, J = 8.0 Hz, 1H), 7.58 (d, J = 8.1 Hz, 2H), 7.54 (d, J = 8.1 Hz, 2H), 7.46 (d, J = 16.3 Hz, 1H), 7.43 (d, J = 8.4 Hz, 2H), 7.38 (d, J = 16.1 Hz, 1H), 7.17 (d, J = 16.3 Hz, 1H), 7.14 (s, 2H), 6.97 (d, J = 16.2 Hz, 1H), 6.75 (br s, 2H), 6.71 (d, J = 8.6 Hz, 2H), 3.81 (s, 2H), 2.93 (s, 6H), 2.87 (s, 3H), 1.26 (s, 9H). Analytical HPLC retention time: 6.84 min. HR-ESI-MS $[M-H]^-$ calculated 773.2191, found 773.2168.

Synthesis of **10**:

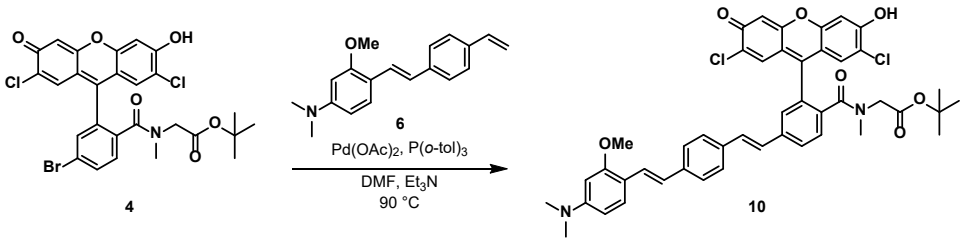

A 25 mL Schlenk flask was charged with fluorophore **4** (38.61 mg, 64.77 µmol), molecular wire **6** (22.64 mg, 81.04 µmol), $Pd(OAc)_2$ (0.63 mg, 2.8 µmol) and P(*o*-Tol)$_3$ (1.26 mg, 4.14 µmol). The flask was evacuated and backfilled with N_2 three times. Solid reagents were dissolved in 1 mL anhydrous DMF and 0.5 mL anhydrous Et_3N, and the reaction stirred at 90 °C for 14 hours. After cooling the reaction was diluted with 25 mL DCM and filtered through a pad of celite. The filtrate was washed with 20 mL 1 M HCl, then washed three times with 20 mL portions of water. The organic phase was dried over magnesium sulfate, decanted, and solvents removed under reduced pressure. The resulting crude was purified by preparative TLC (7.5% MeOH/DCM) to obtain 24.5 mg of **10** (47%). ^{1}H NMR (900 MHz, DMSO-d_6) δ 7.94 (dd, J = 8.1, 1.8 Hz, 1H), 7.79 (d, J = 1.8 Hz, 1H), 7.61 (d, J = 8.0 Hz, 1H), 7.58 (d, J = 8.0 Hz, 2H), 7.50 (d, J = 8.0 Hz, 2H), 7.47 (d, J = 8.8 Hz, 1H), 7.46 (d, J = 16.3 Hz, 1H), 7.37 (d, J = 16.2 Hz, 1H), 7.35 (d, J = 16.4 Hz, 1H), 7.14 (s, 2H), 6.98 (d, J = 16.3 Hz, 1H), 6.34 (dd, J = 8.7, 2.4 Hz, 1H), 6.28 (d, J = 2.5 Hz, 1H), 3.85 (s, 3H), 3.81 (s, 2H), 2.96 (s, 6H), 2.87 (s, 3H), 1.26 (s, 9H). Analytical HPLC retention time: 6.92 min. HR-ESI-MS $[M+H]^+$ calculated 805.2442, found 805.2438.

Synthesis of **11**:

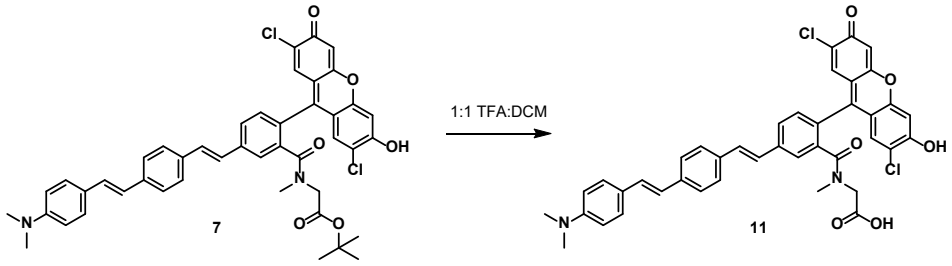

7 (10.5 mg, 13.5 µmol) was dissolved in 0.5 mL DCM, 0.5 mL TFA. After one hour solvents were removed under a stream of nitrogen. Residual TFA was removed azeotropically with toluene. Crude product was purified by preparative TLC (10% MeOH/DCM, eluting with 10% MeOH/1% AcOH/DCM) to obtain 7.4 mg of **11** (76%). ^{1}H NMR (900 MHz, DMSO-d_6) δ 7.93 (dd, J = 8.0, 1.8 Hz, 1H), 7.77 (d, J = 1.7 Hz, 1H), 7.65 (d, J = 7.9 Hz, 2H), 7.58 (d, J = 8.0 Hz, 2H), 7.51 (d, J = 7.8 Hz, 1H), 7.50 (d, J = 16.2 Hz, 1H), 7.46 (d, J = 8.7 Hz, 2H), 7.44 (d, J = 16.5 Hz, 2H), 7.20 (d, J = 16.3 Hz, 1H), 7.04 (s, 2H), 7.01 (d, J = 16.5 Hz, 1H), 6.73 (d, J = 8.8 Hz, 2H), 6.48 (s, 2H), 3.88 (s, 2H), 2.94 (s, 6H), 2.84 (s, 3H). Analytical HPLC retention time: 5.64 min. HR-ESI-MS $[M-H]^-$ calculated 717.1565, found 717.1557.

Synthesis of **12**:

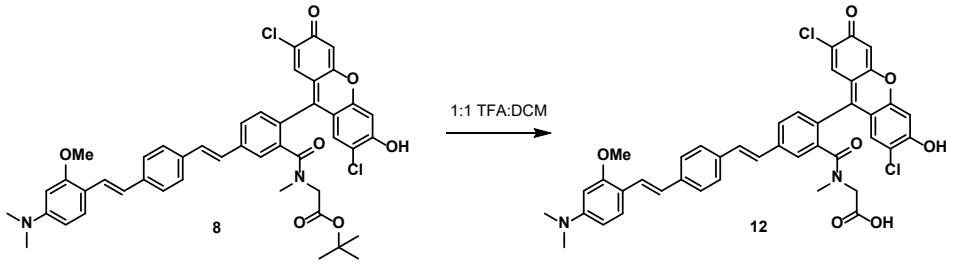

8 (14.7 mg, 18.24 µmol) was dissolved in 0.5 mL DCM, 0.5 mL TFA. After one hour solvents were removed under a stream of nitrogen. Residual TFA was removed azeotropically with toluene. Crude product was purified by preparative TLC (10% MeOH/DCM, eluting with 10% MeOH/1% AcOH/DCM) to obtain 13.0 mg of **12** (95%). ^{1}H NMR (900 MHz, DMSO-d_6) δ 7.91 (dd, J = 8.1, 1.5 Hz, 1H), 7.74 (d, J = 1.6 Hz, 1H), 7.64 (d, J = 7.8 Hz, 2H), 7.53 (d, J = 7.9 Hz, 1H), 7.52 – 7.45 (m, 4H), 7.42 (d, J = 16.5 Hz, 1H), 7.37 (d, J = 16.5 Hz, 1H), 7.01 (d, J = 16.4 Hz, 1H), 6.96 (s, 2H), 6.35 (dd, J = 8.6, 2.4 Hz, 1H), 6.32 (s, 2H), 6.29 (d, J = 2.5 Hz, 1H), 3.87 (m, 5H), 2.97 (d, J = 2.4 Hz, 6H), 2.84 (s, 3H). Analytical HPLC retention time: 5.89 min. HR-ESI-MS $[M-H]^-$ calculated 747.1670, found 747.1651.

Synthesis of **13**:

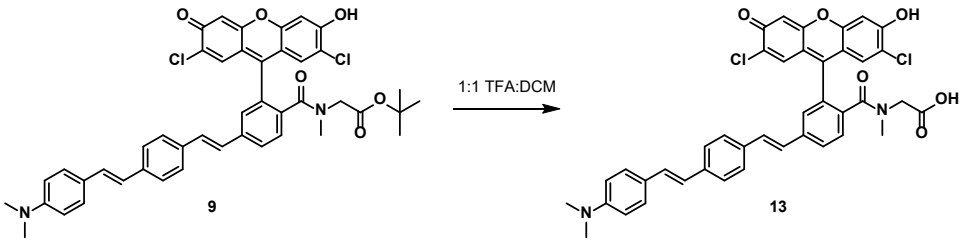

9 (12.6 mg, 16.2 µmol) was dissolved in 0.5 mL DCM, 0.5 mL TFA. After one hour solvents were removed under a stream of nitrogen. Residual TFA was removed azeotropically with toluene. Crude product was purified by preparative TLC (10% MeOH/DCM, eluting with 10% MeOH/1% AcOH/DCM) to obtain 4.7 mg of **13** (40%). ^{1}H NMR (900 MHz, DMSO-d_6) δ 7.89 (d, J = 8.0 Hz, 1H), 7.70 (s, 1H), 7.59 (d, J = 8.2 Hz, 1H), 7.55 (d, J = 8.2 Hz, 2H), 7.54 (d, J = 8.0 Hz, 2H), 7.47 (d, J = 16.2 Hz, 1H), 7.44 (d, J = 8.8 Hz, 2H), 7.37 (d, J = 16.2 Hz, 1H), 7.18 (d, J = 16.3 Hz, 1H), 6.98 (d, J = 16.3 Hz, 1H), 6.89 (s, 2H), 6.72 (d, J = 8.9 Hz, 2H), 6.23 (s, 2H), 3.87 (s, 2H), 2.93 (d, J = 1.7 Hz, 6H), 2.87 (s, 3H). Analytical HPLC retention time 5.62. HR-ESI-MS $[M-H]^-$ calculated 717.1565, found 717.1553.

Synthesis of **14**:

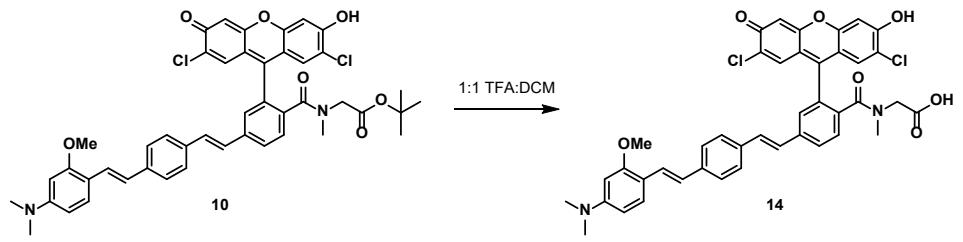

10 (10.9 mg, 13.5 µmol) was dissolved in 0.5 mL DCM, 0.5 mL TFA. After one hour solvents were removed under a stream of nitrogen. Residual TFA was removed azeotropically with toluene. Crude product was purified by preparative TLC (10% MeOH/DCM, eluting with 10% MeOH/1% AcOH/DCM) to obtain 10.0 mg of **14** (99%). ^{1}H NMR (900 MHz, DMSO-d_6) δ 7.91 (d, J = 8.1, 1.6 Hz, 1H), 7.73 (d, J = 1.5 Hz, 1H), 7.58 (d, J = 8.1 Hz, 2H), 7.57 (d, J = 8.0 Hz, 1H), 7.51 – 7.45 (m, 4H), 7.36 (d, J = 16.2 Hz, 1H), 7.35 (d, J = 16.3 Hz, 1H), 6.99 (s, 2H), 6.98 (d, J = 16.6 Hz, 1H), 6.44 (s, 2H), 6.34 (dd, J = 8.7, 2.3 Hz, 1H), 6.28 (d, J = 2.3 Hz, 1H), 3.87 (s, 2H), 3.85 (s, 3H), 2.96 (s, 6H), 2.87 (s, 3H). Analytical HPLC retention time: 5.88. HR-ESI-MS $[M+H]^+$ calculated 749.1824, found 749.1815.

Synthesis of **15**:

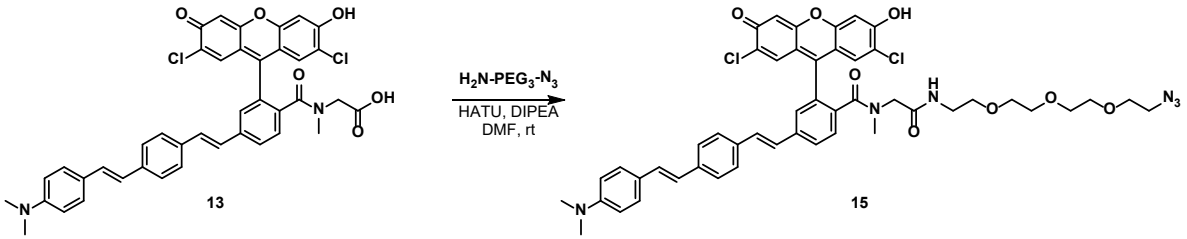

Voltagefluor **13** (27.88 mg, 38.74 µmol), HATU (18.24 mg, 47.97 µmol) and amino-PEG$_3$-azide (10.07 mg, 46.14 µmol) were dissolved in 0.5 mL anhydrous DMF, followed by addition of 36.3 µL (281 µmol) anhydrous DIPEA. After stirring for one hour the reaction was found to have gone to completion by LC-MS. The reaction was acidified with 50 µL AcOH and solvent removed under reduced pressure. Purified by preparative TLC (10% MeOH/DCM) to obtain 31.6 mg of **15** (88.7%). Analytical HPLC retention time: 6.02 min. HR-ESI-MS $[M+H]^+$ calculated 919.2983, found 919.2984.

Synthesis of **16**:

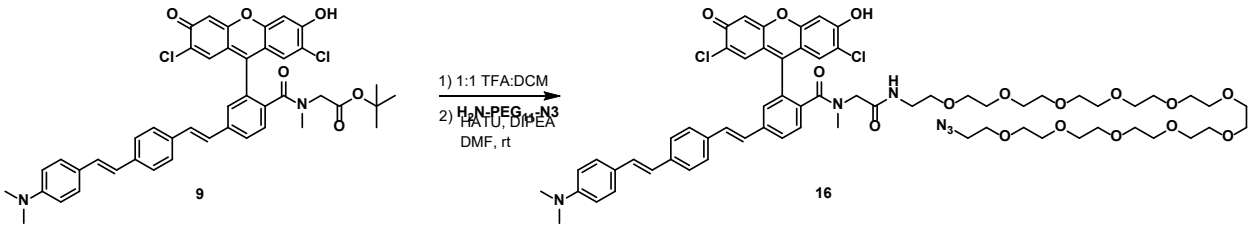

9 (22.5 mg, 29.0 µmol) was dissolved in 250 µL DCM, 250 µL TFA. After two hours solvents were removed under a stream of nitrogen. Residual TFA was removed azeotropically with toluene. To the dram vial containing the deprotected VoltageFluor, added HATU (17.7 mg, 46.5 µmol) and dissolved solid reagents in 0.5 mL anhydrous DMF. Added amino-PEG$_{11}$-azide (19.3 mg, 33.8 µmol) and DIPEA (25.2 µL, 144 µmol). After stirring for 16 hours the reaction was found to have reached completion by LC-MS. Solvent was removed under reduced pressure and the product purified by preparative TLC (10% MeOH/DCM) to obtain 31.9 mg (87%) of **16** as a red gum. Analytical HPLC retention time: 5.68 min. HR-ESI-MS $[M+H]^+$ calculated 1271.5081, found 1271.5110.

Synthesis of **17**:

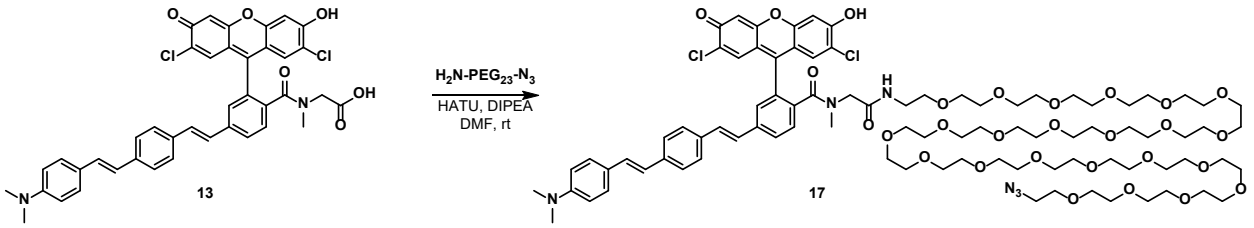

Voltagefluor **13** (14.53 mg, 20.19 µmol), HATU (7.99 mg, 10.01 µmol) and amino-PEG_{23}-azide (27.55 mg, 25.01 µmol) were dissolved in 0.5 mL anhydrous DMF, followed by addition of 18.6 µL (176 µmol) anhydrous DIPEA. After stirring for one hour the reaction was found to have gone to completion by LC-MS. The reaction was acidified with 50 µL AcOH and solvent removed under reduced pressure. Purified by preparative TLC (10% MeOH/DCM) to obtain 26.0 mg of **17** (71.5%). Analytical HPLC retention time: 5.69 min. HR-ESI-MS $[M+H]^+$ calculated 1799.8226, found 1799.8214.

Synthesis of **18**:

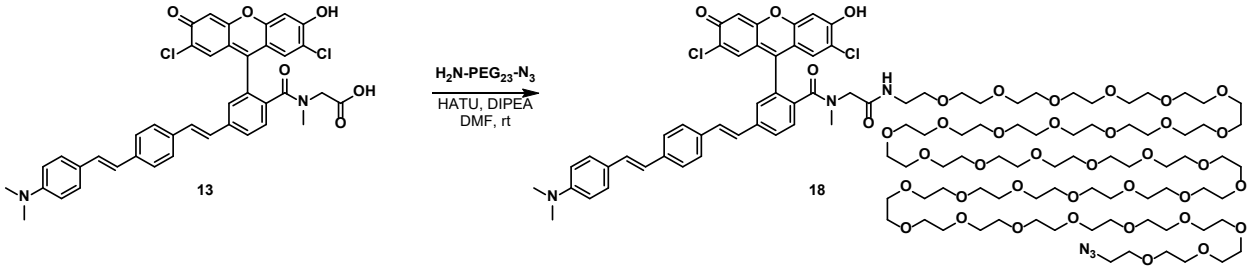

Voltagefluor **13** (15.33 mg, 21.30 µmol), HATU (9.65 mg, 25.38 µmol) and amino-PEG_{35}-azide (38.20 mg, 23.43 µmol) were dissolved in 0.5 mL anhydrous DMF, followed by addition of 18.6 µL (176 µmol) anhydrous DIPEA. After stirring for one hour the reaction was found to have gone to completion by LC-MS. The reaction was acidified with 50 µL AcOH and solvent removed under reduced pressure. Purified by preparative TLC (10% MeOH/DCM) to obtain 29.5 mg of **18** (59.4%). Analytical HPLC retention time: 5.29 min. HR-ESI-MS $[M+2Na]^{2+}$ calculated 1186.5542, found 1186.5563

Synthesis of **19**:

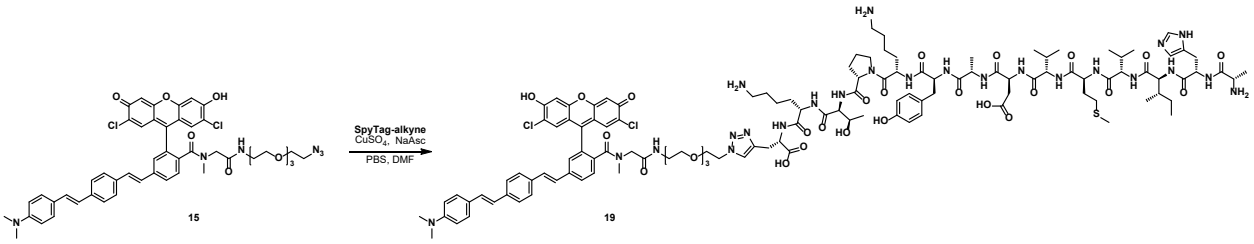

To a 2 mL plastic tube containing 5 mg SpyTag-alkyne (AHIVMVDAYKPTK-propargyl glycine, 3.19 µmol) was added 125 µL DMF, 500 µL PBS pH 7.4 + Triton X-100 and 125 µL of a 25 mM solution of **15** (3.13 µmol) in DMF. The peptide was solubilized by sonication at 40 °C, and the solution transferred to a glass vial. Added 125 µL of a 25 mM solution of copper sulfate and 125 µL of a 25 mM solution of sodium ascorbate, both in PBS pH 7.4 + Triton X-100 and stirred for

16 hours at room temperature under nitrogen. The reaction is cloudy immediately after addition of copper sulfate and sodium ascorbate but all material solubilizes within one hour. After stirring overnight, the reaction was found to have formed a precipitate. Solvents were removed under reduced pressure, and the solid material was suspended in 1.5 mL water and pelleted by centrifugation. The pellet was washed twice with 0.5 mL water and dried once more under high vacuum. The crude was purified by semi-preparative HPLC to obtain 0.089 µmol of **19** (2.8%). Yield was estimated spectroscopically by comparing the maximum absorbance of a stock solution of **19** to that of a standard solution of **13**. Analytical HPLC retention time: 4.26 min. HR-ESI-MS $[M+4H]^{4+}$ calculated 829.3786, found 829.3812.

Synthesis of **20**:

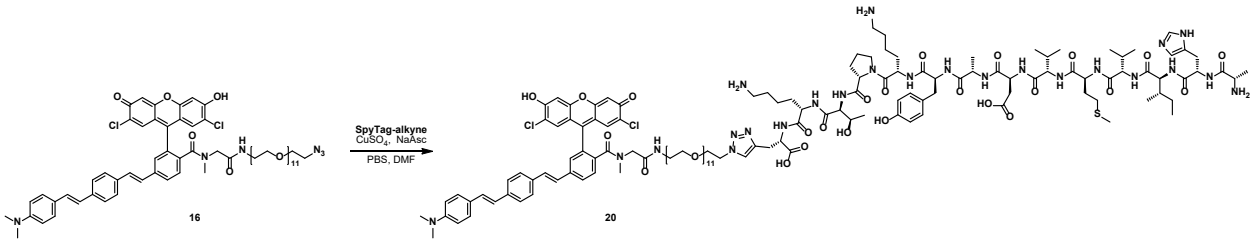

To a 2 mL plastic tube containing 5 mg SpyTag-alkyne (AHIVMVDAYKPTK-propargyl glycine, 3.19 µmol) was added 125 µL DMF, 500 µL PBS pH 7.4 + Triton X-100 and 125 µL of a 25 mM solution of **16** (3.13 µmol) in DMF. The peptide was solubilized by sonication at 40 °C, and the solution transferred to a glass vial. Added 125 µL of a 25 mM solution of copper sulfate and 125 µL of a 25 mM solution of sodium ascorbate, both in PBS pH 7.4 + Triton X-100 and stirred for 16 hours at room temperature under nitrogen. After stirring overnight, a significant precipitate had formed. The precipitate was collected by pelleting the reaction by centrifugation, while the supernatant was concentrated under reduced pressure, suspended in 1 mL H_2O and the resulting solid material was also pelleted by centrifugation. Both pellets were washed 3x with 500 µL of water and dried under high vacuum. Crude material was pooled and purified by semi-preparative HPLC to obtain 0.49 µmol of **20**. Yield was estimated spectroscopically by comparing the maximum absorbance of a stock solution of **20** to that of a standard solution of **13**. Analytical HPLC retention time: 4.67 min. HR-ESI-MS $[M+4H]^{4+}$ calculated 710.3382, found 710.3402.

Synthesis of **21**:

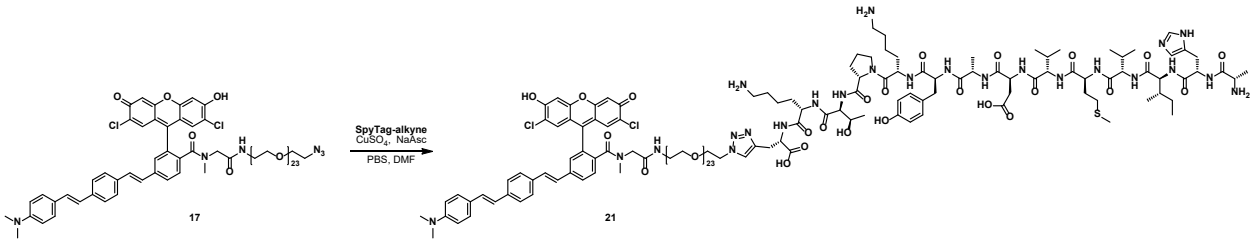

To a 2 mL plastic tube containing 5 mg SpyTag-alkyne (AHIVMVDAYKPTK-propargyl glycine, 3.19 µmol) was added 125 µL DMF, 500 µL PBS pH 7.4 + Triton X-100 and 125 µL of a 25 mM solution of **17** (3.13 µmol) in DMF. The peptide was solubilized by sonication at 40 °C, and the solution transferred to a glass vial. Added 125 µL of a 25 mM solution of copper sulfate and 125 µL of a 25 mM solution of sodium ascorbate, both in PBS pH 7.4 + Triton X-100 and stirred for 16 hours at room temperature under nitrogen. Solvents were removed under reduced pressure, and

the solid material was suspended in 1.5 mL water and pelleted by centrifugation. The pellet was washed twice with 0.5 mL water and dried once more under high vacuum. The crude was purified by semi-preparative HPLC to obtain 0.69 µmol of **21** (22%). Yield was estimated spectroscopically by comparing the maximum absorbance of a stock solution of **21** to that of a standard solution of **13**. Analytical HPLC retention time: 4.50 min. HR-ESI-MS $[M+4H]^{4+}$ calculated 842.4168, found 842.4201.

Synthesis of **22**:

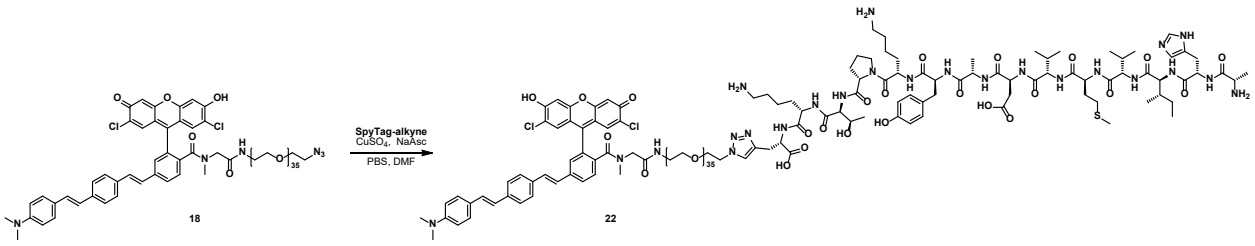

To a 2 mL plastic tube containing 5 mg SpyTag-alkyne (AHIVMVDAYKPTK-propargyl glycine, 3.19 µmol) was added 125 µL DMF, 500 µL PBS pH 7.4 + Triton X-100 and 125 µL of a 25 mM solution of **18** (3.13 µmol) in DMF. The peptide was solubilized by sonication at 40 °C, and the solution transferred to a glass vial. Added 125 µL of a 25 mM solution of copper sulfate and 125 µL of a 25 mM solution of sodium ascorbate, both in PBS pH 7.4 + Triton X-100 and stirred for 16 hours at room temperature under nitrogen. Solvents were removed under reduced pressure, and the solid material was suspended in 1.5 mL water and pelleted by centrifugation. The pellet was washed twice with 0.5 mL water and dried once more under high vacuum. The crude was purified by semi-preparative HPLC to obtain 0.374 µmol of **22** (18%). Yield was estimated spectroscopically by comparing the maximum absorbance of a stock solution of **22** to that of a standard solution of **13**. Analytical HPLC retention time: 4.39 min. HR-ESI-MS $[M+4H]^{4+}$ calculated 974.4955, found 974.4995.

Synthesis of **23**:

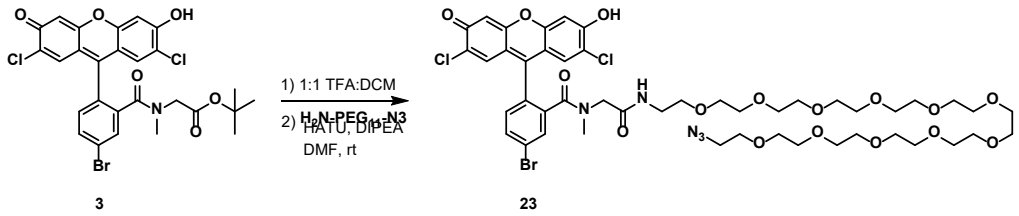

3 (31.5 mg, 51.9 µmol) was dissolved in 1 mL DCM, 1 mL TFA. After one hour solvents were removed under a stream of nitrogen. Residual TFA was removed azeotropically with toluene. To the dram vial containing the deprotected fluorophore, added HATU (21.7 mg, 57.1 µmol) and dissolved solid reagents in 1 mL anhydrous DMF. Added amino-PEG_{11}-azide (38.2 mg, 66.9 µmol) and DIPEA (45.2 µL, 259 µmol). After stirring for 48 hours the reaction was found to have reached completion by LC-MS. The reaction was acidified with 100 µL AcOH and solvent removed under reduced pressure. Purified by preparative TLC (10% MeOH/DCM) to obtain 81.1 mg of **17** (142%). Analytical HPLC retention time: 5.87 min. HR-ESI-MS $[M+H]^{+}$ calculated 1102.2825, found 1102.2842.

Synthesis of **24**:

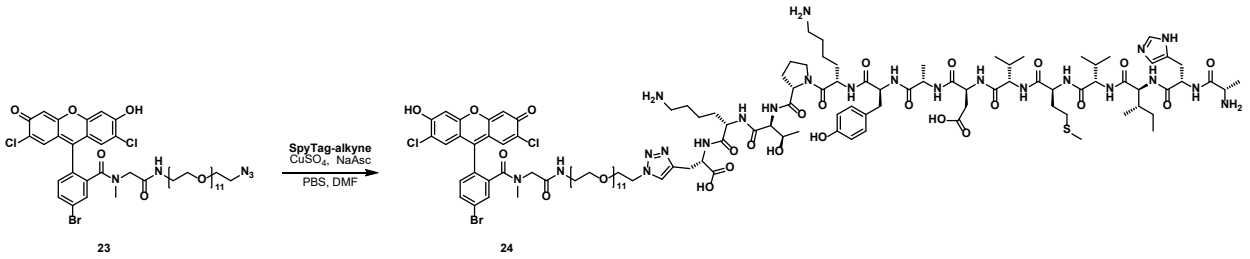

To a solution of SpyTag-alkyne (AHIVMVDAYKPTK-propargyl glycine, 1.62 mg, 1.03 µmol) in 100 µL DMF was added 125 µL of a 25 mM solution **S1** in DMF and 400 µL PBS pH 7.4 + Triton X-100, followed by 125 µL of a 25 mM solution of copper sulfate and 125 µL of a 25 mM solution of sodium ascorbate, both in PBS pH 7.4 + Triton X-100. After stirring for 16 hours complete consumption of SpyTag-alkyne was observed by LC-MS. The reaction was filtered through a 0.22 µm filter and purified by semi-preparative HPLC. Analytical HPLC retention time: 4.07 min. HR-ESI-MS $[M+3H]^{3+}$ calculated 890.3733, found 890.3757.

Scheme 4-1 Genetic targeting of VoltageFluor dyes using SpyTag/SpyCatcher methodology

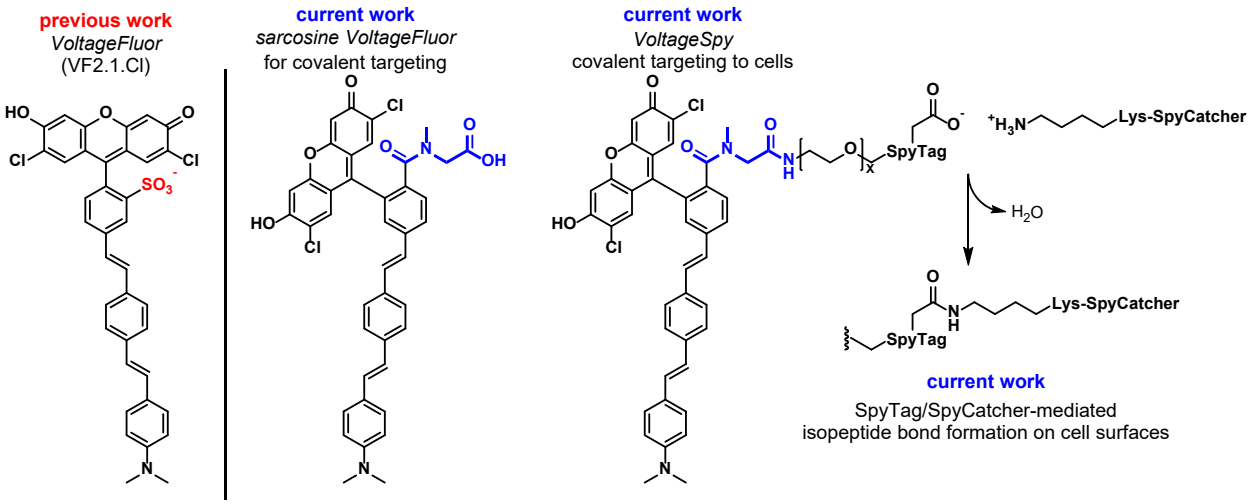

Scheme 4-2 Synthesis of sarcosine VoltageFluors

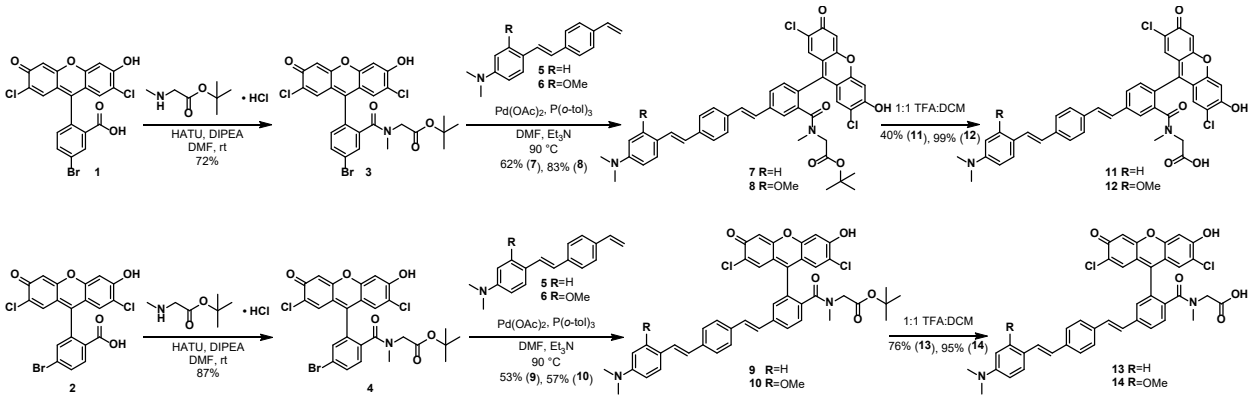

Figure 4-1

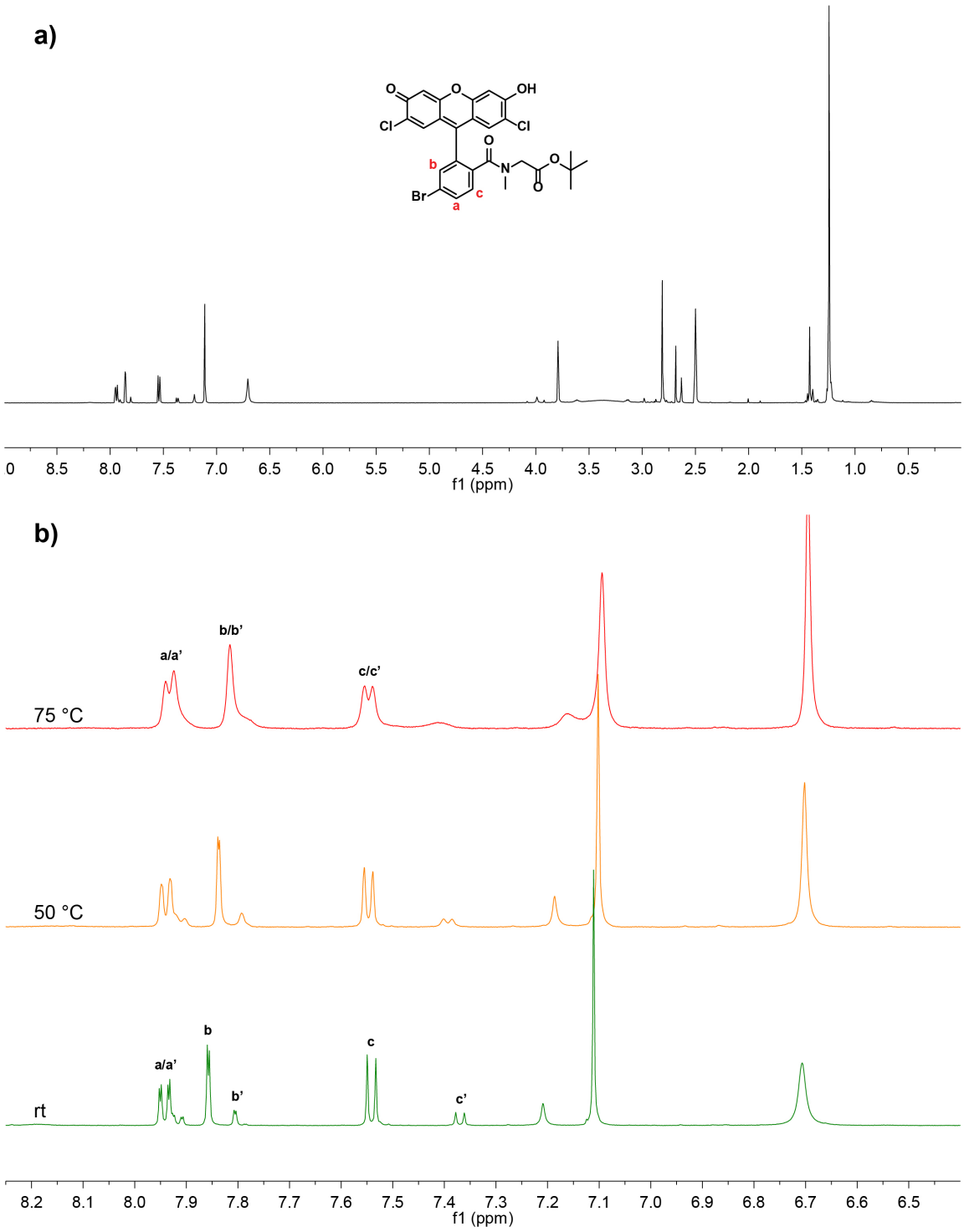

Variable temperature ^{1}H NMR study of compound **4**. a) Room temperature spectrum (ambient temperature of the probe is approximately 25 °C) of **4** from 12 to -2 ppm. **b)** expanded aromatic region at multiple temperatures. Prime peaks are associated with the minor rotamer. Unlabeled peaks in panel (b) correspond to protons on the xanthene chromophore.

Table 4-1 Properties of sarcosine VF dyes, PEGylated intermediates and VoltageSpy indicators

dye	isomer	R	PEG units	λ_{max} (abs)[a]	λ_{max} (em)[a]	Φ[a]	cellular brightness[b]	contrast [b][c]	%ΔF/F [b][d]	effective sensitivity[e]
11	5	-H	---	525	541	2.7	10	---	27.2 ±0.2	7
12	5	-OMe	---	525	540	5.5	1	---	12.2 ±0.4	1
13	6	-H	---	525	540	3.9	40	---	22.7 ±0.1	12
14	6	-OMe	---	524	540	0.8	6	---	29.3 ±0.8	6
15	6	-H	3	526	545	5.8	---	---	---	---
16	6	-H	11	526	544	10.9	---	---	---	---
17	6	-H	23	526	540	9.8	---	---	---	---
18	6	-H	35	526	540	11.2	---	---	---	---
19	6	-H	3	527	544	10.9	---	5.6 ±3.8	12.5 ±0.2	---
20	6	-H	11	526	544	7.9	---	12.6 ±8.6	13.1 ±0.2	---
21	6	-H	23	526	546	13.9	---	17.8 ±9.7	11.6 ±0.2	---
22	6	-H	35	526	546	8.7	---	34.6 ±29.3	12.7 ±0.1	---

[a] Acquired in PBS, pH 7.4 with 0.1% Triton X-100. [b] measured in HEK cells. [c] ratio of fluorescence intensity of SpyCatcher expressing cells and median fluorescence intensity of untransfected cells loaded with 5 nM dye. Data is mean ±SD for 49 to 77 cells. [d] Per 100 mV step, optically sampled at 500 Hz. [e] Relative product of square root of cellular brightness and ΔF/F.

Figure 4-2

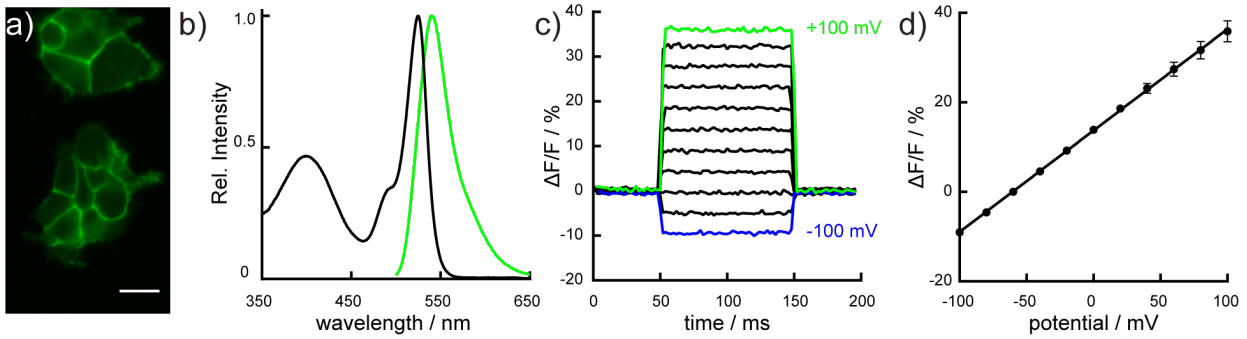

Characterization of sarcosine VoltageFluor dyes. a) Widefield, fluorescence microscopy image of HEK cells loaded with 1 µM sarcosine probe **13**. Scale bar is 10 µM. b) Absorbance (black line) and emission (green line) spectra of **13**. c) Representative plot of fractional change in fluorescence (ΔF/F) vs time from a series of voltage steps (+100 to -100 mV from a holding potential of -60 mV in 20 mV increments) recorded from a HEK cell in whole-cell voltage clamp mode. d) Plot of fractional change in fluorescence vs membrane potential from voltage-clamped HEK cells. Data are mean ±SEM from six cells.

Figure 4-3

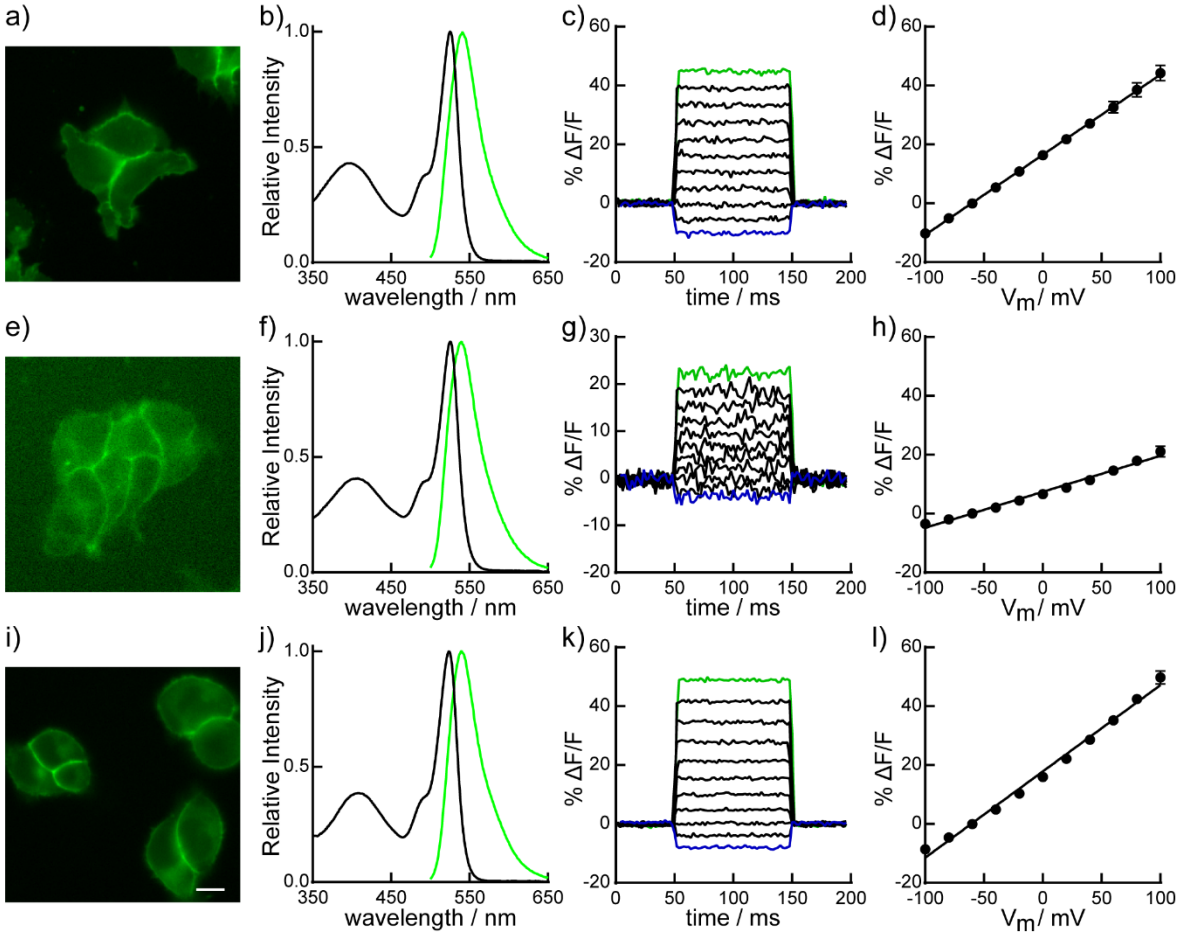

Characterization of sarcosine VoltageFluors. Representative images of staining in HEK cells (a, e, i), absorbance (black) and emission (green) spectra (b,f,j), representative plots of fractional change in fluorescence (ΔF/F) vs time (c,g,k) and plots of fractional change in fluorescence vs membrane potential (d,h,i) for VoltageFluors **11** (a-d), **12** (e-h) and **14** (i-l). Scale bar is 10 μM. Data in panels d, h and l are mean ± SEM from five (d, 11), three (h, 12) and six (l, 14) cells.

Figure 4-4

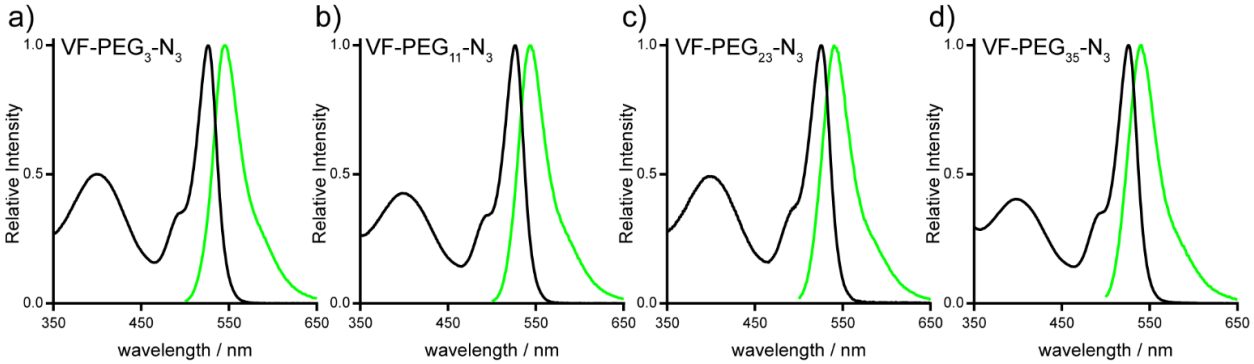

Spectral properties of PEGylated VoltageFluor intermediates. Absorbance (black) and emission (green) spectra of **15** (a), **16** (b), **17** (c) and **18** (d).

Scheme 4-3 Synthesis of VoltageSpy indicators

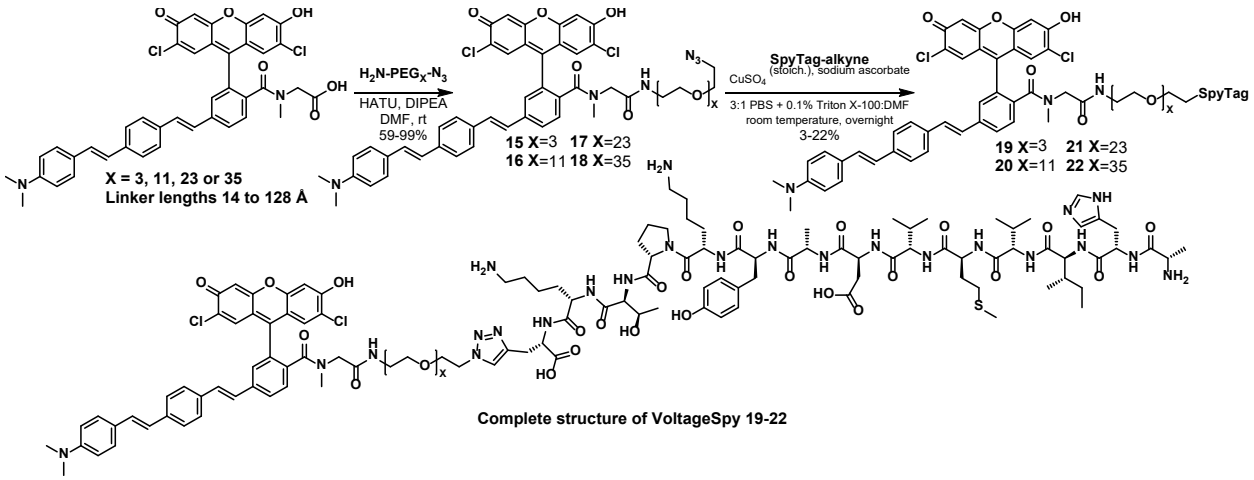

Figure 4-5 Schematic of SpyCatcher constructs

a) PAT3-SpyCatcher-DAF-T2A-NLS-mCherry

b) IgK-SpyCatcher-PDGFR

Figure 4-6

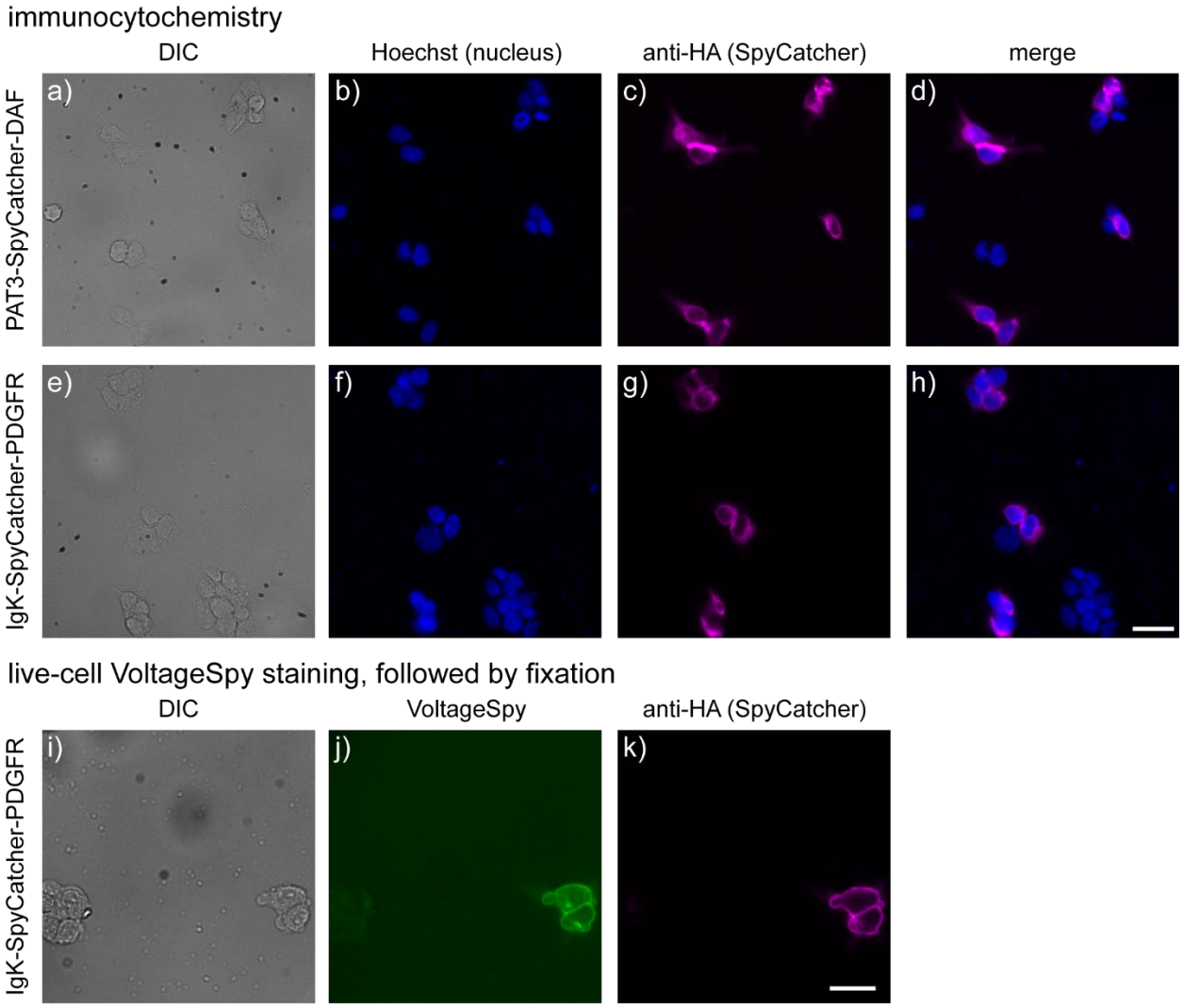

Characterization of SpyCatcher expression in HEK cells. a-h) Widefield DIC and fluorescence microscopy of fixed and permeabilized HEK cells transfected with either PAT3-SpyCatcher-DAF (a-d) or IgK-SpyCatcher-PDGFR (e-h). Using either construct, staining for the HA epitope shows clear expression of the SpyCatcher fusion protein (c, g). Scale bar is 25 µm. i-k) Widefield fluorescence microscopy images of HEK cells labeled with VoltageSpy (i, j) then fixed and stained for SpyCatcher (k), without permeabilization. Scale bar is 25 µm.

Figure 4-7

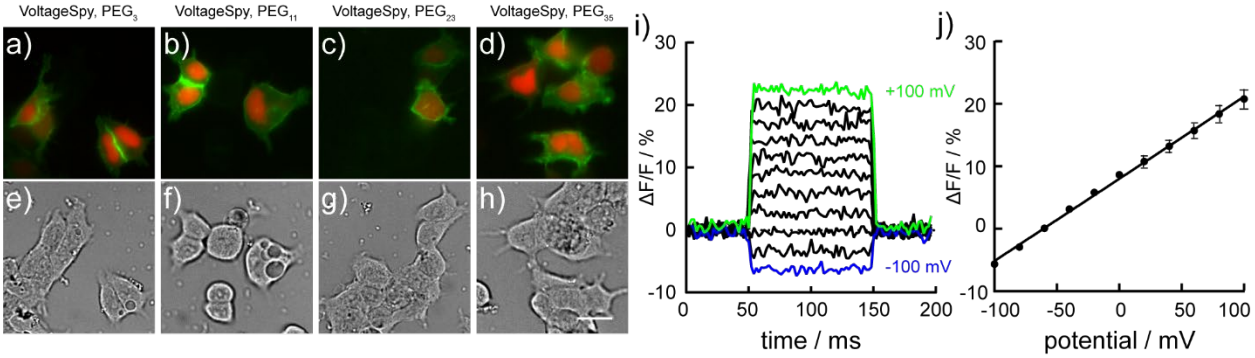

Evaluation of VoltageSpy dyes in HEK cells. a-h) Widefield fluorescence (a-d) and DIC (e-h) microscopy images of HEK cells co-expressing SpyCatcher and nuclear mCherry (red signal) labeled with 5 nM VoltageSpy (green signal) dyes **19** (PEG_3, a, e), **20** (PEG_{11}, b, f), **21** (PEG_{23}, c, g) and **22** (PEG_{35}, d, h). Scale bar is 20 µm. i) Representative plot of fractional change in fluorescence (ΔF/F) vs time from a series of voltage steps (+100 to -100 mV from a holding potential of -60 mV in 20 mV increments) recorded from a HEK cell labeled with **22** in whole-cell voltage clamp mode. j) Plot of fractional change in fluorescence vs membrane potential from voltage-clamped HEK cells labeled with **22**. Data are mean ±SEM from five cells.

Figure 4-8

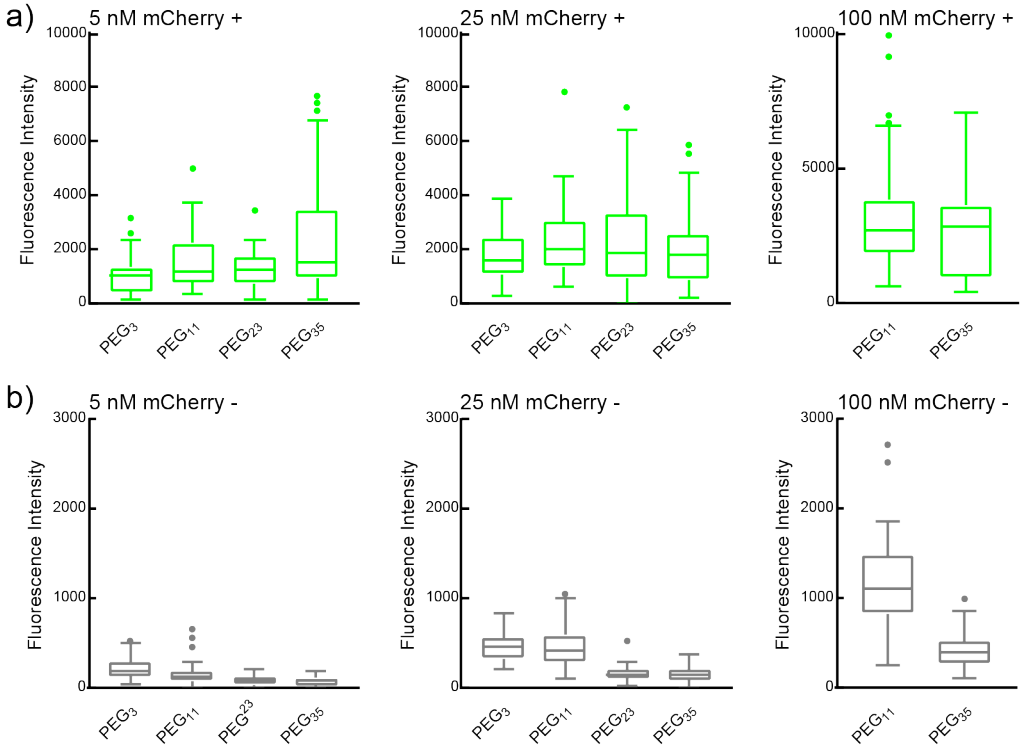

c)

	Contrast		
	Mean	SD	*n*
PEG_3	5.6	3.8	77
PEG_{11}	12.6	8.6	57
PEG_{23}	17.8	9.7	49
PEG_{35}	34.6	29.3	50

	Contrast		
	Mean	SD	*n*
PEG_3	3.9	1.9	40
PEG_{11}	5.4	3.1	55
PEG_{23}	15.8	12.0	58
PEG_{35}	12.9	8.8	87

	Contrast		
	Mean	SD	*n*
PEG_3	3.0	1.9	41
PEG_{11}	6.8	4.1	38

Quantification of VF-PEGx-SpyTag labeling in HEK cells. a) Tukey boxplots (the box defines the first quartile, median, and third quartile; whiskers define minimum and maximum values falling within 1.5 times the inter-quartile range) of cellular fluorescence of SpyCatcher expressing cells labeled with VoltageSpy dyes **19** (PEG_3), **20** (PEG_{11}), **21** (PEG_{23}) and **22** (PEG_{35}). b) Tukey boxplot of cellular fluorescence of untransfected cells exposed to VoltageSpy dyes **19-22**. c) quantification of the contrast (fluorescence intensity of transfected cells divided by the median fluorescence intensity of untransfected cells on the same coverslip) obtained from data in plots (a) and (b). 40-80 cells across all conditions. No wash steps were performed.

Figure 4-9

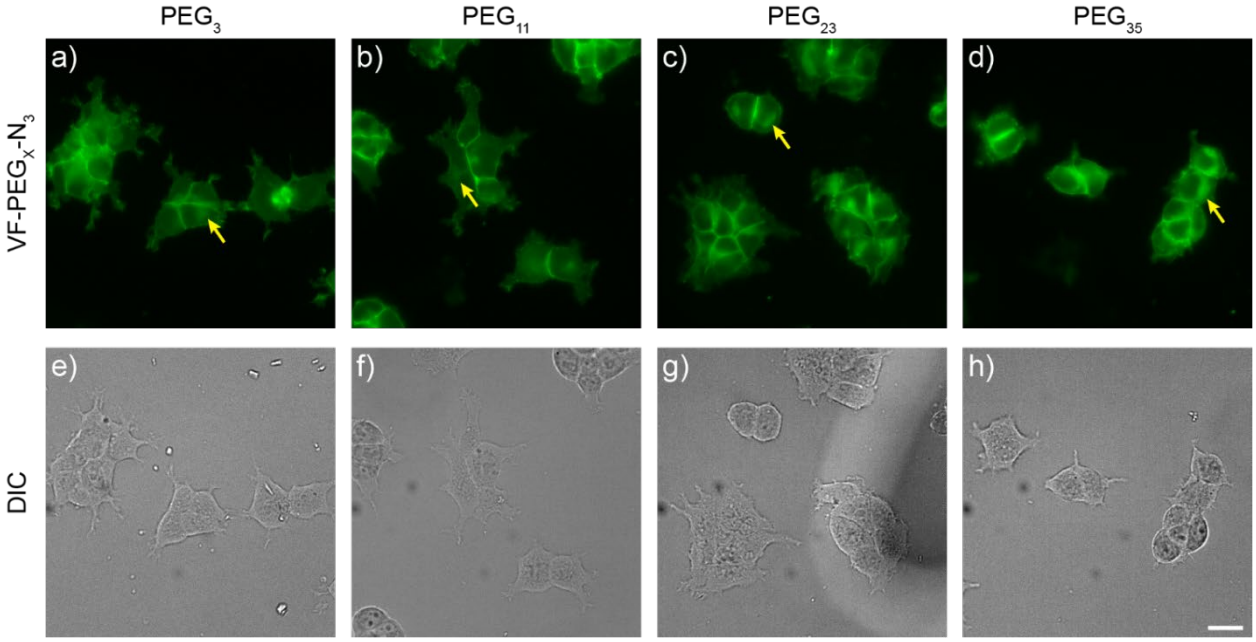

Internalization of VF-PEG$_X$-N$_3$ intermediates. Widefield fluorescence (a-d) and DIC (e-h) images of HEK cells stained with 1 µM PEGylated intermediates **15** (PEG$_3$, a, e), **16** (PEG$_{11}$, b, f), **17** (PEG$_{23}$, c, g) and **18** (PEG$_{35}$, d, h). Yellow arrows denote internal fluorescence not typically observed with VoltageFluor dyes, which becomes increasingly apparent as the length of the PEG linker increases.

Figure 4-10

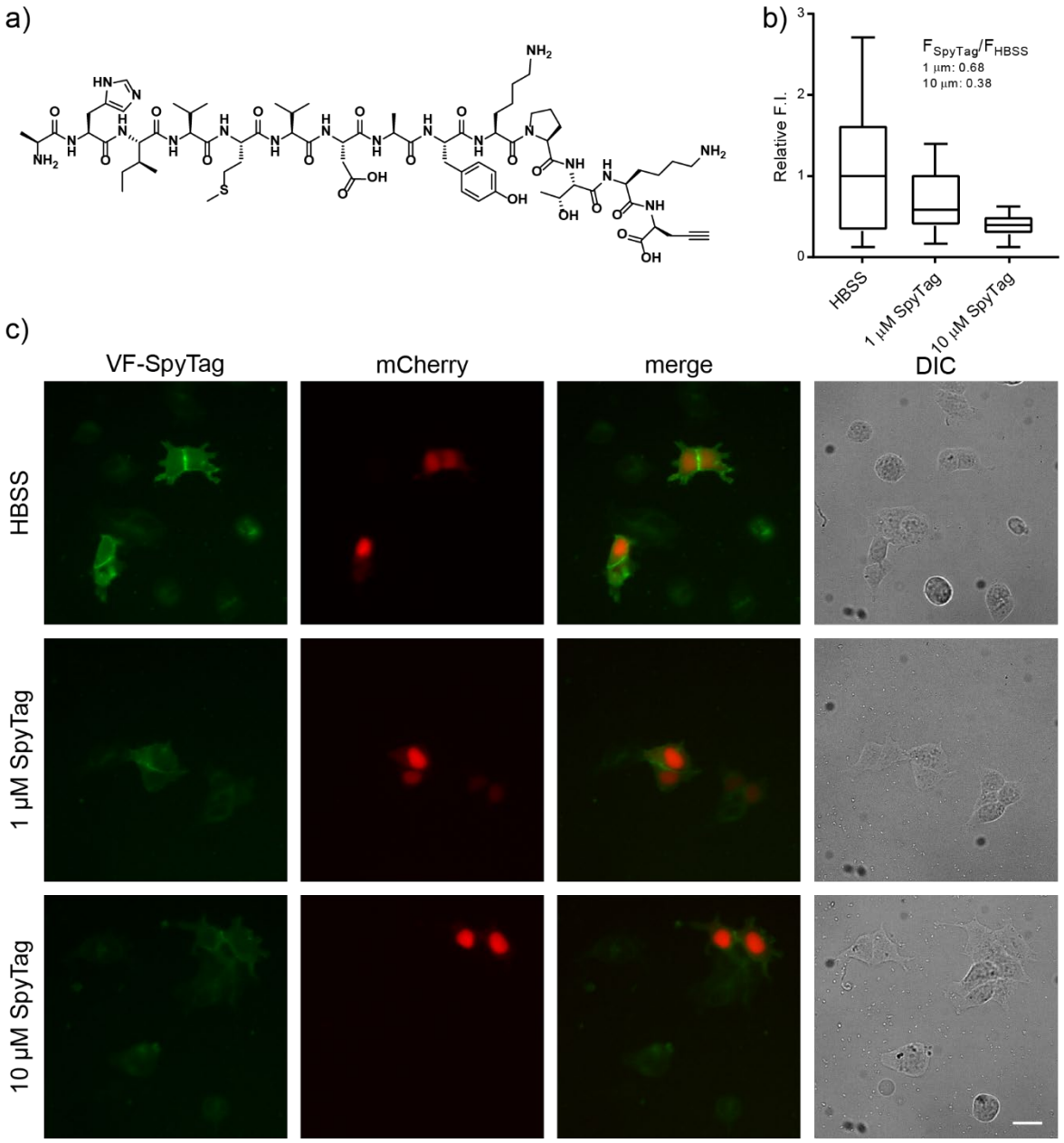

Competition studies with SpyTag/SpyCatcher. a) structure of SpyTag-Pra b) Tukey boxplot (the box defines the first quartile, median, and third quartile; whiskers define minimum and maximum values falling within 1.5 times the inter-quartile range) of cellular fluorescence of SpyCatcher expressing cells (as determined by expression of mCherry marker) after 30 minutes pre-incubation with either HBSS, 1 µM SpyTag-Pra or 10 µM SpyTag-Pra. 15-18 cells per condition. c) Widefield fluorescence and DIC microscopy images of VoltageSpy labeled HEK cells after pre-incubation. Scale bar is 20 µm.

Figure 4-11

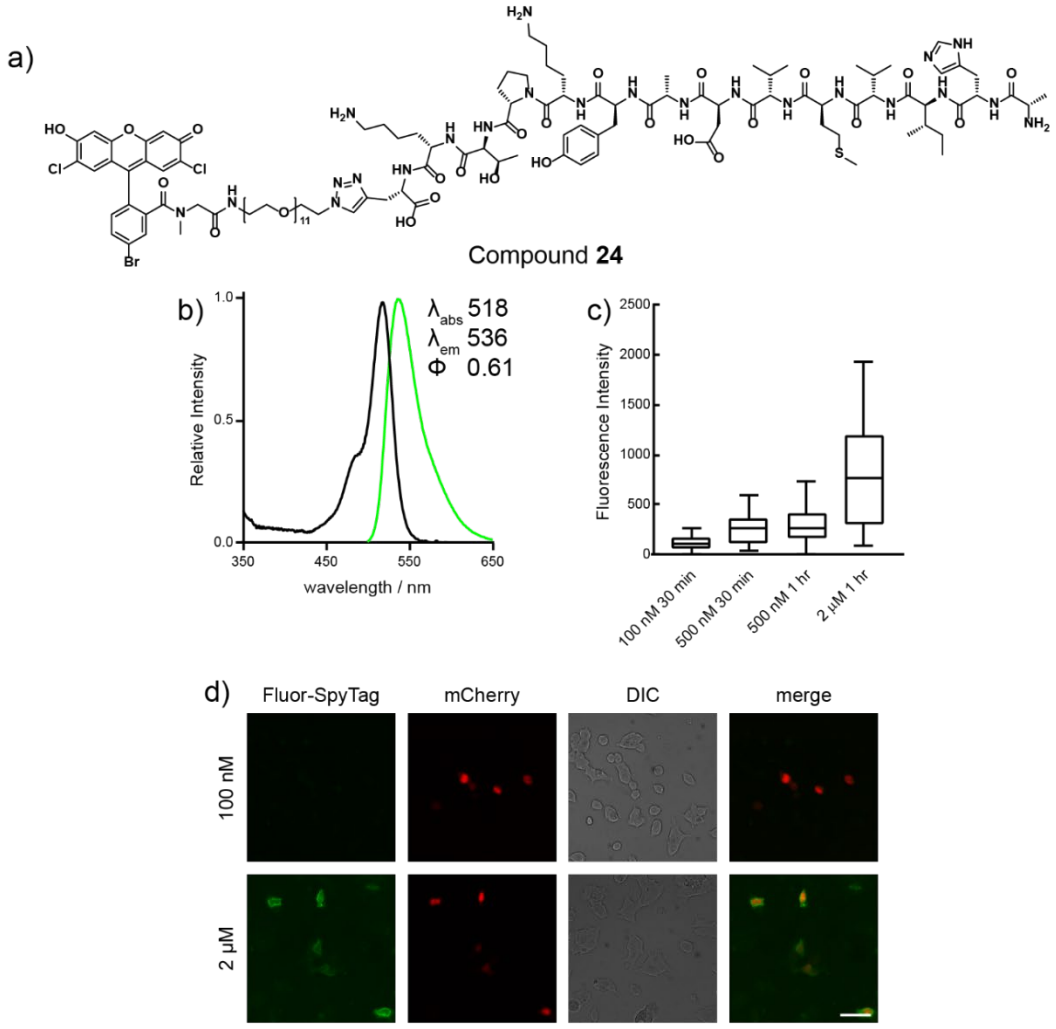

DCF-PEG$_{11}$-SpyTag is a poor substrate for surface-expressed SpyCatcher. a) Structure of DCF-PEG$_{11}$-SpyTag **24**. b) Absorbance (black) and emission (green) spectra of 24. c) Tukey boxplot (the box defines the first quartile, median, and third quartile; whiskers define minimum and maximum values falling within 1.5 times the inter-quartile range) of cellular fluorescence of HEK cells labeled with 24 under the concentrations and loading times. 35-45 cells per condition, no-wash labeling. d) Widefield fluorescence and DIC microscopy images of SpyCatcher expressing HEK cells labeled with **24**. Scale bar is 50 µM

Figure 4-12

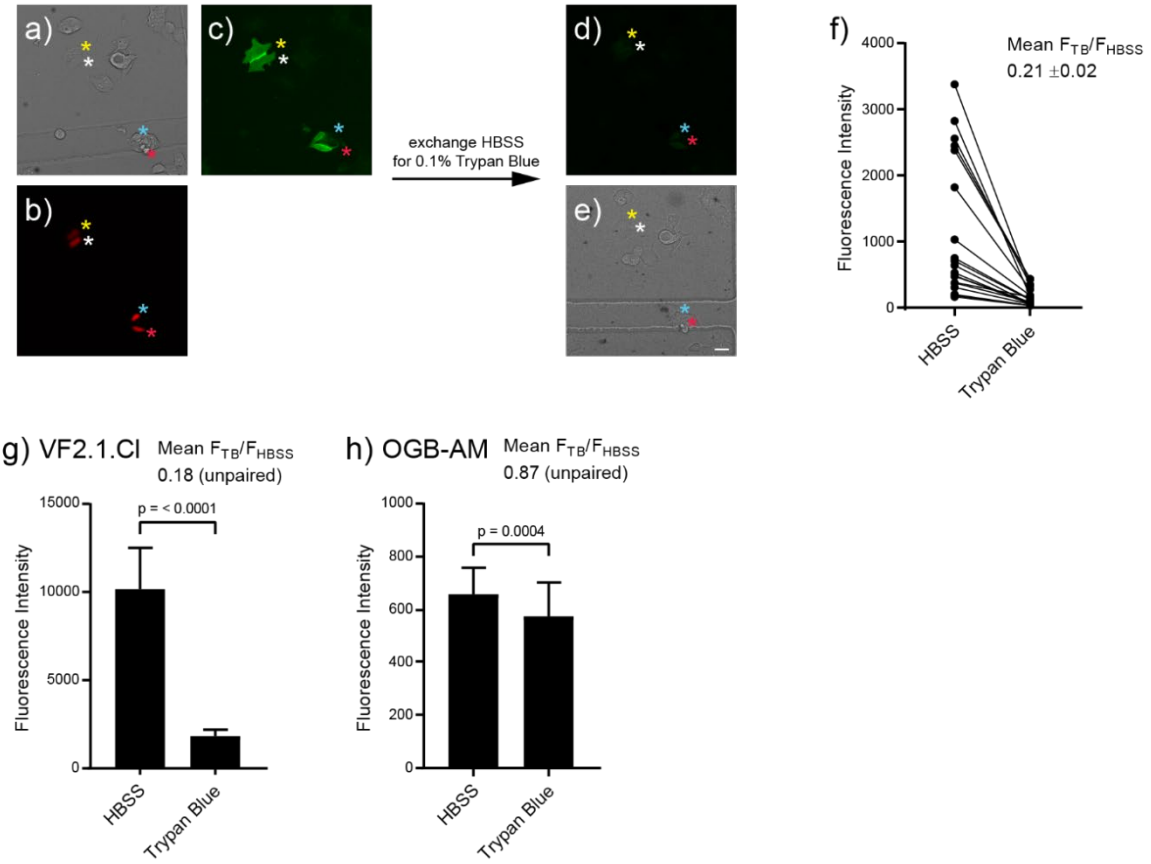

VoltageSpy indicators localize to the extracellular face of the plasma membrane. a-e) Representative widefield fluorescence and DIC images of HEK cells plated on gridded coverslips before (a-c) and after (d-e) quenching of extracelullar fluorescence with Trypan Blue. SpyCatcher expressing cells (a, b) were labeled with VoltageSpy **22** (c). After imaging in HBSS the imaging solution was exchanged with 0.1% Trypan Blue and the same cells (denoted by colored stars) were re-imaged (d-e). f) Quantification of Trypan Blue quenching of VoltageSpy labeled HEK cells. Data are from 19 individual cells. g-h) quantification of Trypan Blue quenching of HEK cells stained with 500 nM VF2.1.Cl, which localizes to the plasma membrane (g) or 1 µM Oregon Green (h), which accumulates in the cytosol and nucleus. Data are mean ± SD for 37 to 53 cells per condition. Scale bar is 20 µm.

Figure 4-13

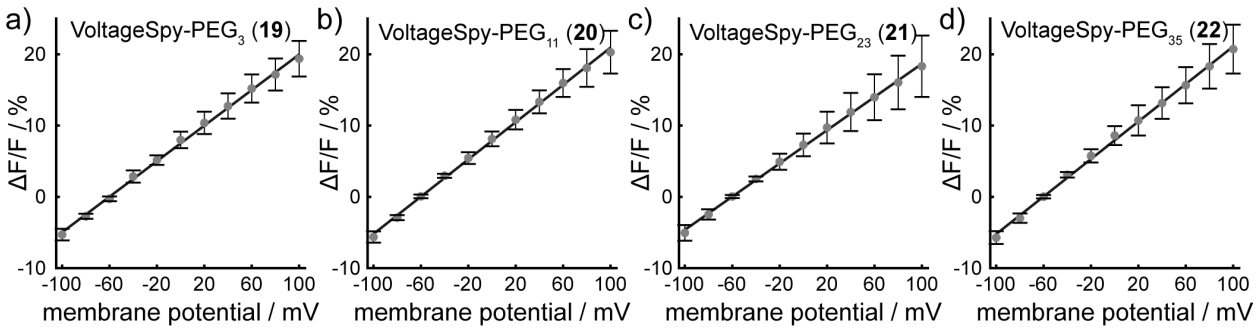

Voltage sensitivities of VoltageSpy compounds. a-d) Plots of fractional change in fluorescence (ΔF/F) vs membrane potential from HEK cells in whole-cell voltage clamp mode for VoltageSpy dyes **19** (a), **20** (b), **21** (c) and **22** (d). Data are mean ± SEM from $n \geq 5$ cells per condition.

Figure 4-14

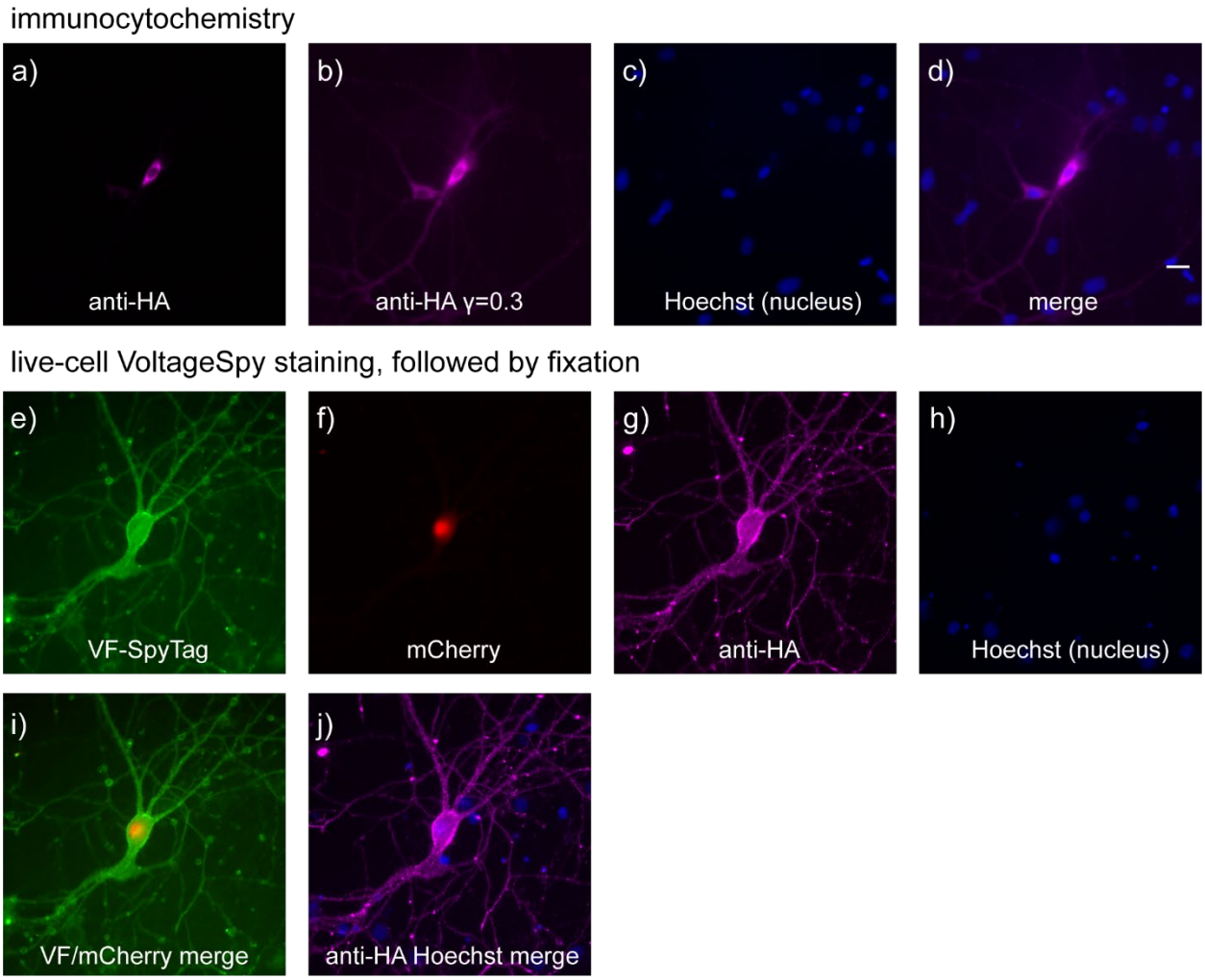

a-d) Widefield fluorescence microscopy of fixed and permeabilized hippocampal neurons. Immunocytochemistry of sparsely transfected neurons expressing SpyCatcher (anti-HA, a) indicates that there exists an appreciable intracellular pool of poorly trafficked SpyCatcher. However, the protein is indeed present throughout the processes of the cell, highlighted in gamma-adjusted panel (b). e-j) Widefield fluorescence microscopy images of a neuron labeled with VoltageSpy 20 (5 nM) (e,f), then fixed and stained for SpyCatcher (g), without permeabilization. Scale bar is 20 μm.

Figure 4-15

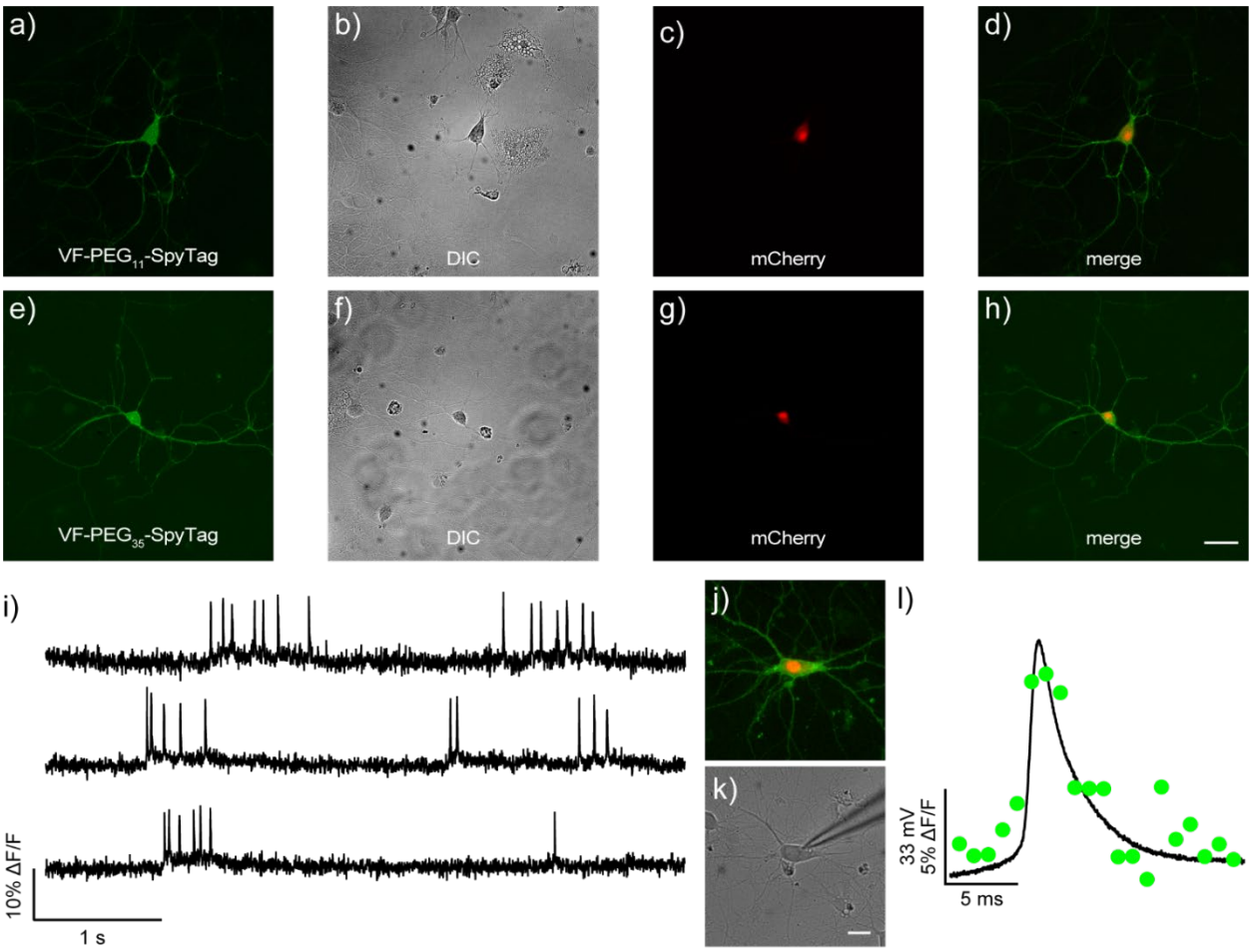

VoltageSpy dyes report on voltage dynamics in cultured hippocampal mammalian neurons. a-h) Widefield fluorescence and DIC microscopy images of neurons co-expressing SpyCatcher and nuclear mCherry labeled with VoltageSpy dyes **20** (a-d) and **22** (e-h). Scale bar is 40 µm. i) Representative ΔF/F traces of spontaneous activity recorded from SpyCatcher expressing neurons labeled with **22**. Traces are ΔF/F from regions of interest at the cell bodies of neurons after background offset and bleach correction. Images were acquired at 500 Hz and represent single-trial acquisitions. Fluorescence (j, merged VoltageSpy and mCherry signals) and DIC (k) microscopy images of a VoltageSpy **22** labeled neuron in whole-cell current clamp mode. Scale bar is 20 µm. l) Overlaid optical and electrophysiology signals from a single action potential in a current-clamped neuron. Optical trace was acquired at 1 kHz.

Figure 4-16

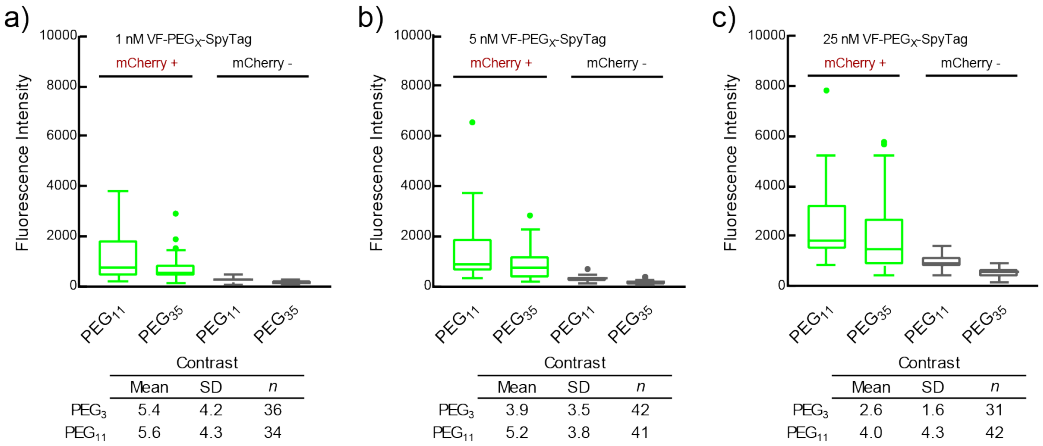

Quantification of VoltageSpy labeling in neurons. a-c) Tukey boxplots (the box defines the first quartile, median, and third quartile; whiskers define minimum and maximum values falling within 1.5 times the inter-quartile range) and quantification of cellular fluorescence of SpyCatcher expressing (mCherry positive) and untrasected (mCherry negative) neurons labeled with VoltageSpy dyes **20** (PEG$_{11}$) or **22** (PEG$_{35}$) at the indicated concentrations.

Figure 4-17

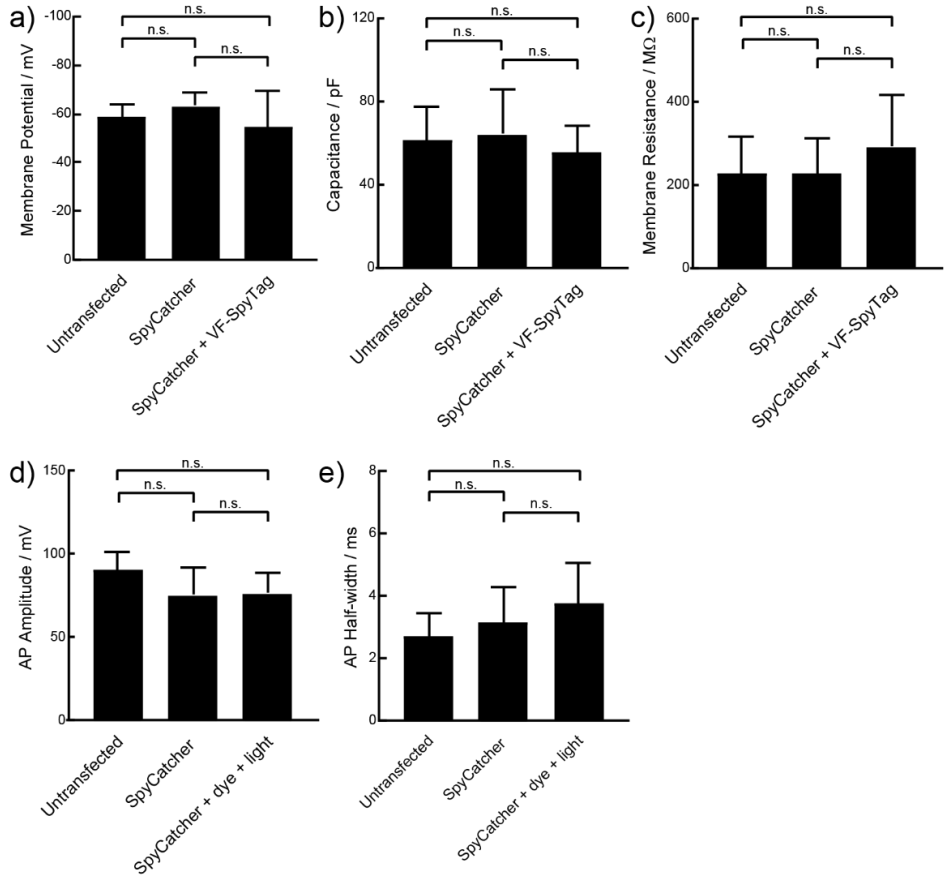

Resting membrane properties and action potential kinetics in SpyCatcher expressing and VoltageSpy labeled neurons. a-c) resting membrane potential (a), capacitance (b) and resistance (c) recorded from cultured mammalian neurons. Data were obtained from ten untransfected neurons, eight neurons expressing SpyCatcher and nine neurons expressing SpyCatcher and labeled with VoltageSpy **22** in whole-cell current-clamp mode. When these cells were induced to fire action potentials (50 ms current injection, 0.05 or 0.1 pA, 10 trials per cell) no differences were observed in action potential amplitude (d) or half-width (e). Data for VoltageSpy labeled cells in panels (d) and (e) were obtained under constant 8 mW/mm^2 illumination.

Figure 4-18

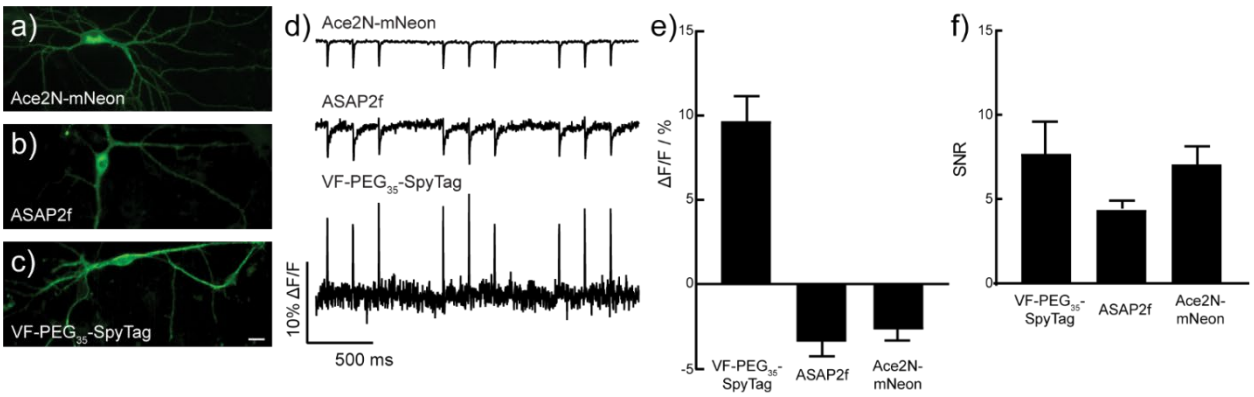

Comparison of VoltageSpy to GEVIs. Widefield fluorescence microscopy images of cultured hippocampal neurons expressing a) Ace2N-mNeon, b) ASAP2f or c) SpyCatcher and labeled with VoltageSpy **22**. Scale bar is 20 µm. d) Representative traces of optically recorded, evoked action potentials from each indicator recorded under identical imaging conditions (. e, f) Quantification of ΔF/F (e) and SNR (f) of evoked spikes. Data are mean ±SD for 17 (VoltageSpy), 15 (ASAP2f) and 15 (Ace2N-mNeon) cells and represent averaged ΔF/F and SNR values from all spikes in a single trace.

Figure 4-19

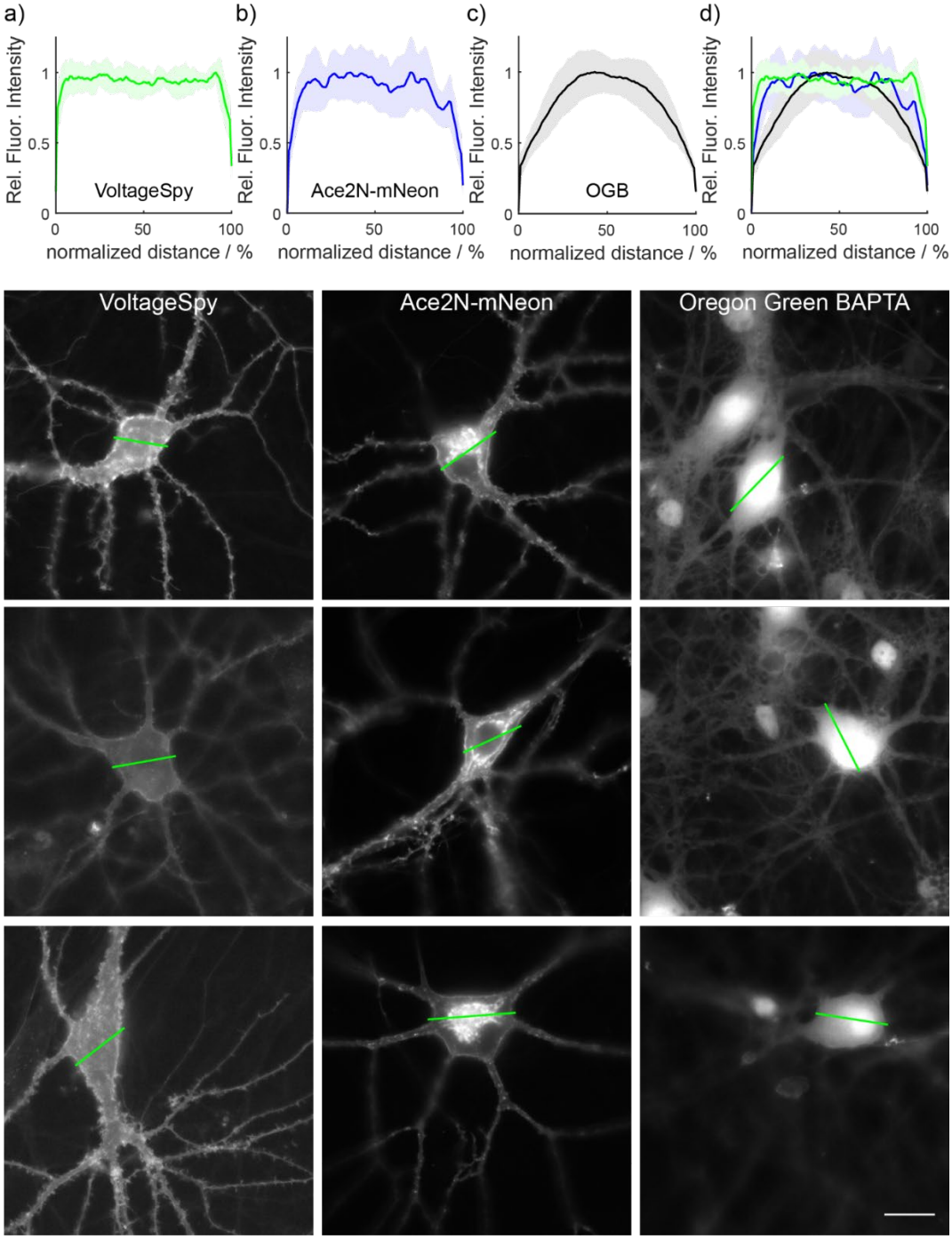

a-d) cellular distribution of membrane-targeted neuronal activity indicators VoltageSpy 22 (a), Ace2N-mNeon (b) as well the small-molecule calcium indicator Oregon-Green (c) which accumulates in the cytosol and nucleus. Line segments were drawn through cell bodies and normalized fluorescence intensity plotted against normalized distance. Images were acquired near the surface of the coverslip where axons and dendrites are in focus. Data represent n = 11, 15, or 11 cells for VoltageSpy, Ace2N-mNeon, or OGB-labeled neurons, respectively. Scale bar is 20 μm.

Figure 4-20

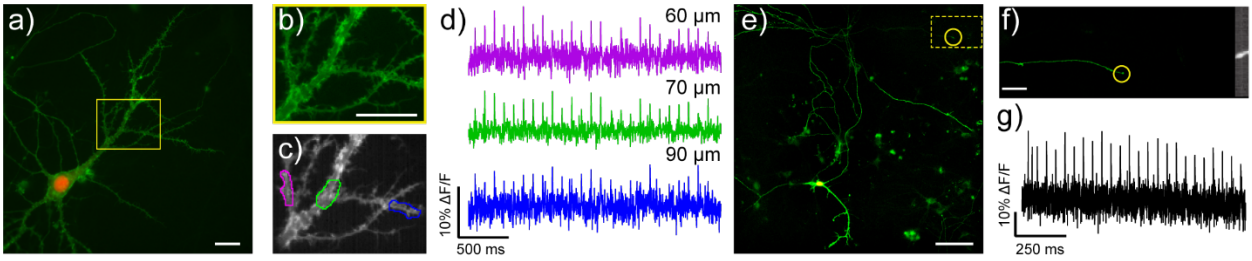

Sub-cellular voltage imaging with VoltageSpy dyes. a-d) imaging evoked action potentials in dendrites. a) Widefield fluorescence microscopy image of a hippocampal neuron co-expressing SpyCatcher and nuclear mCherry (red) and labeled with VoltageSpy **20** (green) under 63X magnification. Scale bar is 20 µm. b) Close-up of boxed region in panel (a). Scale bar is 20 µm. c) Average intensity projection of 2500 frames recorded at 500 Hz. ROIs are 10 µm long. d) ΔF/F traces of an evoked train of 25 APs. Color-coding corresponds to ROIs indicated in panel (c). Approximate distances from the center of the mCherry nucleus are indicated above each trace. e-g) imaging evoked action potentials in axons. e) Widefield fluorescence microscopy image of a hippocampal neuron co-expressing SpyCatcher and nuclear mCherry (red channel) and labeled with VoltageSpy **20** (green signal) under 20X magnification. Scale bar is 100 µm. f) Axon branch of the neuron in panel (e) under 63X magnification and close-up of axon terminal indicated by the yellow circle in panels (e) and (f) averaged intensity projection from 6000 frames imaged at 1.2 kHz. Scale bar is 10 µm. g) ΔF/F trace of an evoked train of 25 APs recorded at 1.2 kHz.

REFERENCES

1. Peterka, D. S.; Takahashi, H.; Yuste, R., Imaging Voltage in Neurons. *Neuron* **2011,** *69* (1), 9-21.

2. Scanziani, M.; Hausser, M., Electrophysiology in the age of light. *Nature* **2009,** *461* (7266), 930-939.

3. Davila, H. V.; Salzberg, B. M.; Cohen, L. B.; Waggoner, A. S., Large Change in Axon Fluorescence That Provides a Promising Method for Measuring Membrane-Potential. *Nature-New Biol* **1973,** *241* (109), 159-160.

4. Salzberg, B. M.; Davila, H. V.; Cohen, L. B., Optical Recording of Impulses in Individual Neurons of an Invertebrate Central Nervous-System. *Nature* **1973,** *246* (5434), 508-509.

5. Gupta, R. K.; Salzberg, B. M.; Grinvald, A.; Cohen, L. B.; Kamino, K.; Lesher, S.; Boyle, M. B.; Waggoner, A. S.; Wang, C. H., Improvements in Optical Methods for Measuring Rapid Changes in Membrane-Potential. *J Membrane Biol* **1981,** *58* (2), 123-137.

6. Fluhler, E.; Burnham, V. G.; Loew, L. M., Spectra, Membrane-Binding, and Potentiometric Responses of New Charge Shift Probes. *Biochemistry-Us* **1985,** *24* (21), 5749-5755.

7. Loew, L. M.; Bonneville, G. W.; Surow, J., Charge Shift Optical Probes of Membrane-Potential - Theory. *Biochemistry-Us* **1978,** *17* (19), 4065-4071.

8. Hubener, G.; Lambacher, A.; Fromherz, P., Anellated hemicyanine dyes with large symmetrical solvatochromism of absorption and fluorescence. *Journal of Physical Chemistry B* **2003,** *107* (31), 7896-7902.

9. Kuhn, B.; Fromherz, P., Anellated hemicyanine dyes in a neuron membrane: Molecular Stark effect and optical voltage recording. *Journal of Physical Chemistry B* **2003,** *107* (31), 7903-7913.

10. Cacciatore, T. W.; Brodfuehrer, P. D.; Gonzalez, J. E.; Jiang, T.; Adams, S. R.; Tsien, R. Y.; Kristan, W. B., Jr.; Kleinfeld, D., Identification of neural circuits by imaging coherent electrical activity with FRET-based dyes. *Neuron* **1999,** *23* (3), 449-59.

11. Gonzalez, J. E.; Tsien, R. Y., Voltage sensing by fluorescence resonance energy transfer in single cells. *Biophys J* **1995,** *69* (4), 1272-80.

12. Gonzalez, J. E.; Tsien, R. Y., Improved indicators of cell membrane potential that use fluorescence resonance energy transfer. *Chem Biol* **1997,** *4* (4), 269-77.

13. Li, L. S., Fluorescence probes for membrane potentials based on mesoscopic electron transfer. *Nano Letters* **2007,** *7*, 2981-2986.

14. De Silva, A. P.; Gunaratne, H. Q. N.; Habibjiwan, J. L.; Mccoy, C. P.; Rice, T. E.; Soumillion, J. P., New Fluorescent Model Compounds for the Study of Photoinduced Electron-Transfer - the Influence of a Molecular Electric-Field in the Excited-State. *Angew Chem Int Edit* **1995,** *34* (16), 1728-1731.

15. Huang, Y.-L.; Walker, A. S.; Miller, E. W., A Photostable Silicon Rhodamine Platform for Optical Voltage Sensing. *Journal of the American Chemical Society* **2015,** *137*, 10767-10776.

16. Kulkarni, R. U.; Kramer, D. J.; Pourmandi, N.; Karbasi, K.; Bateup, H. S.; Miller, E. W., Voltage-sensitive rhodol with enhanced two-photon brightness. *P Natl Acad Sci USA* **2017,** *114* (11), 2813-2818.

17. Kulkarni, R. U.; Yin, H.; Pourmandi, N.; James, F.; Adil, M. M.; Schaffer, D. V.; Wang, Y.; Miller, E. W., A Rationally Designed, General Strategy for Membrane Orientation of Photoinduced Electron Transfer-Based Voltage-Sensitive Dyes. *ACS Chem Biol* **2017,** *12* (2), 407-413.

18. Miller, E. W.; Lin, J. Y.; Frady, E. P.; Steinbach, P. A.; Kristan, W. B.; Tsien, R. Y., Optically monitoring voltage in neurons by photo-induced electron transfer through molecular wires. *P Natl Acad Sci USA* **2012,** *109* (6), 2114-2119.

19. Woodford, C. R.; Frady, E. P.; Smith, R. S.; Morey, B.; Canzi, G.; Palida, S. F.; Araneda, R. C.; Kristan, W. B., Jr.; Kubiak, C. P.; Miller, E. W.; Tsien, R. Y., Improved PeT molecules for optically sensing voltage in neurons. *J Am Chem Soc* **2015,** *137* (5), 1817-24.

20. Yang, H. H.; St-Pierre, F., Genetically Encoded Voltage Indicators: Opportunities and Challenges. *J Neurosci* **2016,** *36* (39), 9977-89.

21. Lin, M. Z.; Schnitzer, M. J., Genetically encoded indicators of neuronal activity. *Nature Neuroscience* **2016,** *19* (9), 1142-1153.

22. Siegel, M. S.; Isacoff, E. Y., A genetically encoded optical probe of membrane voltage. *Neuron* **1997,** *19* (4), 735-41.

23. Sakai, R.; Repunte-Canonigo, V.; Raj, C. D.; Knopfel, T., Design and characterization of a DNA-encoded, voltage-sensitive fluorescent protein. *Eur J Neurosci* **2001,** *13* (12), 2314-2318.

24. Ataka, K.; Pieribone, V. A., A genetically targetable fluorescent probe of channel gating with rapid kinetics. *Biophysical Journal* **2002,** *82* (1), 509-516.

25. St-Pierre, F.; Marshall, J. D.; Yang, Y.; Gong, Y. Y.; Schnitzer, M. J.; Lin, M. Z., High-fidelity optical reporting of neuronal electrical activity with an ultrafast fluorescent voltage sensor. *Nature Neuroscience* **2014,** *17* (6), 884-889.

26. Jin, L.; Han, Z.; Platisa, J.; Wooltorton, J. R. A.; Cohen, L. B.; Pieribone, V. A., Single Action Potentials and Subthreshold Electrical Events Imaged in Neurons with a Fluorescent Protein Voltage Probe. *Neuron* **2012,** *75* (5), 779-785.

27. Abdelfattah, A. S.; Farhi, S. L.; Zhao, Y. X.; Brinks, D.; Zou, P.; Ruangkittisakul, A.; Platisa, J.; Pieribone, V. A.; Ballanyi, K.; Cohen, A. E.; Campbell, R. E., A Bright and Fast Red Fluorescent Protein Voltage Indicator That Reports Neuronal Activity in Organotypic Brain Slices. *J Neurosci* **2016,** *36* (8), 2458-2472.

28. Kralj, J. M.; Douglass, A. D.; Hochbaum, D. R.; Maclaurin, D.; Cohen, A. E., Optical recording of action potentials in mammalian neurons using a microbial rhodopsin. *Nature Methods* **2012,** *9* (1), 90-U130.

29. Hochbaum, D. R.; Zhao, Y.; Farhi, S. L.; Klapoetke, N.; Werley, C. A.; Kapoor, V.; Zou, P.; Kralj, J. M.; Maclaurin, D.; Smedemark-Margulies, N.; Saulnier, J. L.; Boulting, G. L.; Straub, C.; Cho, Y. K.; Melkonian, M.; Wong, G. K. S.; Harrison, D. J.; Murthy, V. N.; Sabatini, B. L.;

Boyden, E. S.; Campbell, R. E.; Cohen, A. E., All-optical electrophysiology in mammalian neurons using engineered microbial rhodopsins. *Nature Methods* **2014,** *11* (8), 825-833.

30. Flytzanis, N. C.; Bedbrook, C. N.; Chiu, H.; Engqvist, M. K. M.; Xiao, C.; Chan, K. Y.; Sternberg, P. W.; Arnold, F. H.; Gradinaru, V., Archaerhodopsin variants with enhanced voltage-sensitive fluorescence in mammalian and Caenorhabditis elegans neurons. *Nature Communications* **2014,** *5*.

31. Herwig, L.; Rice, A. J.; Bedbrook, C. N.; Zhang, R. J. K.; Lignell, A.; Cahn, J. K. B.; Renata, H.; Dodani, S. C.; Cho, I.; Cai, L.; Gradinaru, V.; Arnold, F. H., Directed Evolution of a Bright Near-Infrared Fluorescent Rhodopsin Using a Synthetic Chromophore. *Cell Chem Biol* **2017,** *24* (3), 415-425.

32. Piatkevich, K. D.; Jung, E. E.; Straub, C.; Linghu, C. Y.; Park, D.; Suk, H. J.; Hochbaum, D. R.; Goodwin, D.; Pnevmatikakis, E.; Pak, N.; Kawashima, T.; Yang, C. T.; Rhoades, J. L.; Shemesh, O.; Asano, S.; Yoon, Y. G.; Freifeld, L.; Saulnier, J. L.; Riegler, C.; Engert, F.; Hughes, T.; Drobizhev, M.; Szabo, B.; Ahrens, M. B.; Flavell, S. W.; Sabatini, B. L.; Boyden, E. S., A robotic multidimensional directed evolution approach applied to fluorescent voltage reporters. *Nature Chemical Biology* **2018,** *14* (4), 352-+.

33. Zou, P.; Zhao, Y. X.; Douglass, A. D.; Hochbaum, D. R.; Brinks, D.; Werley, C. A.; Harrison, D. J.; Campbell, R. E.; Cohen, A. E., Bright and fast multicoloured voltage reporters via electrochromic FRET. *Nature Communications* **2014,** *5*.

34. Gong, Y. Y.; Wagner, M. J.; Li, J. Z.; Schnitzer, M. J., Imaging neural spiking in brain tissue using FRET-opsin protein voltage sensors. *Nature Communications* **2014,** *5*.

35. Gong, Y. Y.; Huang, C.; Li, J. Z.; Grewe, B. F.; Zhang, Y. P.; Eismann, S.; Schnitzer, M. J., High-speed recording of neural spikes in awake mice and flies with a fluorescent voltage sensor. *Science* **2015,** *350* (6266), 1361-1366.

36. Baker, B. J.; Lee, H.; Pieribone, V. A.; Cohen, L. B.; Isacoff, E. Y.; Knopfel, T.; Kosmidis, E. K., Three fluorescent protein voltage sensors exhibit low plasma membrane expression in mammalian cells. *J Neurosci Meth* **2007,** *161* (1), 32-38.

37. Baker, B. J.; Lee, H.; Cohen, L.; Ataka, K.; Kosmidis, E.; Isacoff, E.; Knopfel, T.; Pieribone, V., Screening for plasma membrane expression of fluorescent protein (FP)-voltage sensors. *Biophysical Journal* **2005,** *88* (1), 171a-171a.

38. Chanda, B.; Blunck, R.; Faria, L. C.; Schweizer, F. E.; Mody, I.; Bezanilla, F., A hybrid approach to measuring electrical activity in genetically specified neurons. *Nature Neuroscience* **2005,** *8* (11), 1619-1626.

39. Sjulson, L.; Miesenbock, G., Rational optimization and Imaging *in vivo* of a genetically encoded optical voltage reporter. *J Neurosci* **2008,** *28* (21), 5582-5593.

40. Bayguinov, P. O.; Ma, Y. H.; Gao, Y.; Zhao, X. Y.; Jackson, M. B., Imaging Voltage in Genetically Defined Neuronal Subpopulations with a Cre Recombinase-Targeted Hybrid Voltage Sensor. *J Neurosci* **2017,** *37* (38), 9305-9319.

41. Ghitani, N.; Bayguinov, P. O.; Ma, Y. H.; Jackson, M. B., Single-trial imaging of spikes and synaptic potentials in single neurons in brain slices with genetically encoded hybrid voltage sensor. *J Neurophysiol* **2015,** *113* (4), 1249-1259.

42. Wang, D. S.; Zhang, Z.; Chanda, B.; Jackson, M. B., Improved Probes for Hybrid Voltage Sensor Imaging. *Biophysical Journal* **2010,** *99* (7), 2355-2365.

43. Hinner, M. J.; Hbener, G.; Fromherz, P., Enzyme-induced staining of biomembranes with voltage-sensitive fluorescent dyes. *J Phys Chem B* **2004,** *108* (7), 2445-53.

44. Hinner, M. J.; Hubener, G.; Fromherz, P., Genetic targeting of individual cells with a voltage-sensitive dye through enzymatic activation of membrane binding. *Chembiochem* **2006,** *7* (3), 495-505.

45. Ng, D. N.; Fromherz, P., Genetic targeting of a voltage-sensitive dye by enzymatic activation of phosphonooxymethyl-ammonium derivative. *ACS Chem Biol* **2011,** *6* (5), 444-51.

46. Xu, Y. X.; Peng, L. X.; Wang, S. C.; Wang, A. Q.; Ma, R. R.; Zhou, Y.; Yang, J. H.; Sun, D. E.; Lin, W.; Chen, X.; Zou, P., Hybrid Indicators for Fast and Sensitive Voltage Imaging. *Angew Chem Int Edit* **2018,** *57* (15), 3949-3953.

47. Liu, P.; Grenier, V.; Hong, W.; Muller, V. R.; Miller, E. W., Fluorogenic Targeting of Voltage-Sensitive Dyes to Neurons. *J Am Chem Soc* **2017,** *139* (48), 17334-17340.

48. Los, G. V.; Encell, L. P.; McDougall, M. G.; Hartzell, D. D.; Karassina, N.; Zimprich, C.; Wood, M. G.; Learish, R.; Ohane, R. F.; Urh, M.; Simpson, D.; Mendez, J.; Zimmerman, K.; Otto, P.; Vidugiris, G.; Zhu, J.; Darzins, A.; Klaubert, D. H.; Bulleit, R. F.; Wood, K. V., HatoTag: A novel protein labeling technology for cell imaging and protein analysis. *Acs Chemical Biology* **2008,** *3* (6), 373-382.

49. Keppler, A.; Gendreizig, S.; Gronemeyer, T.; Pick, H.; Vogel, H.; Johnsson, K., A general method for the covalent labeling of fusion proteins with small molecules *in vivo*. *Nat Biotechnol* **2003,** *21* (1), 86-89.

50. Gallagher, S. S.; Sable, J. E.; Sheetz, M. P.; Cornish, V. W., An *In Vivo* Covalent TMP-Tag Based on Proximity-Induced Reactivity. *Acs Chemical Biology* **2009,** *4* (7), 547-556.

51. Vivero-Pol, L.; George, N.; Krumm, H.; Johnsson, K.; Johnsson, N., Multicolor Imaging of cell surface proteins. *Journal of the American Chemical Society* **2005,** *127* (37), 12770-12771.

52. Zakeri, B.; Fierer, J. O.; Celik, E.; Chittock, E. C.; Schwarz-Linek, U.; Moy, V. T.; Howarth, M., Peptide tag forming a rapid covalent bond to a protein, through engineering a bacterial adhesin. *Proc Natl Acad Sci U S A* **2012,** *109* (12), E690-7.

53. Deal, P. E.; Kulkarni, R. U.; Al-Abdullatif, S. H.; Miller, E. W., Isomerically Pure Tetramethylrhodamine Voltage Reporters. *J Am Chem Soc* **2016,** *138* (29), 9085-8.

54. Jiao, G. S.; Han, J. W.; Burgess, K., Syntheses of regioisomerically pure 5- or 6-halogenated fluoresceins. *J Org Chem* **2003,** *68* (21), 8264-7.

55. Kim, J.; Zhao, T.; Petralia, R. S.; Yu, Y.; Peng, H.; Myers, E.; Magee, J. C., mGRASP enables mapping mammalian synaptic connectivity with light microscopy. *Nat Methods* **2011,** *9* (1), 96-102.

56. Wakayama, S.; Kiyonaka, S.; Arai, I.; Kakegawa, W.; Matsuda, S.; Ibata, K.; Nemoto, Y. L.; Kusumi, A.; Yuzaki, M.; Hamachi, I., Chemical labelling for visualizing native AMPA receptors in live neurons. *Nat Commun* **2017,** *8*, 14850.

57. Li, L.; Fierer, J. O.; Rapoport, T. A.; Howarth, M., Structural analysis and optimization of the covalent association between SpyCatcher and a peptide Tag. *J Mol Biol* **2014,** *426* (2), 309-17.

58. Yang, H. H.; St-Pierre, F.; Sun, X.; Ding, X.; Lin, M. Z.; Clandinin, T. R., Subcellular Imaging of Voltage and Calcium Signals Reveals Neural Processing *In Vivo*. *Cell* **2016,** *166* (1), 245-57.

59. Gong, Y.; Huang, C.; Li, J. Z.; Grewe, B. F.; Zhang, Y.; Eismann, S.; Schnitzer, M. J., High-speed recording of neural spikes in awake mice and flies with a fluorescent voltage sensor. *Science* **2015,** *350* (6266), 1361-6.

60. St-Pierre, F.; Marshall, J. D.; Yang, Y.; Gong, Y.; Schnitzer, M. J.; Lin, M. Z., High-fidelity optical reporting of neuronal electrical activity with an ultrafast fluorescent voltage sensor. *Nat Neurosci* **2014,** *17* (6), 884-9.

61. Antic, S.; Zecevic, D., Optical Signals from Neurons with Internally Applied Voltage-Sensitive Dyes. *J Neurosci* **1995,** *15* (2), 1392-1405.

62. Yan, P.; Acker, C. D.; Zhou, W. L.; Lee, P.; Bollensdorff, C.; Negrean, A.; Lotti, J.; Sacconi, L.; Antic, S. D.; Kohl, P.; Mansvelder, H. D.; Pavone, F. S.; Loew, L. M., Palette of fluorinated voltage-sensitive hemicyanine dyes. *P Natl Acad Sci USA* **2012,** *109* (50), 20443-20448.

63. Roome, C. J.; Kuhn, B., Simultaneous dendritic voltage and calcium imaging and somatic recording from Purkinje neurons in awake mice. *Nature Communications* **2018,** *9*.

64. Bradley, J.; Luo, R.; Otis, T. S.; DiGregorio, D. A., Submillisecond Optical Reporting of Membrane Potential In Situ Using a Neuronal Tracer Dye. *J Neurosci* **2009,** *29* (29), 9197-9209.

65. Fink, A. E.; Bender, K. J.; Trussell, L. O.; Otis, T. S.; DiGregorio, D. A., Two-Photon Compatibility and Single-Voxel, Single-Trial Detection of Subthreshold Neuronal Activity by a Two-Component Optical Voltage Sensor. *Plos One* **2012,** *7* (8).

66. Hoppa, M. B.; Gouzer, G.; Armbruster, M.; Ryan, T. A., Control and Plasticity of the Presynaptic Action Potential Waveform at Small CNS Nerve Terminals. *Neuron* **2014,** *84* (4), 778-789.

67. Spruston, N.; Jaffe, D. B.; Williams, S. H.; Johnston, D., Voltage- and space-clamp errors associated with the measurement of electrotonically remote synaptic events. *J Neurophysiol* **1993,** *70* (2), 781-802.

68. Keeble, A. H.; Banerjee, A.; Ferla, M. P.; Reddington, S. C.; Anuar, I.; Howarth, M., Evolving Accelerated Amidation by SpyTag/SpyCatcher to Analyze Membrane Dynamics. *Angew Chem Int Ed Engl* **2017,** *56* (52), 16521-16525.

Chapter 5

Mitigating VoltageFluor Photoxicity with Triplet State Quenchers and an Intramolecularly Stabilized VoltageFluor

Portions of this work were completed in collaboration with others:

mVF-PipCys was synthesized in collaboration with Johnathan C. Maza

Introduction

Voltage-sensitive dyes (VSDs) of the VoltageFluor (VF) family[1] have proven to be useful tools for the study of membrane potential and have been applied in a variety of biological contexts including three-dimensional neuronal cultures,[2–5] mouse brain slice,[6] *in vivo* imaging in mice,[7] cultured stem-cell derived cardiomyocytes,[8–15] leech ganglia[16] and pancreatic β-cells.[17] Our lab has invested considerable efforts into facilitating these experiments by developing new VoltageFluors with red-shifted emission,[7,18,19] increased voltage-sensitivity[20,21] and increased two-photon cross-sections.[6,7] However, although a recently disclosed compound with a fluorene molecular wire showed reduced phototoxicity in cardiomyocytes,[8] we have not yet systematically addressed phototoxic effects sometimes encountered when imaging green fluorescein-based VoltageFluors in neurons.

Chapter 4 and its accompanying publication reported the development of genetically-targeted dyes based on a new class of sarcosine VoltageFluors.[22] When we sought to characterize the performance of the best of these VF dyes (referred to here as mVF-sarcosine, Scheme 5-1) using field stimulation in cultured mammalian we sometimes observed aberrant behavior in the neurons under investigation (Figure 5-1), including a progressive drop in action potential ΔF/F across the duration of the recording (it is unclear if this represents a physiological drop in AP amplitude or degradation of active voltage indicator), sharp jumps in the baseline fluorescence intensity and small spikelets which did not track with stimulus pulses (we classify these after "afterdepolarizations" or "non-evoked spikes" depending on whether or not they track with evoked APs). Under most experimental conditions it is possible to mitigate these effects by titrating dye concentration and light power, however in the case of covalently attached, genetically targeted VoltageFluors, the effective concentration of dye in the membrane is governed by expression-levels of a self-labeling protein,[22] making it more difficult to avoid these effects.

Phototoxicity from fluorophores is often driven by intersystem crossing of the excited fluorophore into the triplet state, followed by generation of highly reactive singlet oxygen – a mechanism which has been harnessed for therapeutic applications as photodynamic therapy.[23] It therefore follows that a method to suppress this mechanism might reduce the incidence of phototoxic effects. There exists some precedence for this in the literature: the carotenoid anti-oxidant astaxanthin[24] has been employed to reduce phototoxic effect of oxonol VSDs in cultured cardiomyocytes.[25] In addition, the addition of triplet state quenchers (TSQs)[26] has been used to prevent photobleaching of fluorophores which is also largely driven by the formation of singlet oxygen,[27,28] most prominently in the context of single-molecule imaging.[29,30] We were particularly interested in the work of the Blanchard Lab, who have developed a series of intramolecularly stabilized Cy dyes[31–34] which incorporate a TSQ directly into the structure of the fluorophore. These stabilized fluorophores, commercialized by Lumidyne Technologies, show exceptional resistance to photobleaching without necessitating the addition of high concentrations of free TSQ but have not been exploited in the development of fluorescent indicators. Based on these precedents we set out on a two-pronged effort aimed at developing both i) a protocol for imaging extant VoltageFluors with TSQs and ii) intramolecularly-stabilized VSDs (mVF-Trolox1 and VF-COT1, Scheme 5-1).

Results and Discussion

Imaging mVF-sarcosine with TSQs

The phototoxicity artifacts discussed above and illustrated in Figure 5-1 are prominent in field-stimulation experiments, and we continue to use this system as a testbed for imaging with TSQs. In our protocol, 13-15 DIV embryonic rat hippocampal neurons loaded with 500 nM dye are imaged with 475 nm excitation (LED, 34 nm bandpass) at a light power of 21 mW/mm^2. Stimuli are delivered in three 5 Hz, 400 ms "epochs" in a 2.5 second optical recording (Figure 5-1a,b) in the presence NMDA and AMPA receptor antagonists to suppress spontaneous activity. To quantify possible effects of TSQs on the behavior of our probes we measured the following metrics: cellular fluorescence intensity at the soma; first epoch ΔF/F; the fractional change in ΔF/F between epoch 1 and epoch 3 (the ratio of ΔF/F in epoch 3 divided by ΔF/F in epoch 1); and bleach rate (the slope of a least-squares linear regression fit to the optical trace). In addition to our quantitative analysis, optical traces from individual neurons were qualitatively binned based on the presence of artifacts.

We chose to work with two TSQs: Trolox and cyclooctatetraene (COT). Trolox is a popular antifading agent[29] which appears to quench triplets through a redox cycle,[35,36] while COT is employed in the Blanchard lab's intramolecularly stabilized Cy dyes[31,32,34] and is believed to function through an energy-transfer mechanism.[28,30,37] We imaged neurons without addition of a TSQ, with 1 mM Trolox or with 1 mM COT (n = 33, 26, and 38 cells, respectively) and found that addition of Trolox, but not COT, led to a modest increase in brightness (Figure 5-2a). No significant differences were found in the first epoch ΔF/F, which was 7.4 ±2.1 under control conditions (Figure 5-2b). However, we did find a dramatic effect in the fractional change in sensitivity over the course of the experiment. Whereas control experiments and experiments with 1 mM Trolox showed a decrease in voltage sensitivity (60 ± 14% and 76 ± 10% of initial sensitivity for control and Trolox, respectively), 1 mM COT completely prevents a loss in sensitivity (100 ± 4% of original values; all values are mean ±SD, Figure 5-2c). The effectiveness of the TSQs, and particularly COT, in mitigating the drop in voltage sensitivity across the illumination period was gratifying, and supported our belief that suppressing the population of VoltageFluor in the triplet state would decrease phototoxic effects. We did, however, observe a surprising effect on the rate of photobleaching which increased in the presence of TSQs, the effect being more pronounced with Trolox (Figure 5-2d). This seemingly paradoxical effect has previously been reported with Trolox,[36] and arises in cases where the radical cation formed by electron transfer from the triplet-state fluorophore to Trolox is less stable than the triplet-state fluorophore itself. In solution some Trolox will degrade to form a quinoid species which can an act as an oxidant, rapidly returning the fluorophore to the ground state.[35] It is therefore likely that we could reverse the increased rate of bleaching by imaging with an older stock of Trolox, as is recommended in some imaging protocols.[29,35]

Addition of TSQs had a dramatic effect on the incidence of non-evoked effects in our optical measurements (Table 5-1). Only 12% (4/33) of traces under control conditions showed no obvious artifacts (afterdepolarizations, non-evoked spikes or baseline shifts), compared to 27% in the presence of 1 mM Trolox (7/26) and 89% (34/38) in the presence of 1 mM COT. Our results

suggest that COT may prove to be a broadly useful additive in future imaging experiments where phototoxicity is a concern.

Design and Synthesis of an Intramolecular Stabilized VoltageFluor

We designed two target intramolecularly stabilized VoltageFluors, mVF-Trolox1 and mVF-COT1 (Scheme 5-1, Scheme 5-2), both of which can be accessed in a single step from intermediate VoltageFluor mVF-PipCys. While the sarcosine carboxylic acid handle on mVF-sarcosine would appear to be a natural site for derivatization, or experience with VoltageSpy dyes suggested that introduction of a lipophilic conjugate at this position would likely lead to a cell-permeable compound. By swapping the sarcosine linker for a piperazine-cysteic acid bridge we introduced a constitutively charged sulfonate to maintain cell impermeability and generated a linker with a terminal amine which could serve as a substrate for amide coupling with Trolox of COT-carboxylic acid.[32]

Analogously to the synthesis of mVF-sarcosine, synthesis of mVF-PipCys begins with isomerically pure dichlorofluorescein **1**. HATU-mediated amide coupling with Boc-protected piperazine gave **2** in 89% yield. Heck coupling with a phenylenevinylene molecular wire gave **3** in excellent (92%) yield, after which a subsequent amide coupling with Boc-protected cysteic acid provided intermediate **4** in 50% yield. Although conversion of **3** to **4** was found to be quantitative by LC-MS, **4** adsorbs tightly on silica, complicating recovery by preparative TLC. From **4**, Boc-deprotection and trituration gave novel VoltageFluor mVF-PipCys in 90% yield, while amide coupling with Trolox gave mVF-Trolox1 in 20% yield after purification by preparative HPLC. At the time of writing mVF-COT1 has not yet been synthesized.

Imaging mVF-PipCys and mVF-Trolox 1

We repeated our imaging protocol with 500 nM mVF-PipCys in the absence of TSQs, with 1 mM Trolox or with 1 mM COT (n = 35, 36 and 30 cells, respectively). mVF-PipCys was dimmer than mVF-sarcosine, but maintained a similar first epoch ΔF/F (8.2 ±2.8 in the absence of TSQs, Figure 5-3a,b). Key findings observed with mVF-sarcosine were recapitulated: an improvement in fractional change in sensitivity in the presence of Trolox, which approached 1.0 with addition of COT (Figure 5-3c). TSQs also increased the rate of bleaching, with this effect being more pronounced with Trolox (Figure 5-3d). As with mVF-sarcosine, addition of COT strongly decreased the incidence of non-evoked effects in optical traces (Table 5-2) – 90% (27/30) of traces were free of artifacts, compared to 29% (10/35) for control conditions and 17% with addition of Trolox (6/36).

mVF-Trolox1 behaves quite differently than mVF-PipCys + Trolox. Although both dyes were equally bright when bath applied to neurons, first epoch ΔF/F decreased from 9.3 ±2.5% to 5.5 ±1.6% (Figure 5-4a,b). More prominently, mVF-Trolox showed a fractional change in voltage of sensitivity of 1.09 ±0.09, versus 0.93 ±0.15 for mVF-PipCys + Trolox (Figure 5-4c). That is, ΔF/F increased slightly from epoch 1 to epoch 3 (Figure 5-4). mVF-Trolox also showed a steady increase in fluorescence over time, rather than a bleaching effect (Figure 5-4d, Figure 5-5). It should be noted that while our bleach correction protocol appears to work reasonably well, imperfect bleach correction could, in this case, account for some of the measured increase in

sensitivity. Such a "positive" bleaching effect has been observed in VoltageFluors before, such as our red-shifted, rhodamine-based RhoVRs.[18] It likely arises in situations where the molecular wire moiety is more susceptible to degradation than the fluorophore, breaking the electronic coupling between the aniline electron donor and fluorophore and decreasing quenching of the fluorophore. Photochemical experiments on intramolecularly-stabilized Cy dyes shows that while Cy5-Trolox bleaches at a slower rate than Cy5 alone, the conjugated Trolox does not directly interact with the Cy5 triplet state and may operate through a more general mechanism as an ROS scavenger.[28] If the dichlorofluorescein fluorophore is protected from photodegradation in mVF-Trolox1 but not when Trolox is bath applied to mVF-PipCys, that could account for the observed increase in fluorescence upon illumination.

mVF-Trolox1 reduced the incidence of non-evoked effects in optical recordings (Table 5-2, with 57% (20/35) of traces showing no artifacts, a substantial improvement over control conditions or the addition of external Trolox (which showed no protective effects with mVF-PipCys). While this is a marked improvement, bath-applied COT remains a more effective reagent for combatting phototoxicity.

Concluding Remarks

In keeping with our hypothesis that the phototoxic effects of green VoltageFluors could be mitigated by imaging with TSQs, addition of 1 mM COT to our imaging solution almost completely eliminated non-evoked artifacts in field-stimulation recordings across two different, though structurally related, VoltageFluors. Trolox, which acts through an electron transfer mechanism, showed more mixed results; the decrease in spike amplitude over time was lessened, but there was limited improvement in the appearance of artifacts such as non-evoked activity and jumps in baseline fluorescence intensity.

mVF-Trolox1, an intramolecularly stabilized VoltageFluor, had a greater impact on phototoxic effects than bath applied Trolox. Unexpected differences between the two conditions, such as different bleaching behavior, can be reconciled with existing results on the mechanism of action of intramolecularly stabilized fluorophores. It will be interesting to see if and how VF-COT1 differs from VoltageFluor + COT. Because intramolecular stabilization by COT proceeds through an energy transfer process, the difference may be less stark than what is observed with Trolox.

Should VF-COT1 prove to be a useful probe with minimal phototoxic effects, it could also form the basis for new, intramolecularly stabilized, targeted VoltageFluors which take advantage of a branched linker to incorporate both a TSQ and targeting moiety such as SpyTag, benzyl guanine or a haloalkane.

General Synthetic and Analytical Methods

Chemical reagents and solvents were purchased from commercial suppliers and used without further purification. Thin layer chromatography (TLC) and preparative thin layer chromatography (PTLC) was performed on glass backed plates pre-coated with silica gel (Silicyle, F254, 250 μm (TLC) or 1000 μm (PTLC)). Plates were visualized by fluorescence quenching

under UV light. Flash column chromatography was performed on Silicycle Silica Flash F60 (230–400 Mesh) using a forced flow of air at 0.5–1.0 bar.

^{1}H spectra were collected in DMSO-d_6 at 25 °C on a Bruker AV-600 spectrometer at the College of Chemistry NMR Facility at the University of California, Berkeley. All chemical shifts are reported in the standard δ notation of parts per million using the peak of residual proton signals of DMSO-d_6 as an internal reference. Low resolution LC/ESI-MS was performed on an Advion Expression LC-MS coupled to an Agilent Infinity 1220 HPLC, with a Phenomenex Luna 5 µm C18(2) 75 x 4.6 mm column. Water (eluent A) and acetonitrile (eluent B) were employed as the mobile phase, with 0.05% trifluoroacetic acid present as an additive. For analytical HPLC the mobile phase was ramped from 10 to 100% eluent B over eight minutes, then held at 100% B for two minutes at a flow rate of 1.0 mL/minute. Preparative HPLC was performed using a Waters Acquity Autopurification system (prep UHPLC-MS). The column used for preparative HPLC was an XBridge OBD Prep Column (5 µm, 19mm I.D. x 250 mm) with a flow rate of 30.0 mL/min. The mobile phases were MQ-H2O with 0.05% trifluoroacetic acid (eluent A) and HPLC grade acetonitrile with 0.05% trifluoroacetic acid (eluent B). Signals were monitored at 254 over 20 min with a gradient of 10-100% eluent B and by ESI-MS.

Cell culture, transfection, and dye loading

All animal procedures were approved by the UC Berkeley Animal Care and Use Committees and conformed to the NIH Guide for the Care and Use of Laboratory Animals and the Public Health Service (PHS) Policy.

Hippocampi were dissected from embryonic day 19 Sprague Dawley rats (Charles River Laboratory) in cold, sterile HBSS (zero Ca^{2+}, zero Mg^{2+}, phenol red). All dissection products were supplied by Invitrogen, unless otherwise stated. Hippocampal tissue was treated with trypsin (2.5%) for 15 min at 37 °C. The tissue was triturated using fire polished Pasteur pipettes, in minimum essential media (MEM) supplemented with 5% FBS, 2% B-27, 2% 1M dextrose (Fisher Scientific) and 1% GlutaMax. The dissociated cells were plated onto 12 mm diameter coverslips (Fisher Scientific) pre-treated with PDL at a density of 25-30,000 cells per coverslip in MEM supplemented media. Neurons were maintained at 37 °C in a humidified incubator with 5 % CO_2. At 1 day *in vitro* (DIV) half of the MEM supplemented media was removed and replaced with Neurobasal media containing 2% B-27 supplement and 1% GlutaMax.

Stock solutions of dyes and additives in DMSO were diluted in HBSS to working concentrations. All imaging experiments were performed in HBSS at room temperature.

Epifluorescence microscopy

Imaging was performed on an AxioExaminer Z-1 (Zeiss) equipped with a Spectra-X Light engine LED light (Lumencor), controlled with Slidebook (v6, Intelligent Imaging Innovations) or µManager (Open Imaging). Images were acquired with a W-Plan-Apo 20x/1.0 water objective (20x; Zeiss) and focused onto a OrcaFlash4.0 sCMOS camera (sCMOS; Hamamatsu). For imaging VoltageFluor dyes, excitation light was delivered at 475 nM (LED, 475 nm, 34 nm bandpass) and

emission was collected with a 540/50 nm bandpass filter after passing through a 510 nm longpass dichroic.

Extracellular field stimulation and imaging spontaneous activity

Extracellular field stimulation was delivered by a SD9 Grass Stimulator connected to a recording chamber containing two platinum electrodes (Warner), with triggering provided through a Digidata 1440A digitizer and pCLAMP 10 software (Molecular Devices). To prevent recurrent activity the HBSS bath solution was supplemented with synaptic blockers 10 μM 2,3-Dioxo-6-nitro-1,2,3,4-tetrahydrobenzo[f]quinoxaline-7-sulfonamide (NBQX; Santa Cruz Biotechnology) and 25 μM DL-2-Amino-5-phosphonopentanoic acid (APV; Sigma-Aldrich). Optical recordings of evoked activity were captured on an OrcaFlash4.0 sCMOS camera at 500 Hz, in a restricted 2048x400 imaging window, with 4x4 binning and 21 mW/mm^2 illumination.

Image analysis

For analysis of voltage responses in neurons, regions of interest encompassing cell bodies (all of approximately the same size) were drawn in ImageJ and the mean fluorescence intensity for each frame extracted. ΔF/F values were calculated by first subtracting a mean background value from all raw fluorescence frames to give a background subtracted trace. A least squares linear regression was fit to the background subtracted trace and a bleaching curve, derived from the slope of the regression, was used to correct for photobleaching. A baseline fluorescence value (F_{base}) was calculated from the median of all the frames and was subtracted from each timepoint of the bleach corrected trace to yield a ΔF trace. The ΔF was then divided by F_{base} to give ΔF/F traces. No averaging was applied to any voltage traces.

Synthetic Methods

Synthesis of **2:**

6-bromo-2',7' dichlorofluorescein **1** (317 mg, 660 μmol), Boc-protected piperazine (127.6 mg, 685 μmol) and HATU (695 μmol) were dissolved in 2 mL anhydrous DMF, followed by addition of 575 μL DIPEA (427 mg, 3.30 mmol). After stirring for 24 hours the reaction was diluted with 50 mL 20% iPrOH/DCM and washed five times with 20 mL water. The organic phase was dried over $MgSO_4$, decanted, and solvents removed under reduced pressure. Product was purified by flash column chromatography (10% MeOH/DCM) to obtain **2** (380 mg, 586 μmol, 89%) as a red powder. Analytical HPLC retention time: 6.89 minutes. ESI-MS $[M+H]^+$ calculated 647.0, found 647.2.

Synthesis of **3**:

To an oven-dried Schlenk flask added **2** (350 mg, 540 μmol), phenylene vinylene molecular wire (169 mg, 678 μmol), $Pd(OAc)_2$ (1.80 mg, 8.01 μmol) and P(*o*-Tol)$_3$ (15.5 μmol). The flask was evacuated and backfilled with N_2 three times. Solid reagents were dissolved in 3 mL anhydrous DMF, 1.5 mL anhydrous Et_3N and the reaction stirred for 16 hours at 90 °C. After cooling to rt the reaction was diluted with 20 mL 20% iPrOH/DCM and filtered through a pad of celite. Solvents were removed under reduced pressure and product purified by flash column chromatography (10% MeOH/DCM) to obtain **3** (408 mg, 500 μmol, 92%) as a red powder. Analytical HPLC retention time: 7.10 minutes. ESI-MS $[M+H]^+$ calculated 816.3 , found 816.4.

Synthesis of **4**:

3 (154.3 mg, 188 μmol) was dissolved in 2 mL 1:1 TFA:DCM. After stirring for 30 minutes the reaction was concentrated under a stream of N_2 and residual solvents removed by toluene azeotrope. In the same round bottom, added Boc-protected cysteic acid (56.0 mg, 208 μmol) and HATU (82.5 mg, 217 μmol). Solid reagents were dissolved in 1 mL anhydrous DMF, followed by addition of 164 μL DIPEA (121 mg, 164 μmol). After stirring for 16 hours the reaction was neutralized by drop-wise addition of AcOH and solvents removed under reduced pressure. Crude material was purified by preparative TLC (15% MeOH, 5% AcOH in DCM, material eluted off silica with 10% MeOH/DCM) to obtain pure **4** as a red gum. Trituration with MeCN led to formation of a red powder, which could be isolated by vacuum filtration to obtain **4** (90.0 mg, 93.0 μmol, 50%). Analytical HPLC retention time: 5.15 minutes. ESI-MS $[M+H]^+$ calculated 967.3 , found 967.4.

Synthesis of **mVF-PipCys**:

4 (47.9 mg, 51.7 μmol) was dissolved in 1 mL 1:1 TFA:DCM. After stirring for 30 minutes the reaction was concentrated under a stream of N_2, after which residual solvents were removed by toluene azeotrope. The resulting solid was suspended in MeCN and mVF-PipCys (40.1 mg, 37.3 μmol, 90%) was collected by vacuum filtration as an orange powder. Analytical HPLC retention time: 4.67 minutes. ESI-MS $[M+H]^+$ calculated 867.2 , found 867.2.

Synthesis of **mVF-Trolox1**:

4 (42.1 mg, 43.5 μmol) was dissolved in 1 mL 1:1 TFA:DCM. After stirring for 1 hour the reaction was concentrated under a stream of N_2 and residual solvents removed by toluene azeotrope. In the same round bottom, added Trolox (12.2 mg, 48.6 μmol) and HATU (19.1mg, 50.1 μmol). Solid reagents were dissolved in 1 mL anhydrous DMF, followed by addition of 37.9 μL DIPEA (28.1 mg, 217 μmol). After stirring for 16 hours the reaction was neutralized by addition of 50 μL AcOH and solvents removed under reduced pressure. The crude reaction was dissolved in MeOH, filtered through a 0.22 μm filter and purified by preparative HPLC to obtain mVF-Trolox1 (9.49 mg, 8.63 μmol, 20%) as an orange powder. Analytical HPLC retention time: 5.43 minutes. ESI-MS $[M+H]^+$ calculated 1099.3 , found 1099.5.

Scheme 5-1 Compounds described in this Appendix

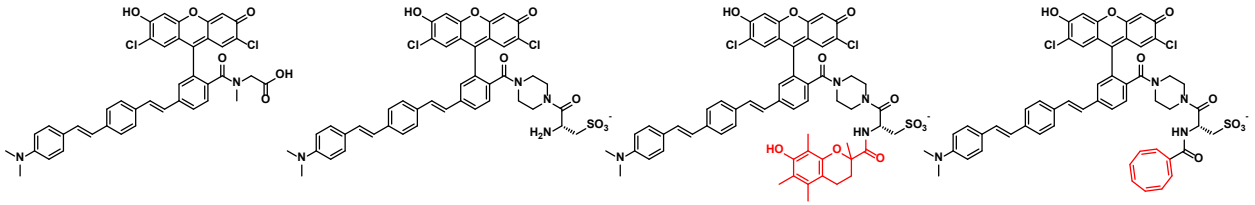

Figure 5-1

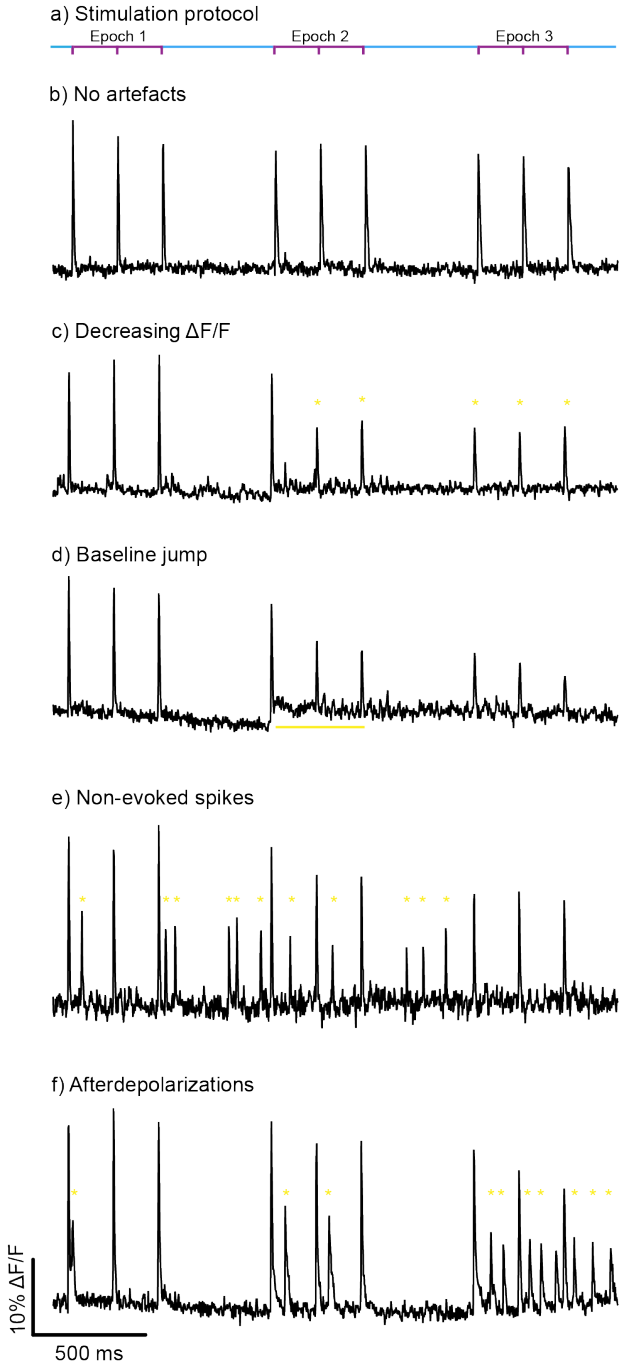

Non-evoked artifacts can be observed in evoked activity traces recorded from mVF-sarcosine despite the presence of synaptic blockers. a-b) pulse program and artifact free traces. c) Example of gradual decrease in evoked AP ΔF/F throughout the duration of the recording. d) Example of a sustained jump in baseline fluorescence intensity. Onset is indicated by the yellow bar. e-f) Examples of non-evoked spikes and afterdepolarizations. Traces were binned to "afterdepolarizations" if the non-evoked spikelets (indicated by yellow stars) exclusively tracked closely with evoked APs.

Figure 5-2

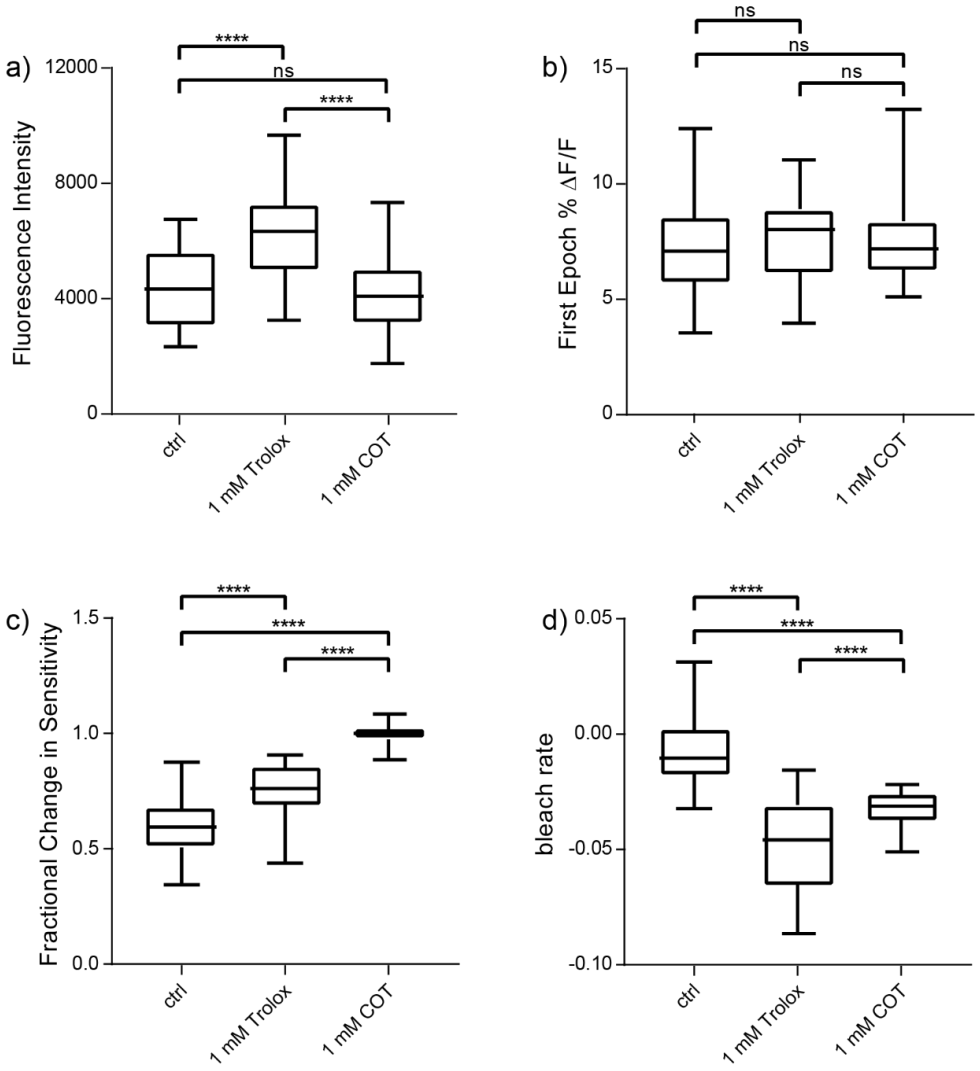

Quantitative analysis of evoked activity traces recorded from 500 nM mVF-sarcosine imaged without TSQs (ctrl), with 1 mM Trolox or with 1 mM COT. Data are from 33, 26 and 38 neurons, respectively. a) Background-corrected cellular fluorescence measured at the soma in the first frame of the recording. b) AP ΔF/F in the first 400 ms stimulation period. In the event where non-evoked spikes overlapped with evoked APs the ΔF/F of the three most intense spikes were averaged. c) Ratio of the mean AP ΔF/F in the third and first 400 ms stimulation period, expressed as a fractional change in sensitivity. A fractional change in sensitivity of 1.0 indicates no change in AP fluorescence amplitude. d) Rate of bleaching, expressed as a unitless parameter describing the slope of a least-squares linear regression fit to the whole trace. Tukey boxplots; box defines the first quartile, median, and third quartile; whiskers define minimum and maximum values falling within 1.5 times the inter-quartile range. * $p < .05$, ** $p < .01$, *** $p < .001$, **** $p < .0001$. Statistics are one-way ANOVA followed by Tukey's test.

Table 5-1 Incidence of non-evoked events in evoked activity traces recorded with mVF-sarcosine

Condition	Number of neurons				
	Total cells	No artifact	Afterdepolarizations	Non-evoked spikes	Baseline shift[a]
No TSQ	33	4	8	14	7
1 mM Trolox	26	7	2	7	10
1 mM COT	38	34	3	1	0

[a] Traces showing a baseline shift were assigned to this category regardless of the presence of other artifacts.

Scheme 5-2 Synthesis of VF-Trolox1

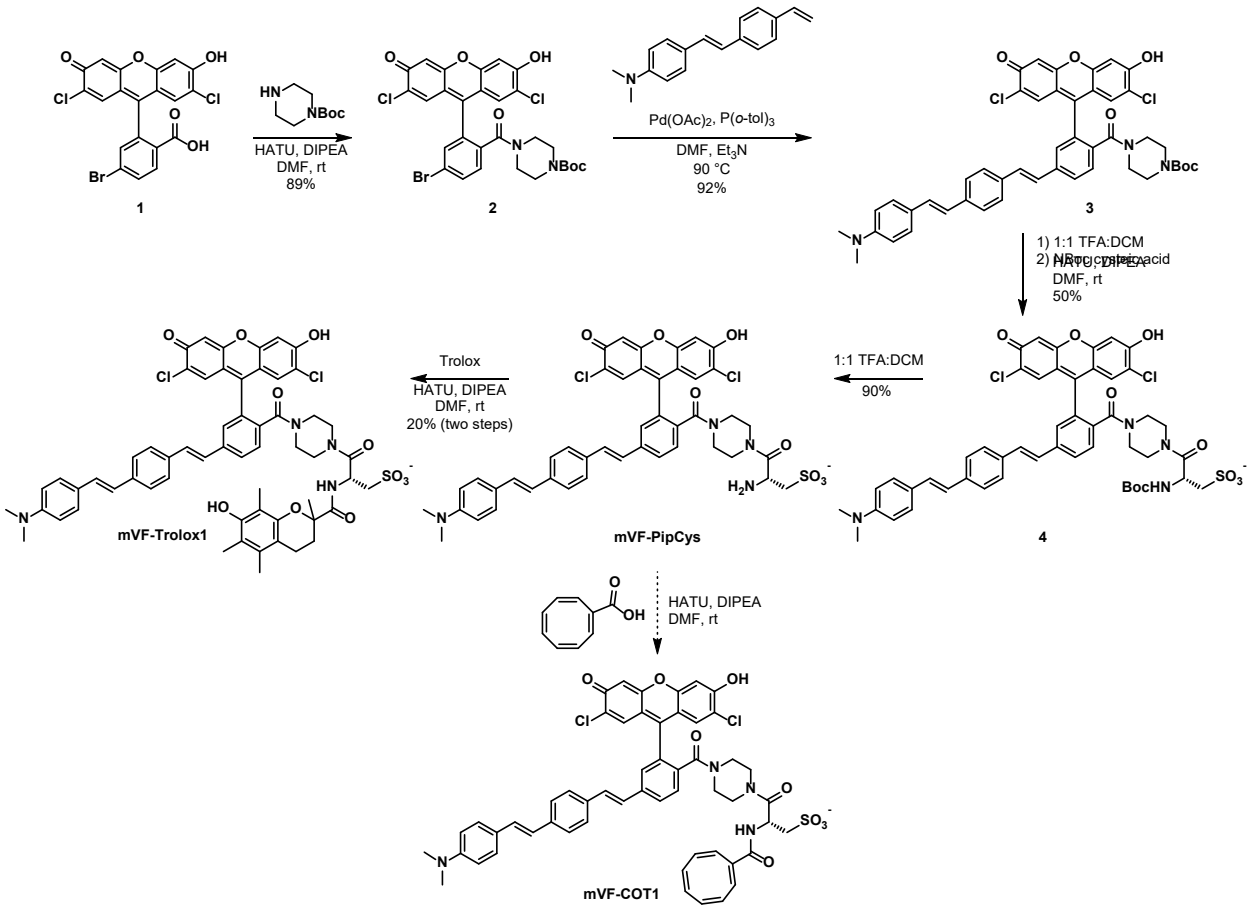

Figure 5-3

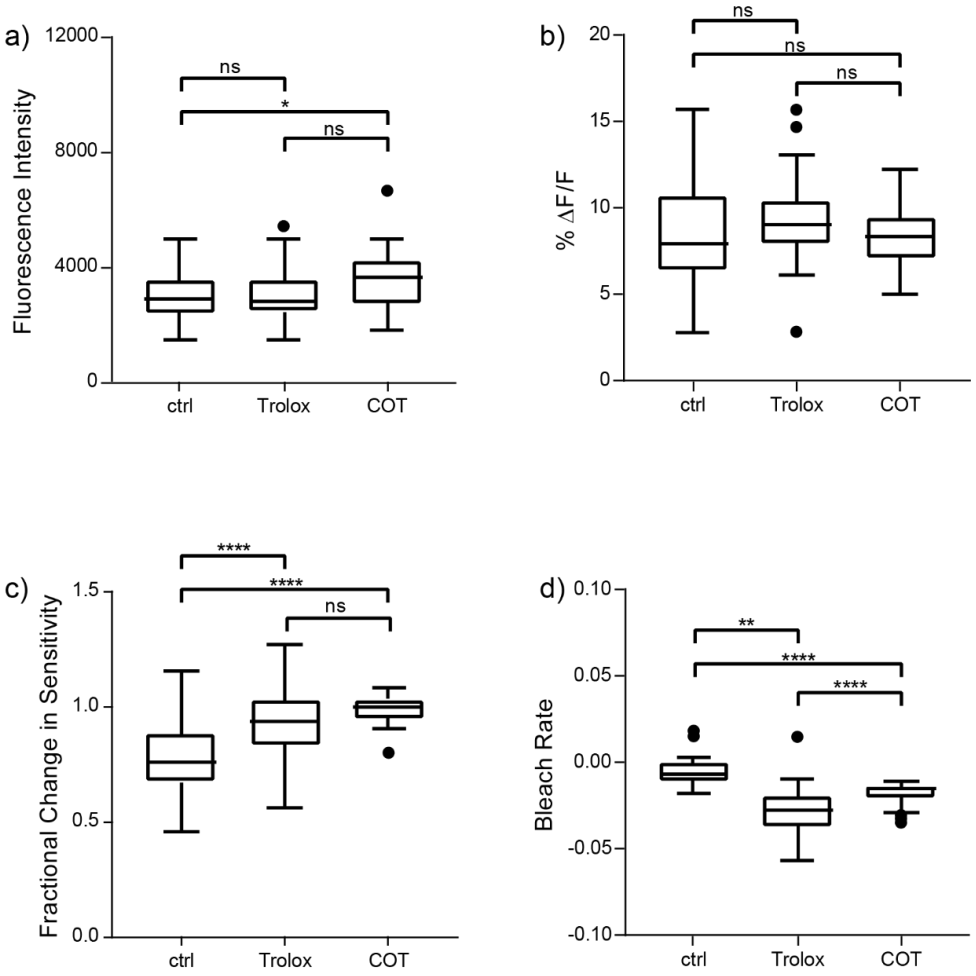

Quantitative analysis of evoked activity traces recorded from 500 nM mVF-PipCys imaged without TSQs (ctrl), with 1 mM Trolox or with 1 mM COT. Data are from 35, 36 and 30 neurons, respectively. a) Background-corrected cellular fluorescence measured at the soma in the first frame of the recording. b) AP ΔF/F in the first 400 ms stimulation period. In the event where non-evoked spikes overlapped with evoked APs the ΔF/F of the three most intense spikes were averaged. c) Ratio of the mean AP ΔF/F in the third and first 400 ms stimulation period, expressed as a fractional change in sensitivity. A fractional change in sensitivity of 1.0 indicates no change in AP fluorescence amplitude. d) Rate of bleaching, expressed as a unitless parameter describing the slope of a least-squares linear regression fit to the whole trace. Tukey boxplots; box defines the first quartile, median, and third quartile; whiskers define minimum and maximum values falling within 1.5 times the inter-quartile range. * $p < .05$, ** $p < .01$, *** $p < .001$, **** $p < .0001$. Statistics are one-way ANOVA followed by Tukey's test.

Table 5-2 Incidence of non-evoked events in evoked activity traces recorded with mVF-PipCys and VF-Trolox1

	Number of neurons				
Condition	Total cells	No artifact	Afterdepolarizations	Non-evoked spikes	Baseline shift[a]
No TSQ	35	10	5	19	1
1 mM Trolox	36	6	19	6	5
1 mM COT	30	27	3	0	0
VF-Trolox1	35	20	12	2	1

[a] Traces showing a baseline shift were assigned to this category regardless of the presence of other artifacts.

Figure 5-4

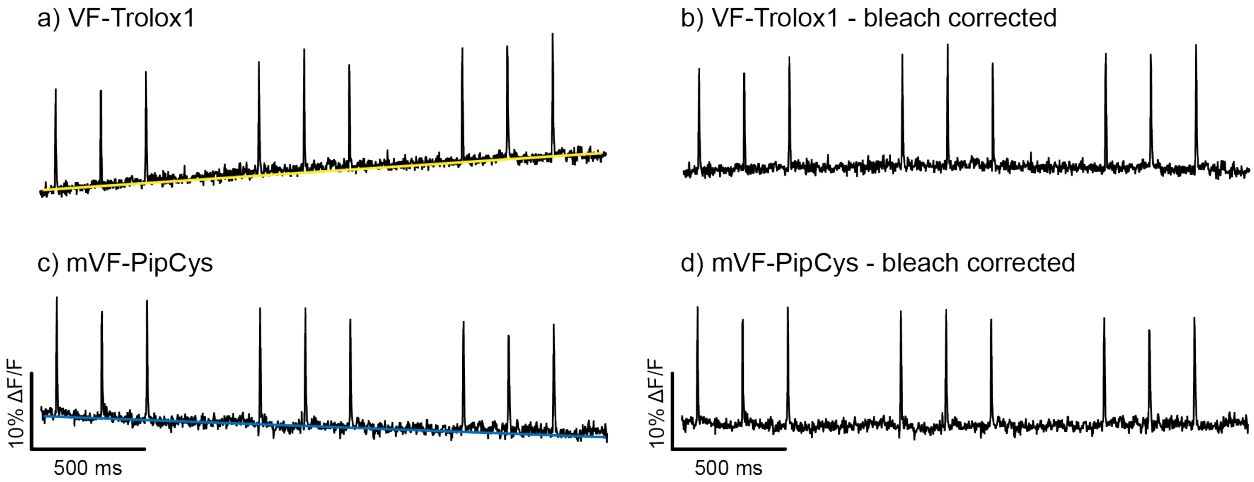

VF-Trolox1 demonstrates an unusual increase in fluorescence throughout the recording. Example traces of VF-Trolox without (a) and with (b) linear bleach correction applied. Example traces of mVF-PipCys without (c) and with (d) linear bleach correction applied.

Figure 5-5

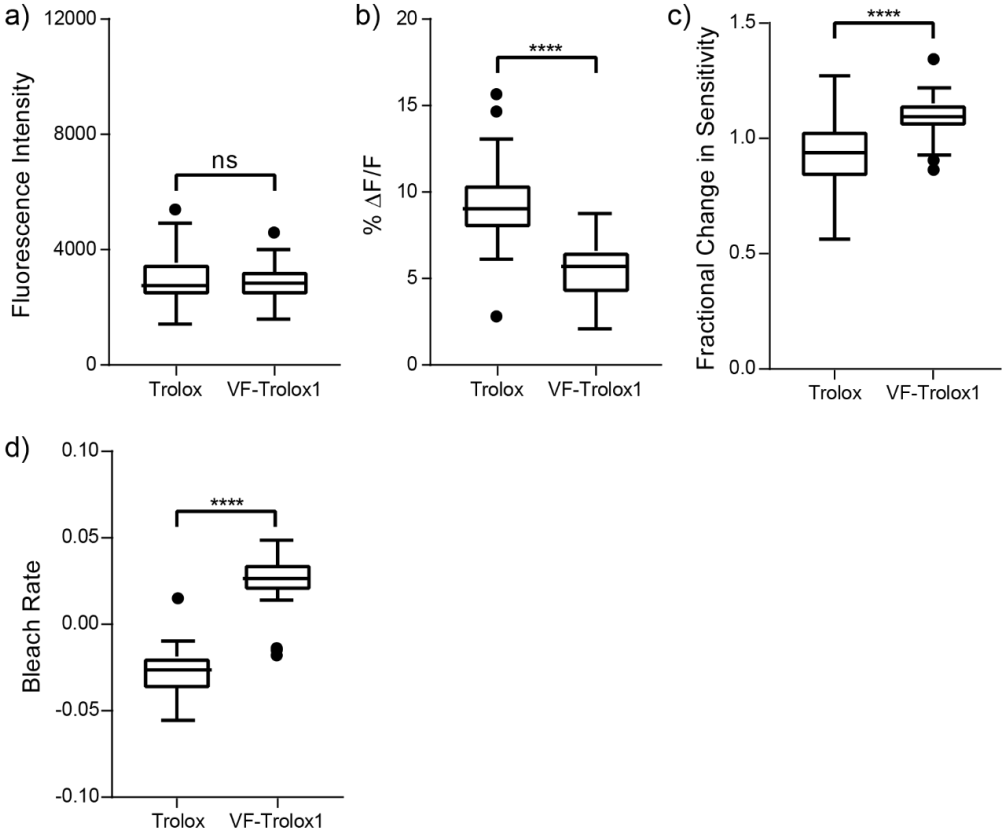

Quantitative analysis of evoked activity traces recorded from mVF-PipCys with 1 mM Trolox (reproduced from Figure 5-3) and VF-Trolox 1 Data are from 36 and 35 neurons, respectively. a) Background-corrected cellular fluorescence measured at the soma in the first frame of the recording. b) AP ΔF/F in the first 400 ms stimulation period. In the event where non-evoked spikes overlapped with evoked APs the ΔF/F of the three most intense spikes were averaged. c) Ratio of the mean AP ΔF/F in the third and first 400 ms stimulation period, expressed as a fractional change in sensitivity. A fractional change in sensitivity of 1.0 indicates no change in AP fluorescence amplitude. d) Rate of bleaching, expressed as a unitless parameter describing the slope of a least-squares linear regression fit to the whole trace. Tukey boxplots; box defines the first quartile, median, and third quartile; whiskers define minimum and maximum values falling within 1.5 times the inter-quartile range. * $p < .05$, ** $p < .01$, *** $p < .001$, **** $p < .0001$. Statistics are one-way ANOVA followed by Tukey's test.

References

(1) Miller, E. W.; Lin, J. Y.; Frady, E. P.; Steinbach, P. a; Kristan, W. B.; Tsien, R. Y. *Proc. Natl. Acad. Sci. U. S. A.* **2012**, *109* (6), 2114–2119.

(2) Rodrigues, G. M. C.; Gaj, T.; Adil, M. M.; Wahba, J.; Rao, A. T.; Lorbeer, F. K.; Kulkarni, R. U.; Diogo, M. M.; Cabral, J. M. S.; Miller, E. W.; Hockemeyer, D.; Schaffer, D. V. *Stem Cell Reports* **2017**, *8* (6), 1770–1783.

(3) Adil, M. M.; Rodrigues, G. M. C.; Kulkarni, R. U.; Rao, A. T.; Chernavsky, N. E.; Miller, E. W.; Schaffer, D. V. *Sci. Rep.* **2017**, *7* (January), 1–11.

(4) Adil, M. M.; Vazin, T.; Ananthanarayanan, B.; Rodrigues, G. M. C.; Rao, A. T.; Kulkarni, R. U.; Miller, E. W.; Kumar, S.; Schaffer, D. V. *Biomaterials* **2017**, *136*, 1–11.

(5) Adil, M. M.; Gaj, T.; Rao, A. T.; Kulkarni, R. U.; Fuentes, C. M.; Ramadoss, G. N.; Ekman, F. K.; Miller, E. W.; Schaffer, D. V. *Stem Cell Reports* **2018**, *10* (5), 1481–1491.

(6) Kulkarni, R. U.; Kramer, D. J.; Pourmandi, N.; Karbasi, K.; Bateup, H. S.; Miller, E. W. *Proc. Natl. Acad. Sci.* **2017**, 201610791.

(7) Kulkarni, R. U.; Vandenberghe, M.; Thunemann, M.; James, F.; Andreassen, O. A.; Djurovic, S.; Devor, A.; Miller, E. W. *ACS Cent. Sci.* **2018**, *4*, acscentsci.8b00422.

(8) Boggess, S.; Gandhi, S.; Siemons, B.; Huebsch, N.; Healy, K.; Miller, E.; *ChemRxiv.* **2018**, Preprint. DOI: 10.36434/chemrxiv.7338683.v1.

(9) Dempsey, G. T.; Chaudhary, K. W.; Atwater, N.; Nguyen, C.; Brown, B. S.; McNeish, J. D.; Cohen, A. E.; Kralj, J. M. *Submitted* **2015**.

(10) Dempsey, G. T.; Chaudhary, K. W.; Atwater, N.; Nguyen, C.; Brown, B. S.; McNeish, J. D.; Cohen, A. E.; Kralj, J. M. *J. Pharmacol. Toxicol. Methods* **2016**, *81*, 240–250.

(11) McPheeters, M. T.; Wang, Y. T.; Werdich, A. A.; Jenkins, M. W.; Laurita, K. R. *PLoS One* **2017**, *12* (8), 1–19.

(12) Bedut, S.; Seminatore-Nole, C.; Lamamy, V.; Caignard, S.; Boutin, J. A.; Nosjean, O.; Stephan, J.-P.; Coge, F. *Am. J. Physiol. - Hear. Circ. Physiol.* **2016**, *311* (1), H44–H53.

(13) Kijlstra, J. D.; Hu, D.; Mittal, N.; Kausel, E.; Van Der Meer, P.; Garakani, A.; Domian, I. J. *Stem Cell Reports* **2015**, *5* (6), 1226–1238.

(14) McKeithan, W. L.; Savchenko, A.; Yu, M. S.; Cerignoli, F.; Bruyneel, A. A. N.; Price, J. H.; Colas, A. R.; Miller, E. W.; Cashman, J. R.; Mercola, M. *Front. Physiol.* **2017**, *8* (OCT), 1–12.

(15) McNamara, H. M.; Dodson, S.; Huang, Y.-L.; Miller, E. W.; Sandstede, B.; Cohen, A. E. *Cell Syst.* **2018**, 1–12.

(16) Moshtagh-Khorasani, M.; Miller, E. W.; Torre, V. *Physiol. Rep.* **2013**, *1* (5), 1–16.

(17) Dolenšek, J.; Stožer, A.; Klemen, M. S.; Miller, E. W.; Rupnik, M. S. *PLoS One* **2013**, *8* (12), 1–16.

(18) Deal, P. E.; Kulkarni, R. U.; Al-Abdullatif, S. H.; Miller, E. W. *J. Am. Chem. Soc.* **2016**, *138* (29), 9085–9088.

(19) Huang, Y.-L.; Walker, A. S.; Miller, E. W. *J. Am. Chem. Soc.* **2015**, *2*, 10767-10776.

(20) Woodford, C. R.; Frady, E. P.; Smith, R. S.; Morey, B.; Canzi, G.; Palida, S. F.; Araneda, R. C.; Kristan, W. B.; Kubiak, C. P.; Miller, E. W.; Tsien, R. Y. *J. Am. Chem. Soc.* **2015**, *137* (5), 1817–1824.

(21) Kulkarni, R. U.; Yin, H.; Pourmandi, N.; James, F.; Adil, M. M.; Schaffer, D. V.; Wang, Y.; Miller, E. W. *ACS Chem. Biol.* **2017**, *12* (2), 407–413.

(22) Grenier, V.; Daws, B.; Liu, P.; Miller, E.; *ChemRxiv* **2018**, Preprint. DOI: 10.26434/chemrxiv.7313657.v1.

(23) Allison, R. R.; Moghissi, K. *Clin. Endosc.* **2013**, *46* (1), 24–29.

(24) Palozza, P.; Krinsky, N. I. *Arch. Biochem. Biophys.* **1992**, *297* (2), 291–295.

(25) González, J. E.; Tsien, R. Y. *Chem. Biol.* **1997**, *4* (4), 269–277.

(26) Zheng, Q.; Jockusch, S.; Rodríguez-Calero, G. G.; Zhou, Z.; Zhao, H.; Altman, R. B.; Abruña, H. D.; Blanchard, S. C. *Photochem. Photobiol. Sci.* **2016**, *15* (2), 196–203.

(27) Zheng, Q.; Jockusch, S.; Zhou, Z.; Blanchard, S. C. *Photochem. Photobiol.* **2014**, *90* (2), 448–454.

(28) Zheng, Q.; Jockusch, S.; Zhou, Z.; Altman, R. B.; Warren, J. D.; Turro, N. J.; Blanchard, S. C. *J. Phys. Chem. Lett.* **2012**, *3* (16), 2200–2203.

(29) Ha, T.; Tinnefeld, P. *Annu. Rev. Phys. Chem.* **2012**, *63* (1), 595–617.

(30) Widengren, J.; Chmyrov, A.; Eggeling, C.; Löfdahl, P. Å.; Seidel, C. A. M. *J. Phys. Chem. A* **2007**, *111* (3), 429–440.

(31) Altman, R. B.; Terry, D. S.; Zhou, Z.; Zheng, Q.; Geggier, P.; Kolster, R. A.; Zhao, Y.; Javitch, J. A.; Warren, J. D.; Blanchard, S. C. *Nat. Methods* **2012**, *9* (1), 68–71.

(32) Zheng, Q.; Jockusch, S.; Zhou, Z.; Altman, R. B.; Zhao, H.; Asher, W.; Holsey, M.; Mathiasen, S.; Geggier, P.; Javitch, J. A.; Blanchard, S. C. *Chem. Sci.* **2016**, *8* (1), 755–762.

(33) Zheng, Q.; Juette, M. F.; Jockusch, S.; Wasserman, M. R.; Zhou, Z.; Altman, R. B.; Blanchard, S. C. *Chem. Soc. Rev.* **2014**, *43* (4), 1044–1056.

(34) Allain, M.; Silvestre, V.; Leriche, P.; Blanchard, P. **2016**, 8–11.

(35) Cordes, T.; Vogelsang, J.; Tinnefeld, P. **2009**, No. iv, 5018–5019.

(36) Vogelsang, J.; Kasper, R.; Steinhauer, C.; Person, B.; Heilemann, M.; Sauer, M.; Tinnefeld, P. *Angew. Chemie - Int. Ed.* **2008**, *47* (29), 5465–5469.

(37) Frutos, L. M.; Castaño, O.; Andrés, J. L.; Merchán, M.; Acuña, A. U. *J. Chem. Phys.* **2004**, *120* (3), 1208–1216.

Appendix 1

Synthesis of a VoltageFluor Activated by β-lactamase Expression

Synopsis

The success of VF-EX2 (see Chapter 3) led us to try and extend our enzymatic-activation strategy to other enzyme-substrate pairs. To that end, I synthesized a Voltagefluor activated by β-lactamase expression (VF-BLX1, Scheme A1-1), modeled off existing cepham-masked fluorescent probes.[1,2]

VF-BLX1 is obtained in two steps from VF2.1.Cl. The phenolic oxygen may be masked with PMB-protected cephem fragment **1** in DIPEA and DMF to yield protected intermediate **2**. **2** was found to decompose under acidic deprotection conditions (1:1 TFA:DCM), but could be deprotected in neat phenol[3] to yield VF-BLX1 in 8.3% yield as a pair of well-resolved diastereomers after purification by semi-preparative HPLC. Regrettably, HEK cells expressing β-lactamase at their cell surface and untransfected cells were equally bright, which we attribute to the hydrolytic instability of VF-BLX1 (unpublished results, Pei Liu).

We proposed an alternate structure, **VF-BLX1** (Scheme A1-2), with an alkene linker between the VoltageFluor and cepham fragment which we believed would be less susceptible to hydrolysis. Reaction of VF2.1.Cl with 2-bromo-1,1-dimethoxyethane appeared to give protected intermediate **3** in adequate yield (67%). Although the desired mass $[M+H]^+$ 772 was clearly observed by LC-MS, ^{1}H NMR analysis suggests that the isolated product may in fact be sulfonate ester **3b**. Deprotection to form the aldehyde with HCl in chloroform or 1:1 TFA:DCM could be achieved on a 10 mg test scale as a concentrated slurry, but could not be made to proceed to completion without decomposition on a larger scale. **3** could be solubilized in chloroform by addition of 10% isopropanol as co-solvent, but the reaction would not proceed beyond a 1:1 ratio of **4** and the intermediate hemiacetal, as assayed by LC-MS.

General Synthetic Methods

Refer to Chapter 3. VF-BLX 1 was isolated using 10 mM ammonium acetate, rather than 0.5% TFA, as HPLC modifier.

Synthesis of VF-BLX1-PMB (2)

In a 4 mL dram vial dissolved VF2.1.Cl (48.7 mg, 71.1 μmol) and commercially available **2** (98.9 μmol) in 500 μL *N,N*-dimethylformamide, followed by addition of diisopropylethylamine (25.4 μL, 146 μmol). After stirring for 17 hours precipitation was induced by addition of 2 mL H_2O. The precipitate was collected by vacuum filtration to obtain **2** (75.7 mg, 94%) as an orange solid. Analytical HPLC retention time: 6.71 minutes. ESI-MS $[M+H]^+$ calculated 1134.2 , found 1134.2.

Synthesis of VF-BLX1:

VF-BLX1-PMB (29.9 mg) was dissolved in 0.5 mL warm phenol. The reaction was stirred for one hour at 45 °C under N_2, at which point the reaction was found to have reached completion by LC-MS. The reaction was added dropwise to diethyl ether, and the resulting orange precipitate collected by vacuum filtration. The precipitate was washed abundantly with diethyl ether to remove residual phenol. The precipitate was then washed off the filter with DCM/MeOH into a clean flask. The crude was purified by semi-preparative HPLC to obtain 2.23 mg (8.3%) of **VF-**

BLX1 as a pair of diastereomers. Analytical HPLC retention time: 5.78 and 5.96 minutes. ESI-MS $[M+2Na]^{2+}$ calculated 529.6, found 529.3.

Synthesis of 3/3b:

In an oven-dried bomb flask dissolved VF2.1.Cl (102 mg, 149 µmol), Cs_2CO_3 (192 mg, 590 µmol) in 1 mL anhydrous DMF, then added 140 µL 2-bromo-1,1-dimethoxyethane (113 mg, 147 µmol). Heated for five days at 120 °C, at which point complete consumption of starting material was observed by LC-MS. The reaction was diluted with 50 mL 20% iPrOH/DCM and filtered to remove residual salts. The filtrate was acidified with 200 µL AcOH and solvents removed under reduced pressure. Crude product was suspended in water and filtered to obtain 77.2 mg (67%) of material as an dull red powder. Analytical HPLC retention time: 6.06 minutes. ^{1}H NMR (600 MHz, DMSO-d_6) δ 8.17 (d, J = 1.7 Hz, 1H), 7.81 – 7.76 (m, 1H), 7.67 (d, J = 8.1 Hz, 2H), 7.57 (d, J = 8.1 Hz, 2H), 7.53 (s, 1H), 7.50 (d, J = 8.1 Hz, 2H), 7.48 – 7.39 (m, 4H), 7.26 (d, J = 7.8 Hz, 1H), 7.21 (d, J = 16.4 Hz, 1H), 7.14 (d, J = 16.6 Hz, 1H), 7.06 (s, 1H), 6.95 (s, 1H), 6.41 (s, 1H), 5.80 (d, J = 17.7 Hz, 1H), 5.21 (d, J = 10.9 Hz, 1H), 4.77 (t, J = 5.1 Hz, 1H), 4.28 (qd, J = 10.7, 5.2 Hz, 2H), 3.37 (s, 6H), 2.97 (s, 6H), 2.95 (s, 6H).

References

(1) Gao, W.; Xing, B.; Tsien, R. Y.; Rao, J. *J. Am. Chem. Soc.* **2003**, *125* (37), 11146–11147.

(2) Zlokarnik, G.; Negulescu, P. A.; Knapp, T. E.; Mere, L.; Burres, N.; Feng, L.; Whitney, M.; Roemer, K.; Tsien, R. Y. *Science (80-.).* **1998**, *279* (5347), 84–88.

(3) Torii, S.; Tanaka, H.; Taniguchi, M.; Kameyama, Y.; Sasaoka, M.; Shiroi, T.; Kikuchi, R.; Kawahara, I.; Shimabayashi, A.; Nagao, S. *J. Org. Chem.* **1991**, *56* (11), 3633–3637.

Scheme A1-1 Synthesis of VF-BLX1

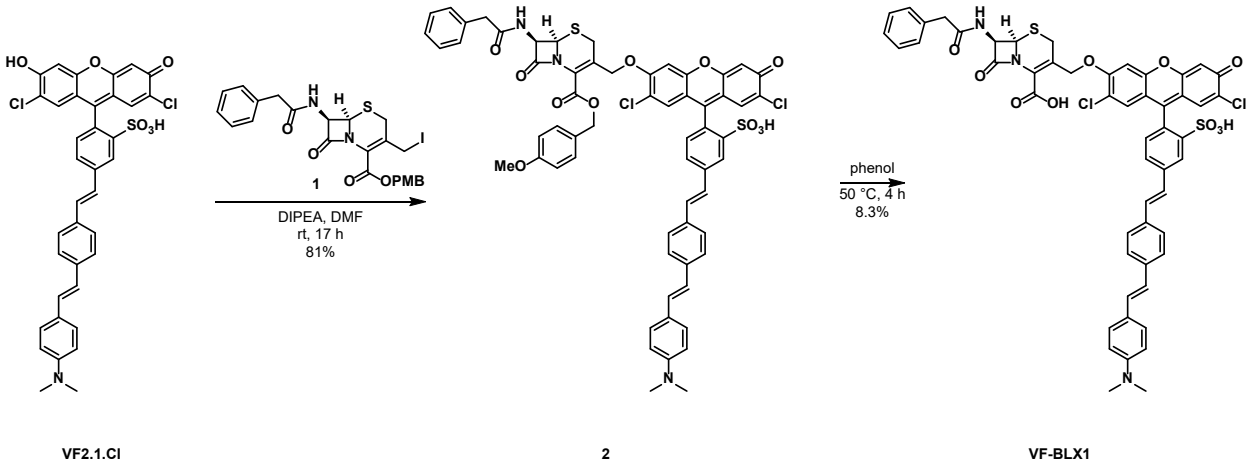

VF2.1.Cl 2 VF-BLX1

Scheme A1-2 Proposed synthesis of VF-BLX1

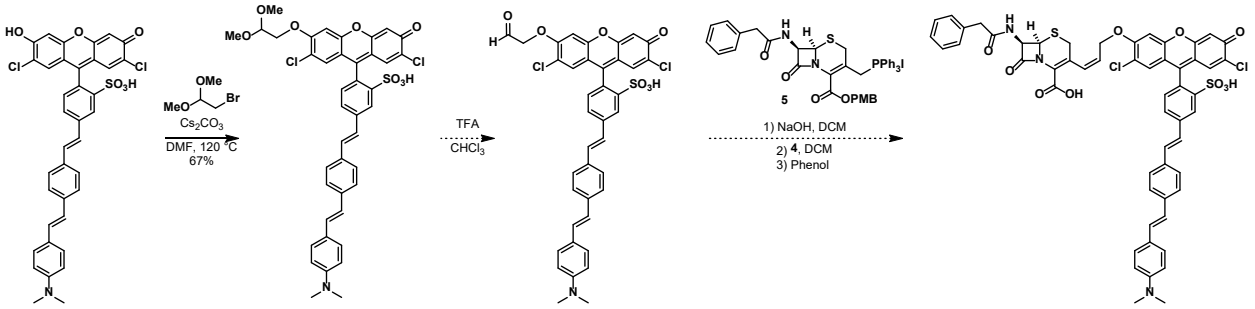

VF2.1.Cl 3 4 VF-BLX2

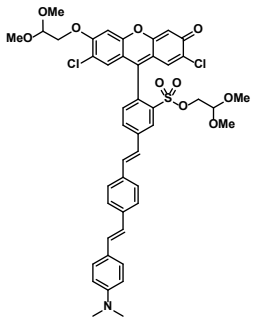

3b
possible side-product

Appendix 2

Application of VoltageSpy Dyes in Mouse Brain Slices

Portions of this work were completed in collaboration with others:

Kiarash Shamardani performed *in utero* electroporation of SpyCatcher plasmid DNA. Pei Liu performed immunohistochemistry experiments. Imaging of brain slices stained with VoltageSpy dye was performed in collaboration with Pei Liu.

Synopsis

Chapter 4 and its accompanying publication[1] reported the design, synthesis and application of a genetically-targeted VoltageFluor. VoltageSpy-PEG$_{35}$ consists of a green VoltageFluor dye coupled to the SpyTag peptide[2] via a PEG linker. When bath applied to cells expressing the SpyTag binding protein, SpyCatcher, an irreversible isopeptide bond is formed between SpyTag and SpyCatcher.[2,3] This covalent labeling method allows for effective labeling of neurons expressing SpyCatcher with single-digit nanomolar concentrations of VoltageSpy-PEG$_{35}$. Given our success in imaging evoked and spontaneous activity in cultured mammalian neurons, we sought to extend this methodology to imaging activity in brain slice.

Embryonic mice were transfected by *in utero* electroporation with a SpyCatcher-fusion protein which bore a PAT3-derived signal peptide,[4] HA epitope tag, and C-terminal glycophosphatidyl inositol (GPI) anchor sequence derived from decay accelerating factor (DAF) under control of a paavCAG promoter. In addition, the SpyCatcher fusion was linked to a nuclear-localized mCherry (NLS-mCherry) via a self-cleaving T2A linker for screening of expression.

Slices from FA-perfused P14 animals showed sparse, nuclear expression of mCherry (Figure A2-1a,b). Staining against the HA-tag demonstrated surface-localized labeling (Figure A2-1c). Signal from anti-HA stained cells correlated tightly with cells expressing NLS-mCherry (Figure A2-1d), confirming expression of SpyCatcher in neurons transfected with our construct.

Live tissue slices from P14 animals stained with 125 nM VoltageSpy-PEG$_{35}$ and expressing NLS-mCherry (Figure A2-1a-c) showed modest dye staining (Figure A2-1d). Whereas immunohistochemistry suggested that SpyCatcher was preferentially localized to the soma, VoltageSpy labeling was most clearly visible in the processes of neurons. While staining of mCherry-expressing neurons at 125 nM was clear, background fluorescence intensity was unacceptably high. Regrettably, no VoltageSpy labeling of mCherry positive cells was observed at lower concentrations, across multiple attempts. We concluded that at present the VoltageSpy system requires further optimization for imaging of neuronal activity in brain slice. Improved genetically-targeted VoltageFluors using alternate tagging chemistries[5,6] and red-shifted fluorophores[7,8] will hopefully show improved performance in ex vivo preparations.

In utero electroporation

All animal procedures were approved by the UC Berkeley Animal Care and Use Committees and conformed to the NIH Guide for the Care and Use of Laboratory Animals and the Public Health Service (PHS) Policy.

Briefly, time-pregnant ICR mice (Charles River, E15-16) were anaesthetized with 2.5% isoflurane. A small vertical incision was made in the abdominal wall and embryos were gently exposed. Embryos were injected with 2 μg of endotoxin-free plasmid DNA using a pressure-controlled glass pipette. Voltage steps were applied via tweezertrodes to achieve sparse cortical transfection. Embryos were returned to the abdomen, which was then sutured.

Immunohistochemistry

To obtain brain slices suitable for immunostaining, animals were anesthetized with a combination of ketamine (100 mg/kg) and xylazine (10mg/kg). Transcardial perfusion was performed with 4% PFA. Brains were collected and fixed in 4% PFA at 4 °C for 24 hours, rinsed with PBS for 3x10 minutes and cryopreserved in 30% sucrose in PBS at 4 °C for 48 hours. Brain sectioning was then performed using a chilled microtome to obtain 40 µm thick slices. Blocking was done in 5% w/v bovine serum albumin (BSA; Sigma Aldrich) in PBS for 1 h. Primary antibody was incubated at 4 °C overnight, followed by AlexaFluor secondary antibody (Life Technologies) at room temperature for 2 hours. All antibodies were used at 1:1000 dilution. Slices were mounted on a glass slide with Fluoromount and sealed under a cover glass.

Name	Primary/Secondary	Manufacturer	Catalog #	Isotype
Anti-HA	Primary	CST	3724S	Rabbit IgG
Anti-rabbit 647	Secondary	Life Technologies	A21244	Goat IgG

Slice labeling

300 µm cortical slices prepared from P14, mCherry expressing animals were incubated with 125 nM VoltageSpy in carbogen-saturated, room temperature ACSF for 1 hour, then transferred to an imaging dish containing fresh ACSF. Tissue was shielded from light during the staining procedure.

Confocal microscopy

Confocal images were acquired on a Zeiss LSM 880 equipped with 405 nm diode, 458, 488 and 514 argon, 561 nm DPSS, 594 and 633 HeNe laser lines. All images were acquired with a Plan-Apochromat 20X/1.0 water immersion objective (Zeiss) Images were processed in Fiji (ImageJ)

Figure A2-1

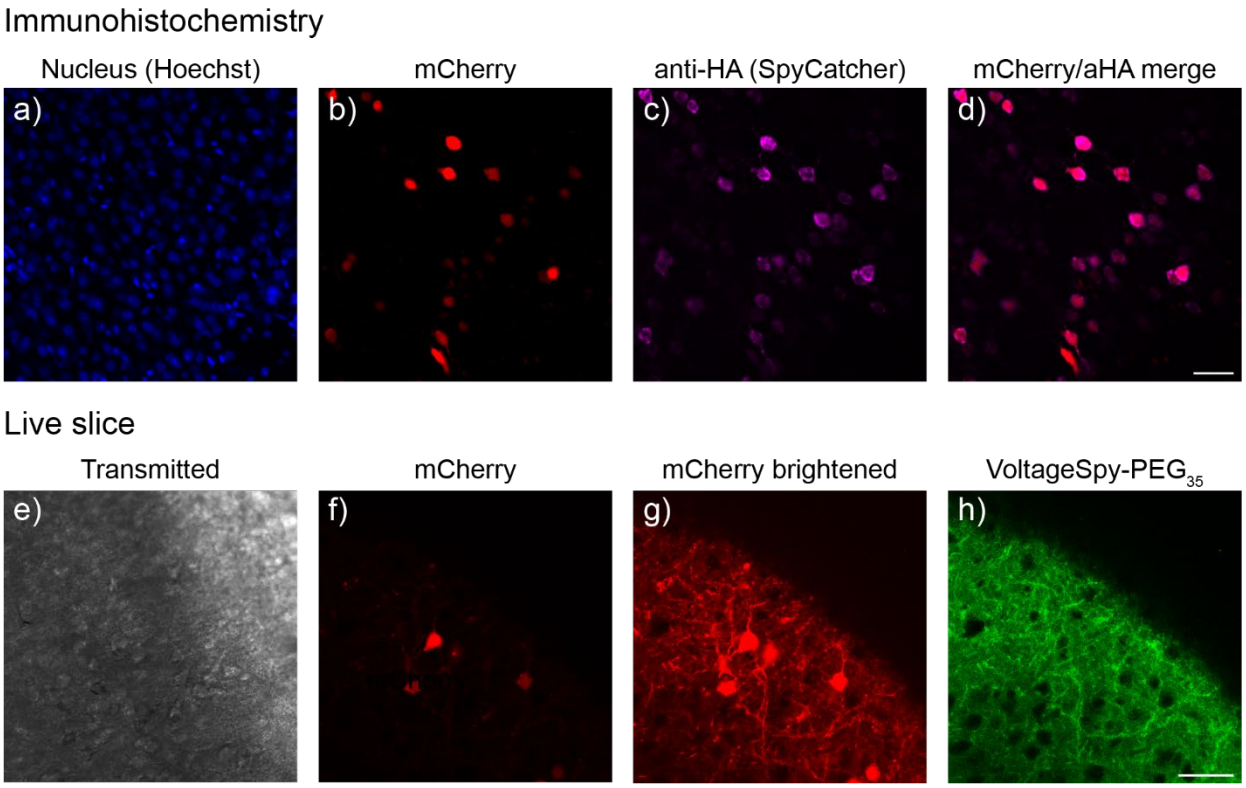

SpyCatcher is expressed in mouse brain slice after *in utero* electroporation. a-d) fixed neurons (a) expressing mCherry (b) show surface expression of SpyCatcher (c, d). mCherry expressing neurons (e-g) in cortical slice labeled with 125 nM VoltageSpy-PEG$_{35}$ (h) show labeling of neuronal processes, though with high background fluorescence. Scale bars are 40 µm.

References

(1) Grenier, V.; Daws, B.; Liu, P.; Miller, E.; Grenier, V.; Daws, B. R.; Liu, P.; Miller, E. W. *ChemRxiv Prepr.* **2018**.

(2) Zakeri, B.; Fierer, J. O.; Celik, E.; Chittock, E. C.; Schwarz-Linek, U.; Moy, V. T.; Howarth, M. *Proc. Natl. Acad. Sci. U. S. A.* **2012**, *109* (12), E690-7.

(3) Li, L.; Fierer, J. O.; Rapoport, T. a; Howarth, M. *J. Mol. Biol.* **2014**, *426* (2), 309–317.

(4) Kim, J.; Zhao, T.; Petralia, R. S.; Yu, Y.; Peng, H.; Myers, E.; Magee, J. C. *Nat. Methods* **2011**, *9* (1), 96–102.

(5) Encell, L. P. *Curr. Chem. Genomics* **2013**, *6* (1), 55–71.

(6) Keppler, A.; Gendreizig, S.; Gronemeyer, T.; Pick, H.; Vogel, H.; Johnsson, K. *Nat. Biotechnol.* **2003**, *21*, 86-89.

(7) Deal, P. E.; Kulkarni, R. U.; Al-Abdullatif, S. H.; Miller, E. W. *J. Am. Chem. Soc.* **2016**, *138* (29), 9085–9088.

(8) Huang, Y.-L.; Walker, A. S.; Miller, E. W. *J. Am. Chem. Soc.* **2015**, *2*, 10767-10776.